https://ntrs.nasa.gov/search.jsp?R=19960003386 2020-06-16T05:38:02+00:00Z

NASA-CR-199176

FINAL TECHNICAL REPORT

on

Two Color Holographic Interferometry for Microgravity Application

Contract No. NAS8-39402
DCN: 1-2-ES-44818

Prepared for:

COTR: William K. Witherow/ES74
NASA Marshall Space Flight Center
Huntsville, Alabama 35812

Period of Performance:

07/21/92 - 02/21/95

Prepared by:

James D. Trolinger, Ph.D. and David C. Weber
MetroLaser
18006 Skypark Circle #108
Irvine, CA 92714

N96-13395
Unclas
G3/35 0064556
(NASA-CR-199176) TWO COLOR HOLOGRAPHIC INTERFEROMETRY FOR MICROGRAVITY APPLICATION Final Report, 21 Jul. 1992 - 21 Feb. 1995 (MetroLaser) 86 p

TABLE OF CONTENTS

1. INTRODUCTION 1

1.1. Background 1

1.2. Two Color Holographic Interferometry (TCHI) 1

1.3. Phase Shift Interferometry 3

2. TECHNICAL APPROACH 5

2.1. Technical Issues 5

2.2. Assessment and Demonstration of the TCHI Technique (Laboratory Breadboard) 6

2.3. Light Weight, Compact, Fiber Optic-Based Holographic Camera System (Flight Breadboard) 6

3. ERROR ANALYSIS 6

3.1. Sensitivity of TCHI Equation to Errors 6

3.2. Change of derivative values over gradient 10

3.3. Experimental Errors 12

3.3.1. Phase Correction to Reference Interferogram 12

3.3.2. Correction of Hologram Tilt 13

3.3.3. Correction of Magnification Differences Due to Chromatic Aberrations 13

4. EXPERIMENTAL PROGRAM WITH LABORATORY BREADBOARD 14

4.1. Breadboard Description 14

4.2. Test Chamber 15

4.3. Control Software 18

4.4. Analysis Software 18

4.4.1. File Format 18

4.4.2. Programs 19

4.5. History of Experiments 23

4.5.1. First Series 23

4.5.2. Second Series 24

4.5.3. Third Series 24

4.5.4. Fourth Series 26

4.5.5. Fifth Series 27

4.5.6. Sixth Series 27

4.5.7. Seventh Series 28
4.6. Experiment Description 30
4.6.1. Data Collection 30
4.6.1.1. Selection and Characterization of Test Solution 31
4.6.1.2. Preparation of Test Solution 33
4.6.1.3. Production of Hologram 34
4.6.1.4. Production of Interferograms 34
4.6.2. Data Reduction 34
5. EXPERIMENTAL RESULTS FROM LABORATORY BREADBOARD 35
5.1. Interferograms 36
5.2. Phase Maps 39
5.3. Determination of Δc and ΔT 42
5.4. Calibration of dn/dT and dn/dc 43
5.5. Data Interpretation 45
5.5.1. Phase Error 46
5.5.2. Reference Interferogram 49
5.5.3. Relative Phase Between Top and Bottom of Test Cell 52
5.5.4. TCHI Results 55
5.5.5. Comparison to Expected Results Based on Error Analysis 62
5.5.6. Comparison of 4 and 5 bucket Algorithms 63
6. FLIGHT BREADBOARD PROGRAM 64
6.1. Breadboard Description 64
6.1.1. Lasers and Associated Hardware 66
6.1.2. Fiber Optic Assembly 68
6.2. Experiment Description 69
6.2.1. Phase Shift Interferometry 69
6.2.2. Demonstration of TCHI 70
6.2.3. Simulation of Microgravity 71
7. EXPERIMENTAL RESULTS FROM FLIGHT BREADBOARD 71
8. CONCLUSIONS 74
REFERENCES 80
APPENDIX A- INSTALLATION INSTRUCTIONS FOR TEST CELL CHAMBER 1

1. INTRODUCTION

1.1 Background

Holographic interferometry is a primary candidate for the determination of temperature and concentration in various crystal growth experiments destined for space. The method actually measures refractive index changes in the fluid in an experimental test cell, which are caused by concentration changes, temperature changes, or a combination of the two. When the refractive index changes are caused by simultaneous temperature and concentration changes the contributions of the two effects cannot be separated by single wavelength interferometry. By using two wavelengths, however, two independent interferograms can provide the additional independent equation required to determine the two unknowns. The two interferograms provide independent equations if the dispersion (dependence of refractive index on wavelength) properties of fluid materials are of sufficient strength. There is no other technique available that can provide this type of information.

The primary objectives of this effort were to experimentally verify the mathematical theory of two color holographic interferometry (TCHI) and to determine the practical value of this technique for space application.

To achieve these objectives, the accuracy and sensitivity of the technique had to be determined for geometries and materials relevant to Materials Processing in the Space program of NASA. This was achieved through the use of two, specially designed TCHI breadboard optical systems. The first system used conventional optical components to demonstrate the feasibility of the technique. The second breadboard was a miniaturized system comprising compact lasers, fiber optics, and fiber optic phase shifting in a lightweight, compact system to test concepts required to make the technique fieldable in space applications. These breadboards were used both to establish limits on the TCHI technique and to provide inputs for the design of an optimum space flight system.

1.2 Two Color Holographic Interferometry (TCHI)

TCHI can be used to measure changes in value of two properties of a test sample whose absolute values directly effect the refractive index of the material. A typical configuration in which TCHI can be utilized is shown in **Figure 1.1,** where a test cell is shown containing a solution with one dimensional gradients in both temperature and concentration of some solute in the solution (e.g., TGS in water). Two beams from a collimated wave front of coherent light are shown passing through the test cell. The phase of each of these beams at the detection plane, seen to the right of the test cell, will be a function of the optical path length (OPL) through which each has traveled. This phase is, in practice, a relative measurement. In this project, the phase was measured relative to a wavefront derived from a hologram of the same test cell containing a solution with no temperature or concentration gradients, and therefore no variations in refractive index. The phases of the two beams measured at the detection plane are the phase differences of each, the difference between the wavefront passing through the "live" test cell and that derived from the hologram of the test cell recorded earlier. If the refractive index of the solution during recording

of the hologram was n', the OPLs of the top beam for the live and holographically recorded wavefront over the entire path, s1, are:

$$OPL_{1,live} = \int_{s1} n\, ds = OPL_{outside\ solution} + \int_{solution} n_1\, ds = OPL_{outside\ solution} + L\, n_1\ ,$$

$$OPL_{1,hologram} = \int_{s1} n\, ds = OPL_{outside\ solution} + \int_{solution} n'\, ds = OPL_{outside\ solution} + L\, n',$$

where L is the cell thickness. The relative change in OPL between the live and recorded conditions are,

$$\Delta OPL_1 = OPL_{1,live} - OPL_{1,hologram} = L\,(n_1 - n'). \tag{1.1}$$

This assumes that nothing in the optical path outside the solution is different between the two different cell conditions (i.e., $OPL_{outside\ solution}$ is a constant). Similarly, for the bottom beam,

$$\Delta OPL_2 = OPL_{2,live} - OPL_{2,hologram} = L\,(n_2 - n'). \tag{1.2}$$

The phase, in terms of fringe order, N, is related to OPL by $OPL = N\lambda$. From Equations 1.1 and 1.2, the phase seen at the Detection Plane for each beam is,

$$\Delta N_1 = L\,(n_1 - n')\,/\,\lambda\ , \tag{1.3}$$

$$\Delta N_2 = L\,(n_2 - n')\,/\,\lambda\ . \tag{1.4}$$

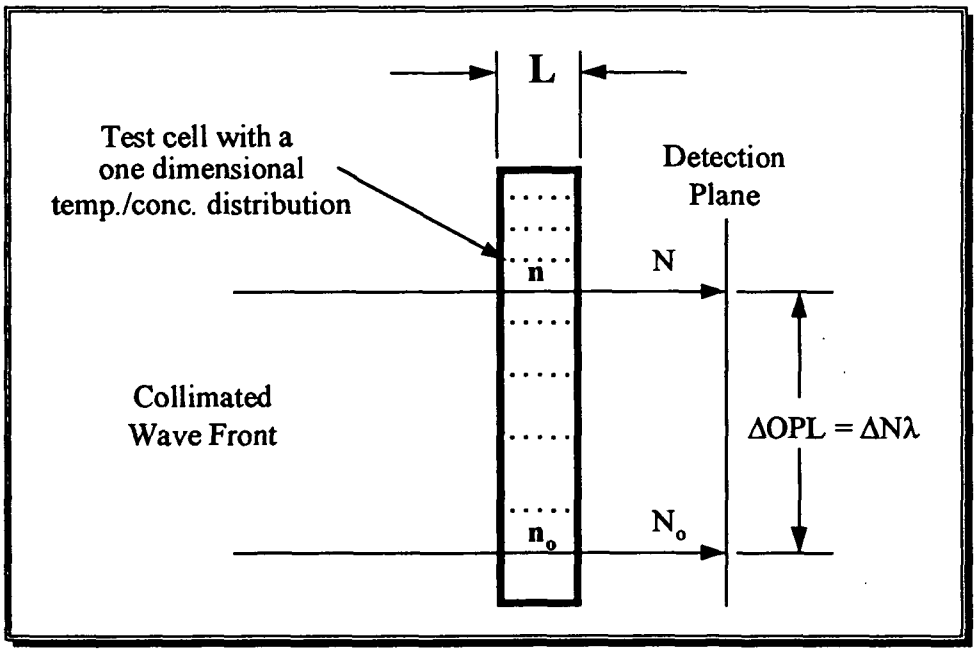

Figure 1.1. Application of TCHI to a test cell with one dimensional temperature and concentration distributions.

If the refractive index n_1 is taken as a reference condition, the refractive index, n_2, in terms of n_1 can be related to changes in temperature and concentration between these two points by the relation,

$$n_2 = n_1 + \left(\frac{\partial n}{\partial c}\right) \Delta c + \left(\frac{\partial n}{\partial T}\right) \Delta T, \tag{1.5}$$

where Δc and ΔT are the changes in concentration and temperature between the two points, $\partial n/\partial c$ and $\partial n/\partial T$ are properties of the solution which depend on the wavelength of the illuminating beam as well as solution temperature and concentration. Combining Equations 1.3 and 1.4 with this relation gives,

$$\frac{\Delta N \lambda}{L} = \left(\frac{\partial n}{\partial c}\right) \Delta c + \left(\frac{\partial n}{\partial T}\right) \Delta T, \tag{1.6}$$

where $\Delta N = \Delta N_2 - \Delta N_1 = L (n_2 - n_1) / \lambda$. Due to dispersion within the solution, $\partial n/\partial c$ and $\partial n/\partial T$ are different at different wavelengths. This relation can be used, therefore, at two different wavelengths to create a set of two independent equations:

$$\frac{\Delta N_j \lambda_j}{L} = \left(\frac{\partial n}{\partial c}\right)_j \Delta c + \left(\frac{\partial n}{\partial T}\right)_j \Delta T, \tag{1.7}$$

$$\frac{\Delta N_k \lambda_k}{L} = \left(\frac{\partial n}{\partial c}\right)_k \Delta c + \left(\frac{\partial n}{\partial T}\right)_k \Delta T, \tag{1.8}$$

where i and j are the two different wavelengths. Since Δc and ΔT are the quantities we are trying to determine, these two equations can be solved for those quantities:

$$\Delta c = \frac{N_j \lambda_j \left(\partial n/\partial T\right)_k - N_k \lambda_k \left(\partial n/\partial T\right)_j}{L\left[\left(\partial n/\partial c\right)_j \left(\partial n/\partial T\right)_k - \left(\partial n/\partial c\right)_k \left(\partial n/\partial T\right)_j\right]}, \tag{1.9}$$

$$\Delta T = \frac{N_j \lambda_j \left(\partial n/\partial c\right)_k - N_k \lambda_k \left(\partial n/\partial c\right)_j}{L\left[\left(\partial n/\partial T\right)_j \left(\partial n/\partial c\right)_k - \left(\partial n/\partial T\right)_k \left(\partial n/\partial c\right)_j\right]}, \tag{1.10}$$

where c and T are the changes in concentration and temperature from the reference condition, L is the width of the test cell, and N is the fringe order.

1.3 Phase Shift Interferometry

The intensity at any point x in an interferogram is a sinusoidal expression,

$$I(x,y) = I_0(x,y)\{1+\gamma(X,Y)Cos[\phi(x,y)+\alpha_i]\}, \quad (1.11)$$

where I is the measured intensity at x and y , I_0 is the background (DC-component) intensity, γ is the contrast of the modulation to I_0, φ is the optical phase, and α is an arbitrary phase that can be chosen. By measuring the intensity in interferograms while varying α, a system of independent equations is generated and subsequently solved for the unknowns, phase being the unknown of primary interest [1,2]. A minimum of three distinct phase shifts are required to obtain a unique solution, but by increasing the number of known phase-shifts, the accuracy of the process can be improved. Phase-shift interferometry has been devised to work for both pulsed and continuous wave laser systems[3]. The significance of this application is that phase-shifts on the order of k /500 are reported, allowing flow field data that are undetectable by other interferometric techniques to be revealed[4].

Phase shift interferometry is a relatively new procedure for improving and analyzing interferometry data. Most phase shift interferometry in use today does not employ holography; however, combining the powers of phase shift interferometry with those of holography lead to an even more powerful capability. This appears to be the first application of phase shift interferometry in a space intended application.

Creath[1] analyzed the errors that often occur in phase shifting interferometry. Tthree-frame, four-frame, and five-frame phase shifting interferometry were described. A single recorded frame of intensity data from an interferogram can be written as:

For the three-frame case where the intensities of interferograms at $\pi/4$, $3\pi/4$, and $5\pi/4$ are recorded, the phase distribution,

$$\phi(x,y) = \tan^{-1}\left[\frac{I_3(x,y)-I_2(x,y)}{I_1(x,y)-I_2(x,y)}\right]. \quad (1.12)$$

The most popular four-frame algorithm uses the intensities of interferograms recorded at 0, π /2, π, and $3\pi/2$, and the phase distribution,

$$\phi(x,y) = \tan^{-1}\left[\frac{I_4(x,y)-I_2(x,y)}{I_1(x,y)-I_3(x,y)}\right]. \quad (1.13)$$

The five-frame algorithm uses intensity data with relative phase shifts of $-\pi$, $-\pi/2$, 0, $\pi/2$, and π. The phase is calculated using

$$\phi(x,y) = \tan^{-1}\left\{\frac{2[I_2(x,y)-I_4(x,y)]}{2I_3(x,y)-I_5(x,y)-I_1(x,y)}\right\}. \quad (1.14)$$

Another method using a four-frame algorithm was first introduced by Carré[3]. This technique assumes an unknown phase shift that is constant from frame to frame, $-3\alpha/2$, $-\alpha/2$, $\alpha/2$, and $3\alpha/2$. The phase distribution of the interferograms is calculated using,

$$\phi(x,y) = \tan^{-1}\left\{\frac{\sqrt{[I_1 - I_4 + I_2 - I_3][3(I_2 - I_3) - (I_1 - I_4)]}}{(I_2 + I_3) - (I_1 + I_4)}\right\}. \quad (1.15)$$

If miscalibration of the phase shifter does happen, the Carré and five-frame algorithms are the least sensitive to miscalibration of the phase shifter. A 10% linear phase shifter error will account for less than 0.2% phase error (waves) by these two methods.

2. TECHNICAL APPROACH

2.1 Technical Issues

The technical issues regarding the use of TCHI in materials processing in space fall into three categories that were treated separately. These are 1) theoretical possibility, 2) experimental possibility and 3) practicality in space. The theory of TCHI is well known. The first question to be answered, therefore, was "Is TCHI sufficiently sensitive, theoretically, to be of use in the desired applications?" This question was answered during the first phase of the project. TCHI was determined to be theoretically applicable if phase shifts in the interferometric measurements could be measured to $\lambda/100$. So the next question to ask is "Can we produce a useful optical system that can perform interferometry over the area of a test cell with this accuracy?" The typical interferometer operates at nearly an order of magnitude less accurate. Finally, if such experimental accuracy is attainable, then the last question is "Is such a measurement possible under the severe weight, volume, power, and other constraints of Spacelab or Space Station operation?'

Therefore, the technical issues were treated in the following separate parallel experimental and theoretical studies:

- **Theoretical**

  A continuing theoretical study to refine the theory based on the experimental results and to search for theoretically optimum parameters and methods. Much of this work was conducted by Dr. Chandra Vikram at the University of Alabama, Huntsville and is reported separately.

- **Laboratory Breadboard**

  A detailed laboratory investigation of TCHI as applied to well known materials to learn the ultimate experimental limitations of TCHI and to develop techniques to advance the technique.

- **Flight Breadboard**

  A laboratory investigation to examine miniaturization techniques that could make the TCHI method applicable in space.

2.2 Assessment and Demonstration of the TCHI Technique (Laboratory Breadboard)

The technical approach included the design and construction of a laboratory breadboard with which to perform experiments to validate the theoretical model, to test the concept, and to develop new procedures that would enhance the TCHI method. A primary objective was to establish the ultimate resolution with which phase shift could be determined using state-of-the-art methods, without regard to the constraints that must be met in space. This allowed us to use mostly existing equipment and well known techniques and hardware. The breadboard employed a large, high stability table, large lasers, and components that would allow us to make measurements with the highest possible accuracy. A series of experiments were performed on this breadboard using two different test solutions. In addition to placing ultimate limits on the TCHI measurement, these experiments provided us with experience in high sensitivity interferometry, allowing us to determine which components were the most critical and which could be simplified. Experience with the laboratory breadboard also provided important design input for a flight breadboard.

2.3 Light Weight, Compact, Fiber Optic-Based Holographic Camera System (Flight Breadboard)

Having proved that TCHI can provide the necessary accuracy and sensitivity to lead to a capability of measuring temperature and concentration in crystal growth experiments, a parallel set of experiments were performed to establish the methods that would allow the measurement to be performed in space. To this end, a flight breadboard was constructed using state-of-the-art procedures to miniaturize the breadboard, and reduce weight and power requirements. Fiber optics were employed to replace beamsplitters, mirrors, and phase shifters. Solid state lasers were used to replace the large HeCd and HeNe lasers used in the laboratory breadboard. The breadboard incorporated much of what had been developed in the laboratory breadboard experiments. Finally, TCHI was performed with simple experiments to determine how the components would react to microgravity.

3. ERROR ANALYSIS

3.1 Sensitivity of TCHI Equation to Errors

The main challenge in the application of the TCHI technique is the extreme sensitivity of the equations for Δc and ΔT to errors in the various parameters involved. The sensitivity of the method to slight errors in the fringe measurements had been the primary concern prior to the current effort; however, in the course of the experimental work done in this program, it was discovered that errors in all the parameters in the TCHI equations could significantly effect the results of the method.

A derivation was done to quantify the effect of errors from each parameter in the TCHI equations in terms of the remaining terms and Δc and ΔT. The validity of the resulting equations were tested against a spreadsheet model of the TCHI equations in which small perturbations could be introduced into any of the parameters to see what effect this had on the resulting calculated values of Δc and ΔT. Good agreement was found in all cases. An exact match was not expected, since the spreadsheet model used a harsher criteria in its definition of error than the one outlined below. Agreement between the two was always a factor of approximately $\sqrt{2}$. Variations from this were attributed to simplifications made during the derivations. This level of agreement is quite acceptable, since quantifying the error in a statistical measurement is somewhat subjective anyway. The purpose here was to obtain a relative feel for the error introduced by slight errors in the TCHI equations.

In deriving the error equations, the starting point was the standard statistical relation,

$$\delta\left(f(x_j,x_k)\right)=\sqrt{\delta\left(x_j\right)\frac{\partial f}{\partial x_j}+\delta\left(x_k\right)\frac{\partial f}{\partial x_k}}, \tag{2.1}$$

where δ is the standard deviation in the measurement a given parameter, x_j and x_k are the parameters in the TCHI equations at the red and blue wavelengths, f is either Δc or ΔT, and $(\partial f / \partial x)$ is the partial derivative of the f (Δc or ΔT) to the parameter whose effect is being studied. This equation assumes that the error in the measurements of x_j and x_k are independent of one another, which is true for all sets of parameters in the TCHI equations. In deriving the equations below it was assumed that $\delta(x_j)$ and $\delta(x_k)$ were equal. In other words, while the error in individual measurements of x_j and x_k are independent, the error on average is assumed to be the same for both. Based on these assumptions and the use of Equation 2.1, the error induced by each parameter was found to be:

$$\%Error\ \Delta c=\left(\%Error\ \frac{dn}{dT}\right)\left(\frac{\sqrt{2}\Delta T}{d\Delta c}\right)\left.\frac{dn}{dT}\right|_{Ave}^{2}, \tag{2.2}$$

$$\%Error\ \Delta c=\left(\%Error\frac{dn}{dc}\right)\left(\frac{\sqrt{2}}{d}\right)\left.\frac{dn}{dT}\right|_{Ave}\left.\frac{dn}{dc}\right|_{Ave}, \tag{2.3}$$

$$\%Error\ \Delta c=\delta(\Delta N)\left(\frac{100\sqrt{2}\ \lambda_{Ave}}{Ld\Delta c}\right)\left.\frac{dn}{dT}\right|_{Ave}, \tag{2.4}$$

$$\%Error\ \Delta c=\delta(\lambda)\left(\frac{100}{d}\right)\left(\frac{\sqrt{\lambda_j^2+\lambda_k^2}}{\lambda_j\lambda_k}\right)\left(\left.\frac{\partial n}{\partial c}\right|_{Ave}+\left.\frac{\partial n}{\partial T}\right|_{Ave}\frac{\Delta T}{\Delta c}\right)\left.\frac{dn}{dT}\right|_{Ave}, \tag{2.5}$$

$$\%\text{Error } \Delta c = \%\text{Error L}, \tag{2.6}$$

$$\%Error\ \Delta T=\left(\%Error\ \frac{dn}{dT}\right)\left(\frac{\sqrt{2}}{d}\right)\left.\frac{dn}{dT}\right|_{Ave}\left.\frac{dn}{dc}\right|_{Ave}, \tag{2.7}$$

$$\%Error\ \Delta T = \left(\%Error\ \frac{dn}{dc}\right)\left(\frac{\sqrt{2}\ \Delta T}{d\Delta c}\right)\left.\frac{dn}{dc}\right|_{Ave}^{2}, \tag{2.8}$$

$$\%Error\ \Delta T = \delta(\Delta N)\left(\frac{100\sqrt{2}\ \lambda_{Ave}}{Ld\Delta T}\right)\left.\frac{dn}{dc}\right|_{Ave}, \tag{2.9}$$

$$\%Error\ \Delta T = \delta(\lambda)\left(\frac{100}{d}\right)\left(\frac{\sqrt{\lambda_j^2+\lambda_k^2}}{\lambda_j\lambda_k}\right)\left(\left.\frac{\partial n}{\partial T}\right|_{Ave}+\left.\frac{\partial n}{\partial c}\right|_{Ave}\frac{\Delta c}{\Delta T}\right)\left.\frac{dn}{dc}\right|_{Ave}, \tag{2.10}$$

$$\%\text{Error } \Delta T = \%\text{Error L}, \tag{2.11}$$

where L is the thickness of the media containing the solution, d is the term $(\partial n/\partial c)_j(\partial n\partial T)_k-(\partial n/\partial c)_k(\partial n/\partial T)_j$ found in the denominator of Equation 2.9, and the Ave subscript refers to the average between the red and blue wavelengths of that parameter. These equations show the percent error in Δc or ΔT in terms of either the magnitude or percent error in the parameter, whichever seems more appropriate for that parameter (e.g., fringe error is typically thought of in terms of parts of a fringe). In these equations,

$$\%\text{Error } x = 100\ \delta(x) / x, \tag{2.12}$$

where x represent any of the parameters in Equations 2.2-2.11.

Several observations can be made for Equations 2.2 - 2.11. First, term d (the term $(\partial n/\partial c)_j(\partial n\partial T)_k-(\partial n/\partial c)_k(\partial n/\partial T)_j$) is found in all the equations. It is dispersion of the material that makes this term other than zero, which in turn is what makes the TCHI technique even possible. Without dispersion $(\partial n/\partial c)_j = (\partial n/\partial c)_k$ and $(\partial n/\partial T)_j = (\partial n\partial T)_k$, since n at any given temperature and concentration would be the same at any wavelength. This in turn would make d equal to zero. The term d can be thought of as a property of the material.

Initially, one is tempted to think of it as a dispersion term; that materials with a higher dispersion would have a correspondingly higher value of d. The physical significance of d, however, is not that simple. The magnitude of d, which is a difference, will grow to the degree that the change of $\partial n/\partial c$ with wavelength is different from the change in $\partial n/\partial T$ with wavelength. If, for example, the relative changes in $\partial n/\partial c$ and $\partial n/\partial T$ with wavelength are the same, the value of d is exactly zero, just as in the case where there is no dispersion, and the TCHI technique would not work for this material.

Since d is always in the denominator of the error equations, the sensitivity of the TCHI technique to errors in the parameters in Equations 1.9 and 1.10 is decreased as d becomes larger, and becomes infinite as d approaches zero. **The success of the TCHI technique depends, to a large extent, therefore, on the value of d for the material of interest. In addition, the value of d will be shown to be very sensitive to temperature and somewhat to concentration. This further suggests that the state of the material in terms of temperature and concentration, may also determine the effectiveness of the TCHI technique for that application.**

Another interesting observation is made by comparing Equations 2.2 and 2.7. In Equation 2.7, the error in ΔT due to inaccuracies in $\partial n/\partial T$ is seen to be independent of ΔT. However, the error in Δc is seen in Equation 2.2 to actually increase in this case as ΔT increases. This implies that if inaccuracies in $\partial n/\partial T$ become significant, the value of ΔT (or more specifically the ratio $\Delta T/\Delta c$) becomes important in determining the limits of practicality of the TCHI technique. Though not as direct, similar observations can be made by comparing Equations 2.1 and 2.6 for the error sensitivity in terms of errors in λ. It will be seen later that error due to inaccuracies in the value of λ are actually very small, so the value of Δc or ΔT are really inconsequential in this case.

Using the relation in Equation 2.12, Equations 2.2 - 2.11 can be put in terms of the absolute error,

$$\delta(\Delta c) = \left(\%Error \frac{\partial n}{\partial T}\right)\left(\frac{\sqrt{2}\Delta T}{100d}\right)\left.\frac{\partial n}{\partial T}\right|^2_{Ave}, \tag{2.13}$$

$$\delta(\Delta c) = \left(\%Error \frac{\partial n}{\partial c}\right)\left(\frac{\sqrt{2}\Delta c}{100d}\right)\left.\frac{\partial n}{\partial T}\right|_{Ave}\left.\frac{\partial n}{\partial c}\right|_{Ave}, \tag{2.14}$$

$$\delta(\Delta c) = \delta(\Delta N)\left(\frac{1}{Ld}\right)\left(\sqrt{\lambda_j^2+\lambda_k^2}\right)\left.\frac{\partial n}{\partial T}\right|_{Ave}, \tag{2.15}$$

$$\delta(\Delta c) = \delta(\lambda)\left(\frac{1}{d}\right)\left(\frac{\sqrt{\lambda_j^2+\lambda_k^2}}{\lambda_j\lambda_k}\right)\left(\left.\frac{\partial n}{\partial c}\right|_{Ave}\Delta c + \left.\frac{\partial n}{\partial T}\right|_{Ave}\Delta T\right)\left.\frac{dn}{dT}\right|_{Ave}, \tag{2.16}$$

$$\delta(\Delta c) = \delta(L)\left(\frac{\Delta c}{L}\right), \tag{2.17}$$

$$\delta(\Delta T) = \left(\%Error \frac{\partial n}{\partial T}\right)\left(\frac{\sqrt{2}\Delta T}{100d}\right)\left.\frac{\partial n}{\partial T}\right|_{Ave}\left.\frac{\partial n}{\partial c}\right|_{Ave}, \tag{2.18}$$

$$\delta(\Delta T) = \left(\%Error \frac{\partial n}{\partial c}\right)\left(\frac{\sqrt{2}\Delta c}{100d}\right)\left.\frac{\partial n}{\partial c}\right|^2_{Ave}, \tag{2.19}$$

$$\delta(\Delta T) = \delta\ (\Delta N)\left(\frac{1}{Ld}\right)\left(\sqrt{\lambda_j^2+\lambda_k^2}\right)\left.\frac{\partial n}{\partial c}\right|_{Ave}, \tag{2.20}$$

$$\delta(\Delta T) = \delta\ (\lambda)\left(\frac{1}{d}\right)\left(\frac{\sqrt{\lambda_j^2+\lambda_k^2}}{\lambda_j\lambda_k}\right)\left(\left.\frac{\partial n}{\partial T}\right|_{Ave}\Delta T + \left.\frac{\partial n}{\partial c}\right|_{Ave}\Delta c\right)\left.\frac{\partial n}{\partial c}\right|_{Ave}, \tag{2.21}$$

$$\delta(\Delta T) = \delta(L)\left(\frac{\Delta T}{L}\right). \tag{2.22}$$

The TCHI demonstration conducted on the laboratory breadboard at MSFC used a salt (NaCl) water solution with an average concentration of around 0.65 g/l and approximately 23°C. Typical

temperature and concentration gradients were approximately 1.35°C and 0.55 g/l, respectively. Under these conditions, the following error sensitivities were found using the above equations.

Table 3.1
Anticipated error in TCHI equations based on uncertainties in the various parameter in those equations.

INPUTS:

Cell Temperature (°C)	22		
Cell Concentration (g/l)	0.65	**ΔT (°C)**	1.35
Cell width (mm)	10	**Δc (g/l)**	0.55

	λ_1	λ_2	Average
Wavelength	0.6328	0.4416	0.5372
dn/dc (g/liter)^-1	2.021E-04	2.199E-04	2.110E-04
dn/dT (1/°C)	-1.369E-04	-1.419E-04	-1.394E-04

Denominator (dndc.j*dndt.k-dndc.k*dndt.j) 1.4281E-09

RESULTS:

		Error		Percent Error	
Param.	**Parameter Error**	**Δc**	**ΔT**	**Δc**	**ΔT**
dn/dT	0.1 %	0.03	-0.04	4.7	-2.9
dn/dc	0.1 %	-0.02	0.02	-2.9	1.8
ΔN	0.01 fringes	-0.08	0.11	-13.7	8.4
L	10 um	0.00	0.00	0.1	0.1
λ	0.05 nm	0.00	0.00	0.2	-0.1
	Total (sqrt. sum of sqrs.)	0.08	0.12	14.8	9.1

From this, it can be seen that the major source of error under these conditions is that introduced by inaccuracies in the phase measurement, ΔN. Variations of only λ/100 introduce errors of 18.5% and 13.7% in the Δc and ΔT measurements, respectively. Error introduced by uncertainty in the values of dn/dc and dn/dT while smaller, are not insignificant. Due to these inaccuracies in dn/dc and dn/dT, improvement in the fringe measurement error, δ(ΔN), beyond approximately a factor of 3 would result in little overall improvement in the measurement of Δc and ΔT. The error introduced by uncertainty in the cell thickness and laser wavelength are seen to be small in comparison to the other parameters evaluated. The total error shown at the bottom of the table is the square root of the sum of the squares of errors introduced by all parameters.

3.2 Change of derivative values over gradient

Since the TCHI equations are so extremely sensitive to slight errors in the partial derivatives, it is important to consider the effect of changes in these partials over the gradients (temperature and concentration) being measured. Since these partials are functions of both temperature and concentration, they will obviously not remain constant over gradients in either parameter. Consider first the effect of changes in $\partial n/\partial T$ due to either temperature or concentration (or for that manner, any other parameter) on Equation 1.9 If the variation at the two wavelengths between the two points in the cell being compared is proportional to the value of $\partial n/\partial T$, then we have

$$\partial n/\partial T_j = m_j * \partial n/\partial T_{j1} ,$$

$$\partial n/\partial T_k = m_k * \partial n/\partial T_{k1} ,$$

where dn/dT_j and dn/dT_k are now considered to the values of these parameter that would produce the correct value of Δc in Equation 1.9, and the subscript 1 refers to the value at one of the two points in the cell over which Δc is being evaluated. If m_j and m_k are equal, which they have been found to be over small variations in T and c, then we have,

$$\partial n/\partial T_j = m * \partial n/\partial T_{j1} ,$$

$$\partial n/\partial T_k = m * \partial n/\partial T_{k1} ,$$

If these values are substituted into Equation 1.9, the m's in the numerator and denominator are seen to cancel and no change in the calculated value of Δc occurs. The implication is that the using the values $\partial n/\partial T_{j1}$ and $\partial n/\partial T_{k1}$ produces no error in the calculation of Δc. Making the same substitution into Equation 1.10 shows that ΔT calculated vs. using $\partial n/\partial T_j$ and $\partial n/\partial T_k$ gives a different answer by a factor of 1/m. For the salt solution and gradients used during the TCHI demonstration, errors of only a few percent would result (i.e., m~1.02 to 1.04). This is small in comparison to other errors.

When the same approach is taken in evaluating the effect of variations of $\partial n/\partial c$ over a gradient, the reciprocal conclusions are made. That is, the factor m cancels out for the ΔT calculation and results in an error of a few percent (1/m) in the calculation of Δc.

Sufficiently precise values of $\partial n/\partial T$ and $\partial n/\partial c$ were found to be extremely difficult to obtain in the literature. For the TCHI demonstration done using the laboratory breadboard, we were essentially forced to obtain these values ourselves experimentally. Because relatively small variations from the assumption $m_j = m_k = m$ can result in large errors when using Equations 1.9 and 1.10 (because the denominators are small in comparison to the individual partials used in their calculation), the exact variations in these parameters over temperature and concentration need to be more fully characterized for the material of interest before a final evaluation of the suitability of TCHI over larger gradients can be made. Generally, the more critical problem will be obtaining

sufficiently accurate answers for very small Δc's and ΔT's. A large gradient can usually be broken into smaller steps as a way of evaluating a larger gradient. The need for accurate characterization of dn/dc and dn/dT is not, however, precluded by this approach, since precise values of these parameters are needed at each step over the larger gradient.

3.3 Experimental Errors

Apart from inaccuracies outlined in the previous sections, other experimental errors were found to effect the measured value of Δc and ΔT. Three corrections were made to data from the TCHI demonstration using the laboratory breadboard before correct values of Δc and ΔT could be obtained. The details of each of these corrections is given here.

In these experiments, errors that are commonly considered negligible in interferometry become important since the required accuracies for TCHI are extremely high. Therefore, we had to address every possible error source, no matter how small.

3.3.1 Phase Correction to Reference Interferogram

As explained in Section 1.2, the interferograms used in the TCHI method are produced by interfering the live (real time) wavefront that passes through the test cell containing the temperature and concentration gradients with a wavefront that has been reconstructed with a hologram of the same test cell with no gradients (i.e., a test cell with either water or solution at a single concentration and with a uniform temperature). Ideally, the only differences in the two wave fronts being interfered are the changes in temperature and concentration. Both wave fronts go through the same test cell, system optics, and the hologram itself.

While this is ideally the comparison, in reality the glass plate upon which the hologram is made must be chemically processed, dried, and placed back into the plate holder for use during recording. Due to factors such as non-uniform shrinkage of the photographic emulsion on the glass plate, minute relative phase variations from those originally recorded occur over the holographic image. For most applications these variations introduce minimal errors. The TCHI technique is, however, sensitive to phase variations of less than $\lambda/100$, so extreme care must be taken to eliminate even these small deviations.

In an attempt to compensate for these errors, a "reference interferogram" was made for each hologram. This interferogram consisted of the hologram compared to the live cell under the same conditions used to make the hologram (i.e., no temperature or concentration gradients). If no errors were introduced between recording and playback of the hologram, this interferogram would contain a constant phase over the entire field of view since the phase information in both images would be exactly equal. The phase errors that in actuality did occur resulted in slight phase variations across the image. The phase variations contained in this interferogram were subtracted from subsequent interferograms made containing temperature and/or concentration gradients, thereby correcting for the phase variations introduced by processing, etc.

Other possible approaches to eliminate such errors include recording the hologram in a "liquid gate". While the method is straightforward, it is not easily adapted to space application, so it was not used.

3.3.2 Correction of Hologram Tilt

Similar to the phase error introduced by processing, failure to return the holographic plate to exactly the same position it had when it was recorded produces interferometric fringes as a result of a slight phase mismatch between the live and recorded images. Unlike the previous phase error, however, alignment mismatch usually results in a very systematic set of fringes. For instance, if the hologram is tilted about a horizontal axis, it will produce a set of straight, horizontal fringes whose spacing will decrease as the amount of tilt increases. Micrometers are used to adjust the position of the plate so as to minimize the amount of mismatch; however, some mismatch is always present and the amount usually changes with time due to factors such as temperature changes and mechanical relaxation of breadboard components.

If this tilt error were static, the method used in the previous method would correct for these deviations as well as those introduced by non-uniform emulsion shrinkage, etc. Temperature and mechanical effects, however, make this error a dynamic process that must be dealt with at the moment the interferogram is recorded. This was accomplished in the current work by designing the experiment so that the field of view contained vertical air gaps to either side of the test cell (c.f., **Figure 4.1**). These air gaps represent a reference area whose phase should remain constant, regardless of the cell condition during the experiment. Tilt correction is achieved by matching the phase variation along the two air gaps of the interferogram under evaluation with air gaps in the reference interferogram. Ideally, the phase variation along the air gap should be zero in the reference interferogram. In practice, however, a condition of "zero" fringes in the test cell of the reference interferogram corresponded to some small amount of phase variation in the vertical direction along the air gaps (usually much less than one fringe). It was this slight phase variation along the air gap that was matched in subsequent interferograms containing gradients in the test cell.

3.3.3 Correction of Magnification Differences Due to Chromatic Aberrations

Once an interferogram containing some test condition is corrected for phase errors, as outlined in the previous sections, differences in magnification of the test cell between the two different colors also had to be made. This difference was minimized through the use of achromatic lenses; however, the very precise phase measurements involved made what typically would be negligible errors important if correct results were to be obtained. A magnification difference of about 3.5 pixels in the vertical direction was noted between the 441.6 nm and 632.8 nm laser light sources. The effect this had on any particular phase measurement depended on the local slope of the gradient where the measurement was being made. Since the change in magnification had the effect of shifting the location of the phase measurement, no error would result if gradients were essentially zero at the location of the phase measurement. This normally turned out to be the case for concentration gradients, since attempts were made during experimentation to keep the top and bottom of the cell at fixed concentrations, while allowing the gradient to be steep in the center.

In the case of temperature gradients, however, the slope was constant from top to bottom, and magnification differences became important.

4. EXPERIMENTAL PROGRAM WITH LABORATORY BREADBOARD

A series of experiments was conducted at the Space Processing Optical Laboratory at NASA Marshall Space Flight Center to demonstrate the TCHI technique. A description of the breadboard, a history of the experiments performed, and the new procedures that were developed is given in the following sections.

4.1 Breadboard Description

A diagram of the TCHI laboratory breadboard is shown in **Figure 3.1**. To minimize vibration problems, the system was constructed on a vibrationally isolated granite table and individual components were damped by pressing modeler's clay around all bases. The room air currents were mitigated with a Plexiglas housing that covered all of the optics. Light for the two colors was provided by a HeNe laser (λ = 632.8 nm) and HeCd laser (λ = 441.6 nm). These lasers were selected from those already available at MSFC in order to maximize the amount of dispersion for the TCHI demonstration.

The beams from the two lasers were combined using a cube beamsplitter, BS1, and split into reference and object beams with BS2 which was a variable beam splitter. Each beam (now a combination of both colors) was spatially filtered and collimated. The object beam passed through a specially built test chamber designed to allow a high degree of control over the temperature and concentration gradients produced in the test cell contained within. After the hologram was made, the interferograms were formed by combining light passing through the test section (object beam) with the reconstructed image of the test cell (using the reference beam). This light passed through a reimaging lens and was recorded by a video camera.

The resulting experimental apparatus is an extremely versatile and sensitive holographic interferometry test laboratory that can be used for a wide range of experiments and measurements. Fringe movements of considerably less than $\lambda/200$ are observable and quantitative measurements of phase changes of less than $\lambda/100$ are measurable. The system is so sensitive that it was ultimately limited by acoustical phenomena. We could observe fringe motion by an airplane passing overhead, or even by rattling paper on the opposite side of the room. Consequently, many of our best experiments were performed after normal work hours.

The details of these components, the test solution used for the TCHI demonstration, and the software developed to record and analyze the interferograms is described below.

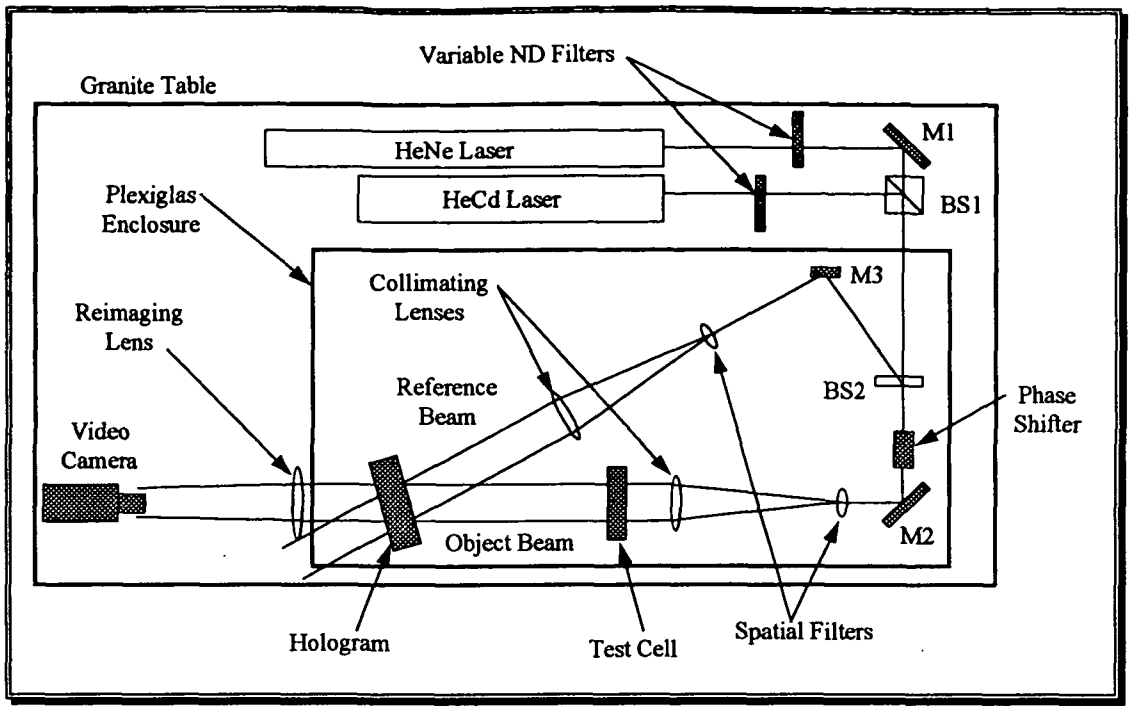

Figure 3.1. Experimental Setup for Two Color Holographic Interferometry.

The phase shifter used during earlier experimentation was a glass slide mounted to a rotation stage. By mounting the slide near normal incidence and by choosing a thin slide, a compromise between sensitivity and linearity was obtained. With this system we could easily determine the smallest measurable phase shift. The main problem with this arrangement was that it was relatively slow for producing the four phase shifted interferograms. The extremely high sensitivity that we sought was limited by temperature changes in the room as well as acoustics, so performing all phase shifts in the least possible time was important. In later experimentation we replaced the glass slide with a piezoelectric phase shifter made by New Focus, Inc. that allowed much faster response time and easy computer interface.

4.2 Test Chamber

A major part of the breadboard design was the design, construction, and implementation of a test chamber that would allow precise control of the temperature and concentration gradients to be set up in the test cell. The design of this chamber was tailored to support the following experimental test:

1. A solution with an optical path distance of approximately 1 centimeter having constant (in space and time), known, and adjustable temperature and concentration with the ability to change concentration and temperature of the solution.

2. A solution with an optical path distance of approximately 1 centimeter with constant temperature (in space and time) and a known concentration gradient.

3. A solution with an optical path distance of approximately 1 centimeter with constant (in space and time) concentration distribution and a known temperature gradient.

The ranges and accuracy of temperature and concentration had to be representative of typical space crystal growth conditions.

A schematic of the test chamber developed to experimentally evaluate the use of two color holography to simultaneously measure both temperature and concentration gradients is shown in **Figure 3.2**. The test liquid was contained in a quartz cell in the center of the chamber. The test cell, shown in **Figure 3.3**, consisted of quartz faces on four sides and the bottom with the top being capped by an aluminum cap. To control the temperature of the test liquid, or to introduce a temperature gradient, thermo-electrics were located above and below the quartz cell. The top set of thermo-electrics were attached to an aluminum block that was in direct contact with the test liquid via the open top of the quartz cell. The bottom thermo-electrics were attached to a copper block upon which the cell sat. A thin layer of mineral oil was placed between the copper block and the quartz cell to assure good thermal contact.

The quartz cell and thermo-electrics were mounted inside a copper enclosure with thick side walls and two open faces to allow optical access to the test liquid. This enclosure acted as a heat sink and due to the high thermal conductivity of the copper, tended to maintain an even temperature distribution throughout. To insulate the copper enclosure from any ambient temperature variations, it was contained inside a second enclosure made of polypropylene. Glass windows were placed on the front and rear faces of the outer enclosure to permit optical access and insulate the inner cell with an air layer. The copper enclosure sat on the polypropylene enclosure and was secured by contact at the top corners. An air gap between the two enclosures acted to further insulate the copper enclosure from outside ambient conditions.

An access port in the top of the outside enclosure allowed an elongated fixture containing four thermocouples, mounted at different vertical positions, to be placed into the test liquid. This was to allow the temperature of the test fluid to be monitored at different locations throughout the test cell. In this way, any induced temperature gradients could be measured directly to confirm the holographic results. (Ultimatjely, they were not used because they interfered with the temperature gradient itself.) The monitoring of these thermocouples, along with the operation of the two sets of thermo-electrics, was under computer control using software developed at MetroLaser for this project. Layers of different solute concentrations could be introduced using a pipette via the same access port.

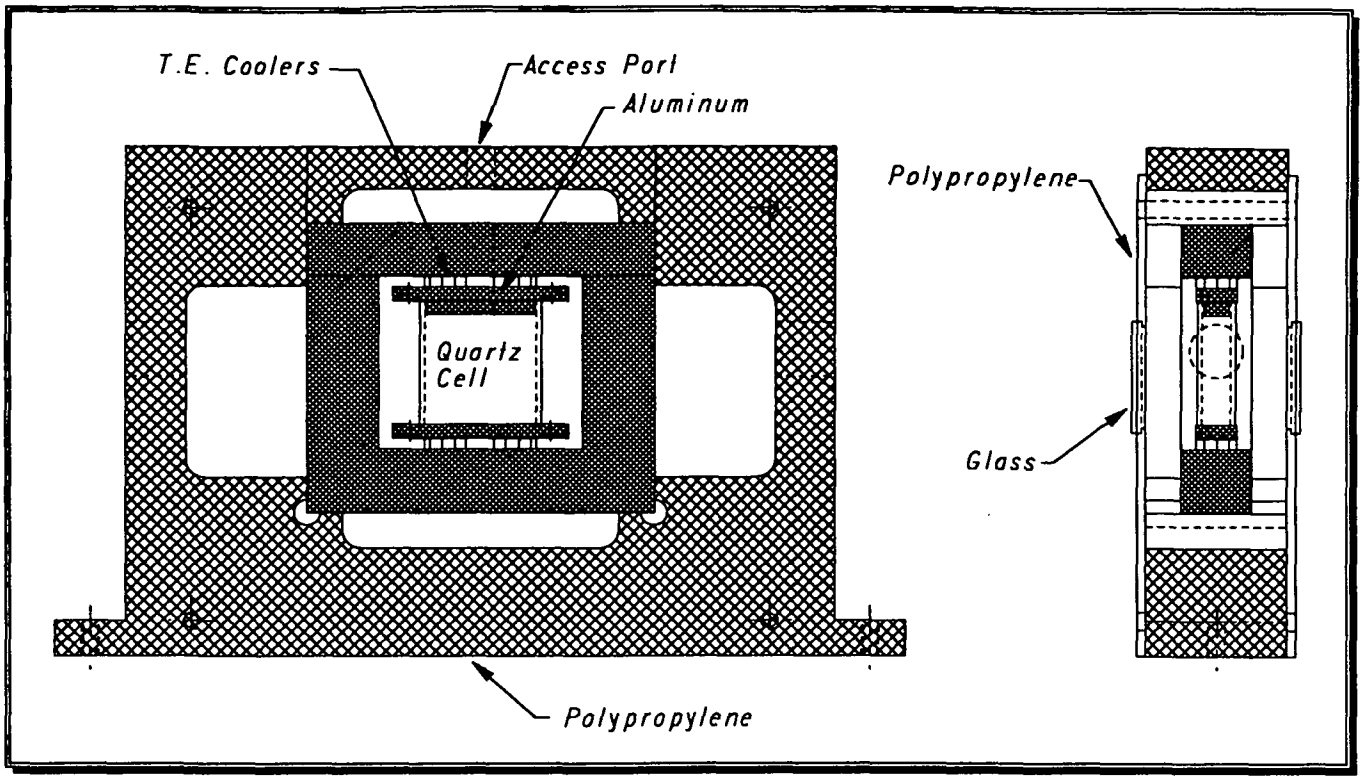

Figure 3.2 Test chamber developed to confirm the two color holography technique experimentally. The chamber consisted of the inner quartz cell, thermo-electrics, and two enclosures (made of copper and polypropylene).

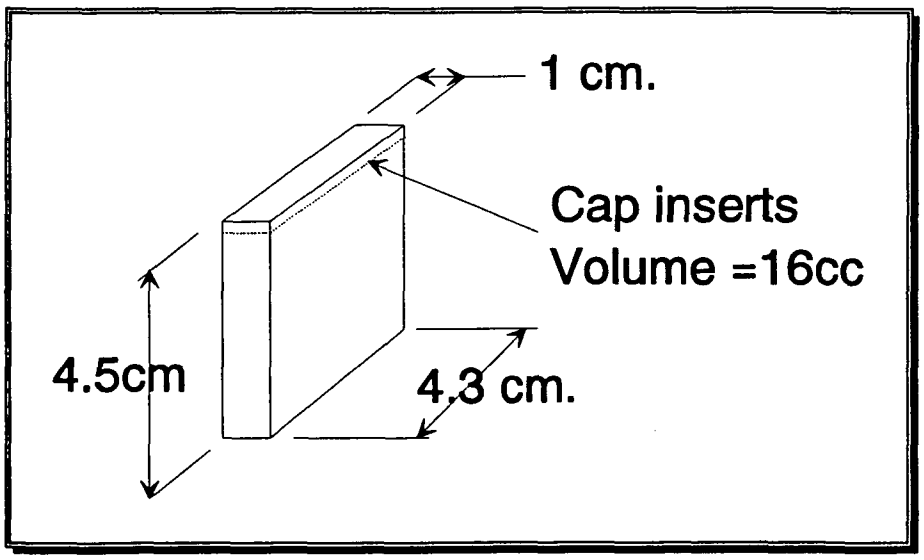

Figure 3.3. Quartz Test Cell Geometry

Two types of cell temperature control were possible with the cell: water bath and thermoelectric. The advantage of thermoelectric coolers/heaters were that: 1) they contained no moving parts and

therefore introduced no vibrations into the system, and 2) were small, lightweight and responded quickly to current inputs. The main disadvantage to this system was that it had large thermal expansion coefficients and had to be mechanically decoupled from the test cell. Constant temperature water baths that may be used to cool or heat the cell are commercially available; however, the circulating water would introduce vibrations that could upset the holographic measurements. Additionally, the degree of accuracy required in both the control and monitoring of the test solution temperature (0.1°C) present a challenge for both methods of temperature control. Ultimately, the thermoelectrics proved to provide very stable temperature gradients, so use of the water bath never became necessary.

The first set of experiments used a diode detector and a pinhole to demonstrate that the required fringe accuracy could be obtained with the breadboard system. Soon afterwards the diode detector was replaced with a video camera whose output was sent to a recorder. There was a considerable amount of electrical noise on the video signal after it was digitized at MetroLaser due to the fact that the data went through seven devices (cameras, video recorders, etc.) and each device added noise. This noise was reduced considerably by directly digitizing the camera output. Several frames were collected and averaged to further reduce noise. The amount of noise reduction was found to not be reduced as much as had been hoped (presumably by the square root of the number of frames taken at a particular phase). This indicated that the noise was in the optical system itself and not electronic. This was confirmed by the fact that two phase maps made close together in time exhibited very similar noise structure as one traversed the cell.

4.3 Control Software

Control software for the TCHI experiment that digitized multiple frames of interferograms at five different phases and at two wavelengths, produced phase maps, and saved all images to computer disk was developed by Bill Witherow at MSFC. This allowed the required interferograms to be obtained within seconds, minimizing phase noise due to air currents or other time fluctuations of phase.

4.4 Analysis Software

A number of DOS utilities were written at MetroLaser to aid in viewing and analyzing the images made using the laboratory breadboard.

4.4.1 File Format

The input image files and the output image files described an image that was 512 pixels wide by 480 pixels high and with 8 bits, a value of 0 to 255 of gray scale. The format of the files required by the programs or produced by them was the following:

The first four bytes describe the width and height and had to be 00h, 02h, E0h, and 01h.

The next 245,760 bytes described the image intensity from the upper left hand corner to the lower right. They were written as consecutive horizontal lines. Each pixel was one byte long and was interpreted as a value from 0 to 255.

The output from the phase unwrapping program was to add a 4 byte footer to the end of the file. The footer was a four byte floating point number with the value of the full scale OPD, or in other words, the points with values of 255 had the footer as their OPD.

4.4.2 Programs

Programs to analyze the data, **phase.exe** and **unwrap.exe**, display the data, **display.exe**, **xsec.exe** and **y.exe**, and to transfer the data **tif.exe**, **dt2dip**, and **3dcon.exe** are described below.

display.exe

"display.exe" displays a 512 pixel x 480 pixel x 8 bit image on the computer VGA monitor at a resolution of 512 pixels x 480 pixels x 4 bits. The gray scale is reduced due to limitations of the VGA display. The program is entered from the DOS prompt by:

display [*source*]

source is the file name with no extension. ".img" is the assumed extension. If source is not given the user will be prompted for it. After examination of the image, a new image name followed by the "Enter" key, "↵", can be typed and it will be displayed. If just the "↵" is pressed, the program exits to DOS.

Example:

C:\>**display abc**

Image abc.img is displayed on the computer's VGA screen.

If a new file name is entered and "*" followed by the enter key is inputted, the screen will toggle between a monochrome and pseudo color display.

phase.exe

This program solves the set of simultaneous equations using a four frame algorithm. It requires that the phase steps be equal in size but not necessarily known. It displays the first of the four images used as input data. Then it calculates the phase step with statistics. These statistics are the standard deviation of the phase step, the number of pixels used to calculate the phase step, the number of pixels with too low of modulation to use for the calculation, and cases of round-off errors causing a divide by zero or taking a cosine of a number greater than one. Finally it calculates the phase map, writes it to a file and displays it on the VGA monitor. The program is entered from the DOS prompt by:

phase *source destination* [*nd*]

The *source* is the root name of the phase stepped frames. It may have up to 7 characters. These data files have names ending in 1, 2, 3, and 4 corresponding to the phase step and an extension of ".img". If the root name of the files is abcdefg, the names of the files will be abcdefg1.img, abcdefg2.img, abcdefg3.img, and abcdefg4.img. The *destination* is the file name for the output phase mapped data without its extension. The extension will be ".img". The source and destination are required. *nd* is optional and will suppress the display of the images. This will speed up the analysis.

Examples:

C:\>phase abcdefg output

This will take data from abcdefg1.img, abcdefg2.img, abcdefg3.img, and abcdefg4.img. do all the calculations, display the data, and store it in output.img. Hit the "Enter" key, ↵, to return to DOS.

C:\>phase abcdefg output nd

This will do the same as the above but with no displays. After execution, the program will return to DOS.

tif.exe

This program creates a tiff file from an image file. The tiff file is a common image format and can be imported into many programs used for word processing and graphics. The program is entered from the DOS prompt by:

tif *source*

source is the file name of the image to be converted without its extension. ".img" is the assumed extension. The program produces a tiff file with the same name but with an extension of ".tif".

Example:

C:\>tif abc

The tiff file abc.tif is created from the image file abc.img.

1. nh2dip

This program creates a Dipix format image file from an image file with no header. The Dipix format is the format used by display.exe, phase.exe, tif.exe, unwrap.exe, xsec.exe, and 3dcon.exe.

It is assumed that the image is 512 pixels wide by 480 pixels high. The program is entered from the DOS prompt by:

nh2dip ***source destination***

source is the file name of the image to be converted with its extension. The program produces a Dipix format image file with ***destination*** as its name.

Example:

C:\>**nh2dip abs.img cde.img**

The file with no header, abc.tif, is converted to the file cde.img with the Dipix header.

it2dip

This program creates a Dipix format image file from an image file with an Imaging Technology header. The Dipix format is the format used by display.exe, phase.exe, tif.exe, unwrap.exe, xsec.exe, and 3dcon.exe. It is assumed that the image is 512 pixels wide by 480 pixels high. The program checks for "IM" at the beginning of the Imaging Technology file and that the image is 512 pixels wide by 480 pixels high. The program is entered from the DOS prompt by:

it2dip ***source destination***

source is the file name of the image to be converted with its extension. The program produces a Dipix format image file with ***destination*** as its name.

Example:

C:\>**it2dip abs.img cde.img**

The file with an Imaging Technology header, abc.tif, is converted to the file cde.img with the Dipix header.

2. dt2dip

This program creates a Dipix format image file from an image file with an Data Translation header. The Dipix format is the format used by display.exe, phase.exe, tif.exe, unwrap.exe, xsec.exe, and 3dcon.exe. It is assumed that the image is 512 pixels wide by 480 pixels high. The program checks for "DT-IMAGE" at the beginning of the Imaging Technology file and that the image is 512 pixels wide. The program is entered from the DOS prompt by:

dt2dip ***source destination***

source is the file name of the image to be converted with its extension. The program produces a Dipix format image file with ***destination*** as its name.

Example:

C:\>it2dip abs.img cde.img

The file with an Data Translation header, abc.tif, is converted to the file cde.img with the Dipix header.

xsec.exe

This program displays a 512 pixel x 480 pixel x 8 bit image at a resolution of 128 pixels x 120 pixels x 4 bits and displays a horizontal or vertical cross section. The cross sections may be moved one line at a time by the use of the arrow keys or eight lines at a time by use of the Num Lock arrow keys. The cross sectional lines are displayed over the image for reference. "5" toggles between a black and white display or a pseudo color display. It displays the x and y cross sectional position and the value of that pixel. If the footer generated from unwrap.exe is present, it incorporates the scale factor and also displays the OPD. The cross sections may be saved to an HPGL file with the extension ".hgl" by entering "f" for file. The user is prompted for a file name (with no extension). The program is entered from the DOS prompt by:

xsec ***source***

source is the image to be examined with no extension. ".img" is the assumed extension. If no source is given, the user is prompted for one. To examine a new image, press the "Enter "key, "↵". The user is prompted for a new name followed by a "↵". If just a "↵" is entered, the program is exited.

Example:

C:\>xsec abc

Image abc.img is displayed with cross sections.

y.exe

This program displays a 512 pixel x 480 pixel x 8 bit image at a resolution of 256 pixels x 240 pixels x 4 bits and displays both horizontal and vertical cross sections. The cross sections may be moved one line at a time by the use of the arrow keys or eight lines at a time by use of the Num Lock arrow keys. The cross sectional lines are displayed over the image for reference. "5" toggles between a black and white display or a pseudo color display. It displays the x and y cross sectional position and the value of that pixel. The full screen may be saved to a monochrome

"Tiff" file with extension ".tif" by entering "f" for file. The user is prompted for a file name (with no extension). The program is entered from the DOS prompt by:

xsec ***source***

source is the image to be examined with no extension. ".img" is the assumed extension. If no source is given, the user is prompted for one. To examine a new image press the "Enter "key, "↵". The user is prompted for a new name followed by a "↵". If just a "↵" is entered, the program is exited.

Example:

C:\>y abc

Image abc.img is displayed with cross sections.

3dcon.exe

This program converts a 512 pixel x 480 pixel image (.img) file to a 64 x 60 data (.txt) file for import to EXCEL or other spreadsheet programs primarily for 3D plotting. If the image file has scale, the scale is incorporated. The ".txt" file uses commas to separate x values and <CR> to separate lines of data. When inputted into a spreadsheet, the horizontal lines of cells correspond to a horizontal image line and the columns to a vertical image line. Each spreadsheet cell is the average of a 8 x 8 pixel kernel of the image. The program is entered from the DOS prompt by:

3dcon ***source***

source is the input image file with no extension . ".img" is the assumed extension. The output file will have the same name as the input file but with extension of ".txt".

Example:

C:\>3dcon abc

The text file abc.txt is created from image file abc.img.

4.5 History of Experiments

A series of seven experiments were performed at MSFC using the laboratory breadboard. Significant events from each of these is reported in this section.

4.5.1 First Series

In the first series of experiments, most of the effort was spent in dealing with problems of optimizing the recording of two wavelengths on a single hologram and producing interferograms with high contrast. During these experiments, we also fully realized the importance of vibration

isolation, air currents, acoustical phenomena and temperature variations. Many such effects that are normally negligible made themselves quite obvious when we pushed the measurements to high sensitivity.

4.5.2 Second Series

During the second series, most of the operational problems were solved, but much of the effort was devoted to technique refinement and development. The required sensitivity was clearly available. Two color holographic interferograms were produced with concentration and temperature variations, but the quality of the data was still far from what was needed to produce acceptable results.

4.5.3 Third Series

During this experiment series, we selected temperature changes from the following:

$dn/dt = 10^{-4}/^{0}C$ which produces

1. 6 fringes/^{0}C for HeNe.
2. 2.26 fringes/^{0}C for HeCd.

We found that the phase shifter had the following calibration:

The number of steps of the stepper motor driving the phase shift wedge for a 360 degrees phase shift was:

= 30,000 for blue
= 43,000 for red.

We ran approximately thirty experiments to include constant T and C at various values, then to include gradients in T and C. During this experimental series we became familiar with the operating characteristics of the cell. We experimented with methods to induce temperature and concentration gradients into the solution. The cell temperature was increased by raising the temperature of the top and bottom, independently, with gradients being introduced by observing before equilibrium was reached or by setting the top and bottom of the cell to different temperatures.

The following table provides the experiment values that correspond to the tapes that were produced. Each experiment recorded on tape includes five interferograms of the condition with an equal phase difference being introduced in each one.

Exp No	Condition	Top T	Bott T	Notes
1	Const T & C	22.01	22.13	Pure Water
2	Temp. Grad.	22.31	22.43	delta of .3 C
3	20 min. later			const. T
4	Raise T .3 C	22.60	22.71	t=10:40
5		22.90	23.00	10:59
6	Temp. Grad.	22.90	22.7	11:25
7	Fill cell to top	22.89	22.69	11:51
8		22.71	22.70	13:44
9	1/5000 sucrose			sucrose on bottom
10	stirred			
11	4/10000			
12				14:24
13	+3 to top and bot	23.00	23.00	
14		23.30	23.30	14:40
15		23.60	23.60	
16		23.3	23.3	
17	6/10000 sucrose	23.3	24.6	
18	4/10000 sucrose	22.74	22.98	Next day 13:05
19	6/10000 sucrose			
20	Const C 3/10000	23.75	24.02	Stir 14:02 data 14:12
21	Bad data			
22	Bad data			
23	Clean cell			Pure water
24	1/500 sucrose	23.10	23.21	
25		23.09	23.21	
26		24.07	23.21	T drops to 23.8 in meas.17:31
27		23.65	23.21	
28		25.07	23.21	18:12 Heaters shut off
29				13:25
30		24.02	23.30	13:32 dropped .3 during meas.
31		24.02	22.30	Faster stepping 14:04

From the constant T and C experiments we can determine the values of dn/dT and dn/dC required to solve the equations for T and C after we determine the refractive index.

4.5.4 Fourth Series

Our objective during this series was to take the highest quality data possible and to add a combined temperature and concentration gradient. The following table provides the conditions for the experiment series.

Exp No	Condition	Top T	Bott T	Notes
1				
2	1/1000	21.32	21.26	Constant C
3		21.82	21.72	
4		21.32	21.26	
5	1/500 suc.rep.2cc	21.32	21.26	
		21.51	21.43	
6	1/500 suc rep 2cc	22.51	22.43	next day
5b				Cleaned windows
6b				
6c	Repeat cond. 6			Rem/ret cell
7a	Pure water			Ref. wave generator
7b	dup 7a			
8	Conc. grad. Const T	21.26	50.72	mix with 7a,Top T faulty
9	Same as 8			Hol 8

We learned by experience that we cannot add water taken from a different room without adding a T gradient that delays the experiment. Enough data had been reduced to lead to the following conclusions.

1. To achieve the highest possible sensitivity requires that fewer steps must be used to produce the interferogram that is ultimately analyzed.

2. The required sensitivity to extract temperature and concentration for the interferograms is achievable.

3. Optical noise in the images limits overall accuracy of the data. Procedures are needed to reduce some of the noise effects.

4. The blue image is approximately 10% smaller than the red image, a result for which we have

no concrete explanation.

4.5.5 Fifth Series

The objective of this series of experiments was to improve the quality of the data taken using the MSFC breadboard by directly digitizing the images of the interferograms produced between a hologram and the live cell. In addition to this objective, this experimental series was also used to begin development of an automated data collection system which incorporated the ability of the Data Translation frame grabber to store multiple frames.

Analysis of the interferograms revealed that the interferometric breadboard at MSFC was not well suited to obtain sufficiently accurate values of the partials used in the two color holography equations. It was also observed that the variation of ΔT between the top and bottom of the cell was approximately 2.5%, while the variation in ΔT was even larger by about 6%. Because of these factors, it could not be determined if the two-color holography method worked for the resulting errors in the phase measurements.

In reviewing the results from the fifth test series, it became evident that two improvements would have to be made before satisfactory results could be obtained for the two color holography demonstration. From previous analysis, it had been demonstrated that the current breadboard at MSFC could be used to determine the phase in the test liquid to within about $\lambda/50$. While this approached the desired result, an accuracy of at least $\lambda/100$ was preferable.

The second area of needed improvement for the two color demonstration was the accurate determination of the derivatives used in the two color equation. While the data could be made to fit the conditions in the test cell, relatively large corrections in the values of these derivatives had to be made to accomplish this. To really demonstrate the technique, better values for these derivatives needed to be found. Three possible methods of increasing the accuracy were discussed. The first was to measure the values in the current setup at MSFC, similar to what was done before, but to increase the accuracy in the fringe measurement. The second method was to adapt a refractometer at MSFC to measure refractive index at the two desired wavelengths. The last method discussed was to use another material which was better characterized than the sucrose solution previously used. A gel is currently being evaluated at MSFC as a possible candidate as a replacement for sucrose.

4.5.6 Sixth Series

Using the newly obtained data for salt solutions, a similar series of experiments were conducted using a 0.13% salt solution similar to those previously run using sucrose solutions. The following procedure was used to obtain TCHI interferograms.

1. Make a hologram of the test cell filled with pure water.
2. Make five, phase-shifted reference interferograms using the wavefront reconstructed from the hologram and the live cell with pure water.

3. Introduce a concentration gradient into test cell using a 0.1% salt solution.
4. Make five phase-shifted interferograms of the concentration gradient.
5. Introduce a temperature gradient of approximately 2°C by setting the upper and lower thermoelectrics to 1.5°C above and below ambient, respectively.
6. Make five phase-shifted interferograms of the temperature and concentration gradients (TCHI demonstration).
7. Turn off the thermoelectrics and allow cell temperature to equalize.
8. Make a second set of phase-shifted interferograms of the remaining concentration gradient.
9. Reintroduce the temperature gradient as in (5).
10. Make a hologram of both the temperature and concentration gradients.
11. Turn off thermoelectrics.
12. Make phase-shifted interferograms of the live cell (concentration gradient only) with the hologram containing both temperature and concentration gradients.
13. Fill test cell with pure water.
14. Make phase-shifted interferograms of the live cell (no gradients) with the hologram containing both temperature and concentration gradients.

The complete test procedure was performed the next day and both sets of data are currently being reduced. The interferogram in (12) was used to determine the temperature gradient that existed in the test cell during the TCHI demonstration.

While the resulting data may be usable, improvements in the system for the seventh series produced better interferograms and this data is what has been presented in this report.

4.5.7 Seventh Series

The experimental series was performed to demonstrate end-to-end, from hologram recording through two-dimensional image processing and data analysis, the TCHI concept as applied to a known temperature and concentration distribution. To date, the concept has been demonstrated only on individual critical steps in the procedure and not on the entire integrated process.
Before beginning experimentation, the path match and polarization of the reference and object beams were examined in an attempt to improve the interferogram quality over those made in previous experiments. The polarization was found to be quite adequate for holography, with the extinction ratio at the hologram plane being around 60:1 for both reference and object beams and for both the HeNe and HeCd lasers. The extinction ratios for each were closer to 1000:1 at the lasers.

Path matching between the reference and object beams was found to be off by several inches. The reference beam was lengthened and the path match between it and the object beam was determined by maximizing the fringe contrast between a hologram of the test cell and the live cell.

The diffraction efficiency of the blue holograms were significantly improved. As a result of this adjustment, the accuracy of the phase change measurement between the top and bottom of the test cell was increased for both colors by about a factor of two to approximately $\lambda/100$.

Characterization of the reference and temperature gradient interferograms over time was also accomplished during the seventh experimental series. The objective was to test the stability and repeatability of the setup and, in the case of the temperature gradient, to characterize the temperature distribution over the cell produced by the thermoelectrics. The temperature gradient was evaluated by utilizing the relation,

$$\Delta T = \lambda / [\text{cell length} * dn/dT(\lambda, c, T)].$$

This equation was used to determine ΔT using the HeNe interferogram fringes, since precise data was available for dn/dT at the 632.8 nm wavelength. The value of dn/dT at 441.6 nm was also determined using this equation, since ΔT was already known from the phase change measurement at 632.8 nm. A similar approach was used to deduce the values of Δc and dn/dc in the test cell that contained only a concentration gradient.

The front and rear windows of the test enclosure were removed during experimentation in an attempt to eliminate the horizontal fringes that developed in the air gaps to either side of the test cell during previous experiments. Their removal did not change the formation of these fringes over time. The absence of these windows also did not result in any apparent increased convective effect, so they were never reinstalled since their absence meant less sources of potential aberrations or retroreflections. The formation of fringes in the air gaps was later determined to be a very linear phenomena over time that was probably due to relaxation of some component in the breadboard, the hologram holder being the most likely source.

Table 4.1 gives a time line of the events, holograms, and interferograms produced during this series. Each hologram and interferogram listed gives all related data including room temperature, cell temperature (top and bottom), salt concentration, and gradient conditions. Interferogram names ("Interf. Name") are designated as follows:

First Character:	Hologram number.
Second Character:	Cell condition when interferogram was made (R-reference, C-concentration gradient, T-temperature gradient, B-both temperature and concentration gradients).
Third Character:	Number to distinguish between different interferograms made with the same hologram and gradient condition.

Table 4.1.

Time line of interferograms made during the seventh experimental series at MSFC.

		Temperatures				Holo.	Interf.	Live Cell		
Date	Time	Top	Bottom	Room	Conc.	#	Name	Delta T	Delta C	Comments
		°C	deg C	deg C	g/liter			deg C	g/liter	
26-Oct					**0.00**	**4**		**0.00**	**0.00**	Front and rear windows on test chamber
					0.00		4R1	0.00		
27-Oct					**0.00**	**5**		**0.00**	**0.00**	Front and rear windows removed from test chamber
					0.00		5R1	0.00		
					0.00		5R2	0.00		
	13:00	22.60	22.60	22.60	0.00		5R3	0.00		
	14:40	23.96	23.96	23.96	0.00		5R4	0.00		
	17:10	23.95	23.95	23.95	0.00		5R5	0.00		
	17:40	**25.5**	**22.5**							***TEs on***
	19:05	25.47	22.54	24.50	0.00		5T1	2.93		
	19:08	25.48	22.54	24.50	0.00		5T2	2.94		Changed DC offset to 5.65 (from 5.05)
	20:15	25.48	22.57	24.67	0.00		5T3	2.91		Reset DC offset to 5.05
	20:20	**26.3**	**23.3**							***Inc. top/bottom TEs by 0.8°C***
	21:05	26.26	23.33	24.70	0.00		5T4	2.93		
	21:40	24.66	24.66	24.66	0.00		5R6	0.00		***TEs off at ~9:10??***
		24.66	24.66	24.66	0.00		5R7	0.00		Adjusted lab jack to return to infinite fringe
28-Oct	08:45	23.14	23.14	23.14	0.00			0.00		Approximately one fringe at 4416 nm
	12:00				**0.00**	**6**		**0.00**	**0.00**	Time is only approximate
	13:30	24.26	24.26	24.26	0.00		6R1	0.00		
	13:50	24.34	24.34	24.34	0.00		6R2	0.00		
	14:15	24.40	24.40	24.40	0.00		6R3	0.00		
	14:30				?					Add concentration gradient (SUCROSE!!!)
	14:50				?		6C1	0.00		
	16:25	23.76	23.76	23.76	?		6C2	0.00		
29-Oct	11:20	19.90	19.90	19.90	0.00	**B**		0.00		
	11:50	20.12	20.12	20.12	0.00		BR1	0.00		
	12:07	20.22	20.22	20.22	0.00		BR2	0.00		
	12:22	20.28	20.28	20.28	0.00		BR3	0.00		
	12:50	20.46	20.46	20.46	0.35			0.00	-0.70	Add concentration gradient (top=.03%, bottom=.1%)
	12:58				0.35		BC1	0.00	-0.70	
	13:13	20.66	20.66	20.66	0.35		BC2	0.00	-0.70	
							BC3			Data lost due to disk being full
	14:30	20.98	20.98	20.98	0.35		BC4	0.00	-0.70	
	14:45	21.04	21.04	21.04	0.35		BC5	0.00	-0.70	
	14:47	**22.70**	**19.70**							***TEs on***
	15:22	22.67	19.73	21.27	0.35		BB1	2.94	-0.70	
	16:00	22.67	19.73	21.53	0.35		BB2	2.94	-0.70	Removed object beam pinhole and changed beam
	17:10	22.67	19.75	21.83	0.35		BB3	2.92	-0.70	ratio at ~4:30. Returned each to org. before 17:10
	17:14									***TEs off***
	17:55	21.93	21.93	21.93	0.35		BC6	0.00	-0.70	
	18:12	21.96	21.96	21.96	0.35		BC7	0.00	-0.70	
	18:22									Rinse cell once and added distilled water
	18:34	22.03	22.03	22.03	0.00		BR4	0.00	0.00	

4.6 Experiment Description

4.6.1 Data Collection

Measurements of various cell conditions were made during the sixth and seventh experimental series by directly digitizing the data from the CCD camera. The frame grabber's ability to store several images simultaneously was utilized to produce wrapped phase maps in essentially real

time. The raw images used to produce the phase maps and the phase maps themselves were stored onto floppy disks and later to Bernoulli disks for further analysis. The image files containing the raw data and phase maps were named using the convention outlined below.

Char. Pos.	Significance	Examples
1, 2	Type of phase map	up - unwrapped wp - wrapped
3	Color of laser light; phase map algorithm	r (s) - red b (c) - blue
4	Hologram number	6, 7, 8, 9, a, or b
5	Designator of type of relative gradient(s) formed between hologram and live cell	r - reference c - conc. grad. t - temp. grad. b - temp. & conc.
6	Used to distinguish between multiple interferograms of the same type and using the same hologram	0, 1, 2, 3, or 4
7	Filter code (never used)	0
8	Image number (raw interferograms only)	1, 2, 3, 4, or 5

In the case of the image files containing phase maps, only the first seven characters were used. The image files containing the interferograms used to produce the phase maps utilize the last six characters.

The first two characters (phase maps only) designate rather the data is a wrapped or unwrapped phase map. The third character tells if the file was for red or blue laser light. In the case of phase maps, this character also shows the type of algorithm used to produce the phase map; where r (red) or b (blue) signifies that the MetroLaser algorithm was used, and s (red) or c (blue) that the algorithm developed by Bill Witherow at MSFC was used. Since both algorithms gave essentially equivalent-looking phase maps, the MetroLaser algorithm was used in the analysis described below.

The fifth character shows the type of relative gradient which existed between the live cell and the hologram with which it was interfered. If, for example, the character were "c", then either the live cell or the hologram contained a concentration gradient, while the other contained no gradient. If the live cell (which may or may not have a gradient) and hologram contained the same condition, "r" was used to designate a reference interferogram.

The sixth character was used to differentiate between different interferograms files which would otherwise have the same name (i.e., same hologram, color light, and relative cell conditions). The filter code (seventh character) was never used since filtering the raw images did not significantly improve the final results. The last character was used to differentiate between the five phase shifted interferograms which were used to obtain each phase map.

4.6.1.1. Selection and Characterization of Test Solution

Two solutions were used in the experimentation performed with the laboratory breadboard. Initial experimentation was performed using a sucrose solution. This solution was abandoned for reasons previously outlined. A salt solution (NaCl in water) was eventually used to demonstrate the TCHI technique in the last two experimental series performed at MSFC.

In a paper published in Applied Optics by W. Lu and W. Worek[5], a salt solution was characterized with sufficient accuracy to apparently meet the precision requirements of our TCHI demonstration. Data for refractive index was given over a temperature range of about 18 to 25 °C and for concentrations up to 0.4% solution. In this paper, the data was used to determine the constants, A_n, in the following equation:

$$n(T,c) = A_1 + A_2T + A_3T^2 + A_4c + A_5c^2 + A_6cT + A_7T^2c^2, \quad (4.1)$$

where T is the solution temperature in degrees centigrade and c is the concentration in percent solution. This equation allows the first derivative with respect to temperature and concentration to be determined directly. The result is easily seen to be:

$$dn/dT\,(T,c) = A_2 + 2A_3T + A_6c + 2A_7Tc^2, \quad (4.2)$$

$$dn/dc\,(T,c) = A_4 + 2A_5c + A_6T + 2A_7T^2c. \quad (4.3)$$

The values of the coefficients in these equations were given for two wavelengths:

For λ = 632.8 nm:	**For λ = 457.9 nm:**
$A_1 = 1.332876681$	$A_1 = 1.339675476$
$A_2 = -2.637899 \times 10^{-5}$	$A_2 = -1.909458 \times 10^{-5}$
$A_3 = -1.513549 \times 10^{-6}$	$A_3 = -1.674018 \times 10^{-6}$
$A_4 = 1.477013 \times 10^{-3}$	$A_4 = 1.781316 \times 10^{-3}$
$A_5 = 2.312523 \times 10^{-4}$	$A_5 = 2.31062 \times 10^{-4}$
$A_6 = -1.137696 \times 10^{-5}$	$A_6 = -2.191775 \times 10^{-5}$
$A_7 = 2.192279 \times 10^{-9}$	$A_7 = 5.880504 \times 10^{-10}$

The 632.8 nm condition corresponds to one of the two lasers used in our demonstration. The other condition is slightly different from the 441.6 nm produced by the HeCd laser used in the MSFC breadboard. To obtain values at the proper wavelengths, two approaches were evaluated. The first approach was to perform a linear extrapolation of the constants to the 441.6 nm conditions. The advantage here is that it allows the first derivatives to be determined directly. Using this method produces the following coefficients at λ = 441.6 nm:

$A_1 = 1.340309097$
$A_2 = -1.841570 \times 10^{-5}$
$A_3 = -1.688973 \times 10^{-6}$

$$A_4 = 1.8096758565 \times 10^{-3}$$
$$A_5 = 2.310442 \times 10^{-4}$$
$$A_6 = -2.290011 \times 10^{-5}$$
$$A_7 = 4.385425 \times 10^{-10}$$

The second method was to use Cauchy's equation, $n_\lambda = A + B / \lambda^2$, to determine n_{4416} from n_{6328} and n_{4579}. To obtain the derivative in this case, the local slope of n_{4416} would be determined by finding the refractive indices at values of c and T just above and below the nominal condition.

While these relations seemed to provide an easy way of determining the values of dn/dT and dn/dc needed to solve the TCHI equations, the accuracy of this data proved to be inadequate. Initially, the values at the red and blue wavelengths were found to be off relative to one another. It is important that these relative values be accurate due to the extreme sensitivity of the denominators in the TCHI equations to these parameters. This conclusion was reached due to the observation that, for cell conditions where there was either a temperature or concentration gradient, but not both, the calculated magnitude of that gradient was different for the 441.6 nm and 632.8 nm fringe data based on values of dn/dT and dn/dc given from the Equations 4.2 and 4.3 above. Our conclusions were confirmed by calculating dn/dT based on data from the NBS paper by Tilton and Taylor[6] on the refractive index of pure water at various temperatures and wavelengths. The Lu's equations for calculating n were compared at zero concentration to values given by the NBS paper on the refractive index of pure water. The result was a disagreement in the two sets of data at the blue wavelength by over 100 parts in a million in refractive index and by several percent when dn/dT was calculated from each data set. The agreement was much better at the longer wavelength, thus confirming the accuracy of the equations at 632.8 nm. When the values of dn/dT calculated from the NBS values of n at 632.8 nm and 441.6 nm were used with our experimental data, there was agreement in the calculated temperature gradient at the two different wavelengths.

Later, when ΔT and Δc were estimated for the test cell conditions used in the TCHI demonstration (Section 5.3), it was discovered that the absolute values of dn/dT and dn/dc were also off by 30 to 60%. Using the method outlined in Section 5.4, values for dn/dT and dn/dc were ultimately determined experimentally to sufficient accuracy to do the TCHI demonstration. This proved to be a valuable exercise since it demonstrated that the required accuracies could be obtained for dn/dT and dn/dc for any solution of interest from the same experimental setup used to apply the TCHI technique.

4.6.1.2. Preparation of Test Solution

Holograms were initially made with the test cell filled with distilled water at room temperature in order to establish the stability of the interferograms over time and to characterize the temperature gradient resulting from maintaining a 3°C temperature difference between the top and bottom of the test cell. In the first case, sufficient time was given for the water temperature to equalized throughout the cell. For later experimentation with concentration gradients, all fluids were added and extracted from the test cell using a pipette that was attached to a syringe via a small diameter

Tygon tube. This allowed the introduction and extraction of fluid in a very controlled manner that would not disturb the test cell.

For determination of dn/dc and for the TCHI demonstration, a concentration gradient was set up in the test cell. To accomplish this, the water that was in the cell for making the reference hologram was first removed and the cell was refilled approximately half way with a low concentration solution (0.03 % for the final TCHI demo). The pipette was then withdrawn and filled with a higher concentration solution (0.10 % for the final TCHI demo). This solution was introduced from the bottom of the test cell, where it would naturally want to settle. Using this method, the top and bottom of the cell contained solutions at nearly constant concentrations in the vertical direction, while the center of the cell contained a gradient due to mixing of the two solutions. The cell was allowed to set while the gradient settled out into horizontal layers of constant concentration.

The two salt solutions used to form the concentration gradients were prepared by weighing the proper amount of salt and adding it to a partially filled volumetric flask. The flask was then filled to its calibration mark in order to obtain the proper solution strength. The density of each solution was later measured and correlated to solution strength using the CRC Handbook of Chemistry. These measurements confirmed that the solution strengths were 0.03 % and 0.10 %.

4.6.1.3. Production of Hologram

Holograms of the test cell were made on Agfa-Gevaert 4" x 5" 10E75 glass plates using exposure times of approximately 1/8th second. A single shutter was used that exposed the plate to both laser beams simultaneously. Holograms were processed in the normal manner in Kodak D-19 developer and placed back into the experimental setup. To ensure proper alignment of the hologram after processing, a two piece plate holder made by Jodan was used. The glass plate was mounted into a metal frame in which it remained during exposure, processing, and placement back into the setup. The combined glass plate/frame was placed in the main plate holder that used micrometers to allow very minor adjustments in the plate position after processing. This allowed adjustment that would return the plate to precisely the same position it had been during recording.

4.6.1.4. Production of Interferograms

Interferograms were formed combining the hologram of the test cell with the live cell. Initially the live cell was unmodified from its condition when the hologram was recorded. This permitted minor adjustments in the plate position after chemical processing so that an "infinite fringe" condition could be obtained. The ideal infinite fringe interferogram could not actually be obtained at that time, but by digitizing the interferogram that was obtained, corrections could be made to later interferograms made with a live test cell containing temperature and/or concentration gradients. In this manner the interferogram is essentially normalized to the infinite fringe condition.

4.6.2 Data Reduction

As stated earlier, the MetroLaser algorithm was used to produce phase maps of each set of phase shifted interferograms. Software was written to use these images to produce unwrapped phase maps of the same data. For selected images, the data from each type of phase map was put into a spreadsheet to make sure that the relative phase at various points within the image corresponded between the two representations. The unwrapping software left a few isolated vertical discontinuities in some of the images. Since such discontinuities were rare and obvious, they were simply eliminated in later analysis when they occurred. These discontinuities could probably be eliminated with further refinements in the unwrapping software, but for the moment, the current algorithm is an acceptable conversion.

A number of approaches were tried in attempting to reduce the megabytes of image data into some useful format. In the end, the data was reduced by making each data "point" the average of a number of pixels with the same horizontal position, as outlined in **Figure 4.1**. Images from the test cell were taken at two horizontal positions for each phase map, one near the top of the cell and the other near the bottom. At each position, data points consisted of arrays of 1x10 pixels inside the test cell, and 1x30 pixels in the air gaps to either side of the test cell. This grouping of pixels seemed reasonable since the temperature and concentration along any horizontal line within the cell should be approximately constant for the gradients set up during this test series.

The average of each pixel array, along with the standard deviation of the pixel values within that array, was saved to an ASCII file for each phase map. The data for each unwrapped phase map was read into a spreadsheet for analysis.

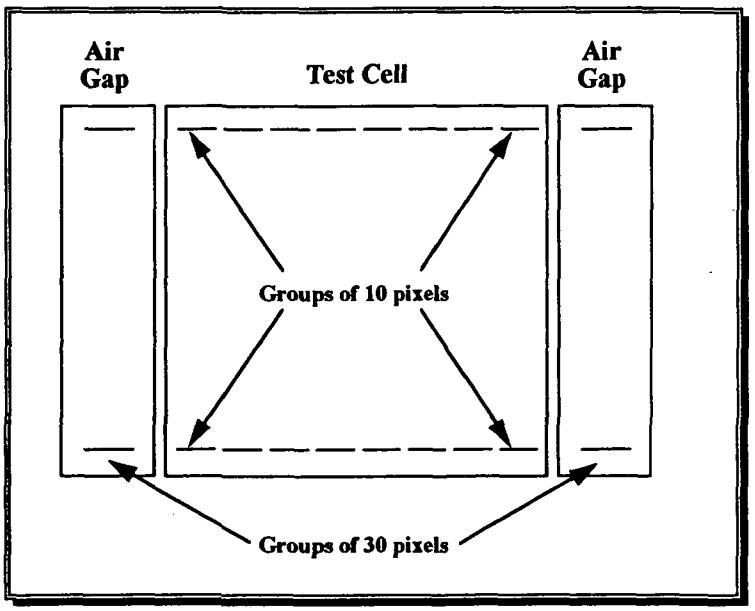

Figure 4.1. Pixel arrays used to determine data points within each phase map.

5. EXPERIMENTAL RESULTS FROM LABORATORY BREADBOARD

The results reported here are primarily from the seventh experimental series at MSFC, since it represents the culmination of all previous work. Representative samples of the data, from raw interferograms to the final plots showing the successful measurement of ΔT and Δc, are presented in the following sections.

5.1 Interferograms

Representative sets of four interferograms in which the test cell contained both temperature and concentration gradients are shown in **Figures 5.1** and **5.2** for red and blue light, respectively. Each successive interferogram was phase shifted 90° from the previous using the control software developed by Bill Witherow. Each dark, horizontal fringe represents a change in phase by 2π. The closer fringe spacing in **Figure 5.2** is a result of the shorter wavelength of this light, which essentially increases the difference in optical path length between any two vertical points. The areas of essentially constant intensity to either side of these horizontal fringes are the air gaps to either side of the test cell. The tilting fringes and the slight difference of intensity between the left and right air gaps indicate a slight tilt of the hologram along a vertical axis. This tilt does not effect the TCHI results, since the phase difference between two points along a vertical line are seen to stay constant. The gradual change in intensity from top to bottom indicates a very slight tilt of the hologram in the other axis, and this tilt would effect the TCHI results if it were not taken into account as we have done.

The plots shown in **Figure 5.3** show how the intensity of the first interferogram from each color varies along a vertical line near the center of each interferogram. The noise in these interferograms is especially evident at the peak intensities for each cycle. Overall, however, the fringe contrast can be seen to be very good, the minimum intensity going to essentially zero in each cycle.

These interferograms were used to produce the wrapped and unwrapped phase maps shown in the next section.

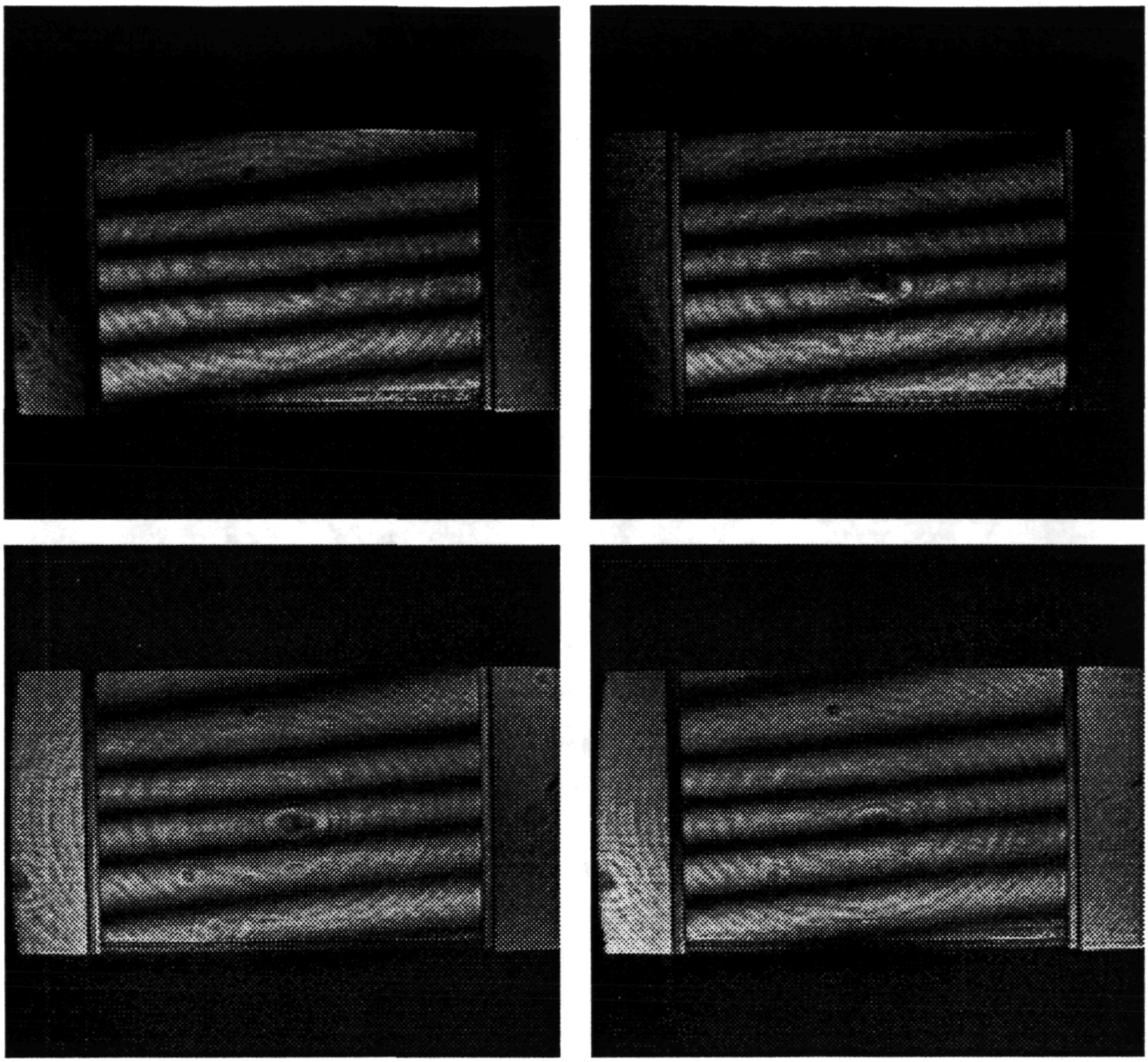

Figure 5.1. Four red light interferogram (number BB1 from the seventh experimental series) in which the test cell contained both temperature and concentration gradients. Each interferogram is phase shifted 90° from the previous.

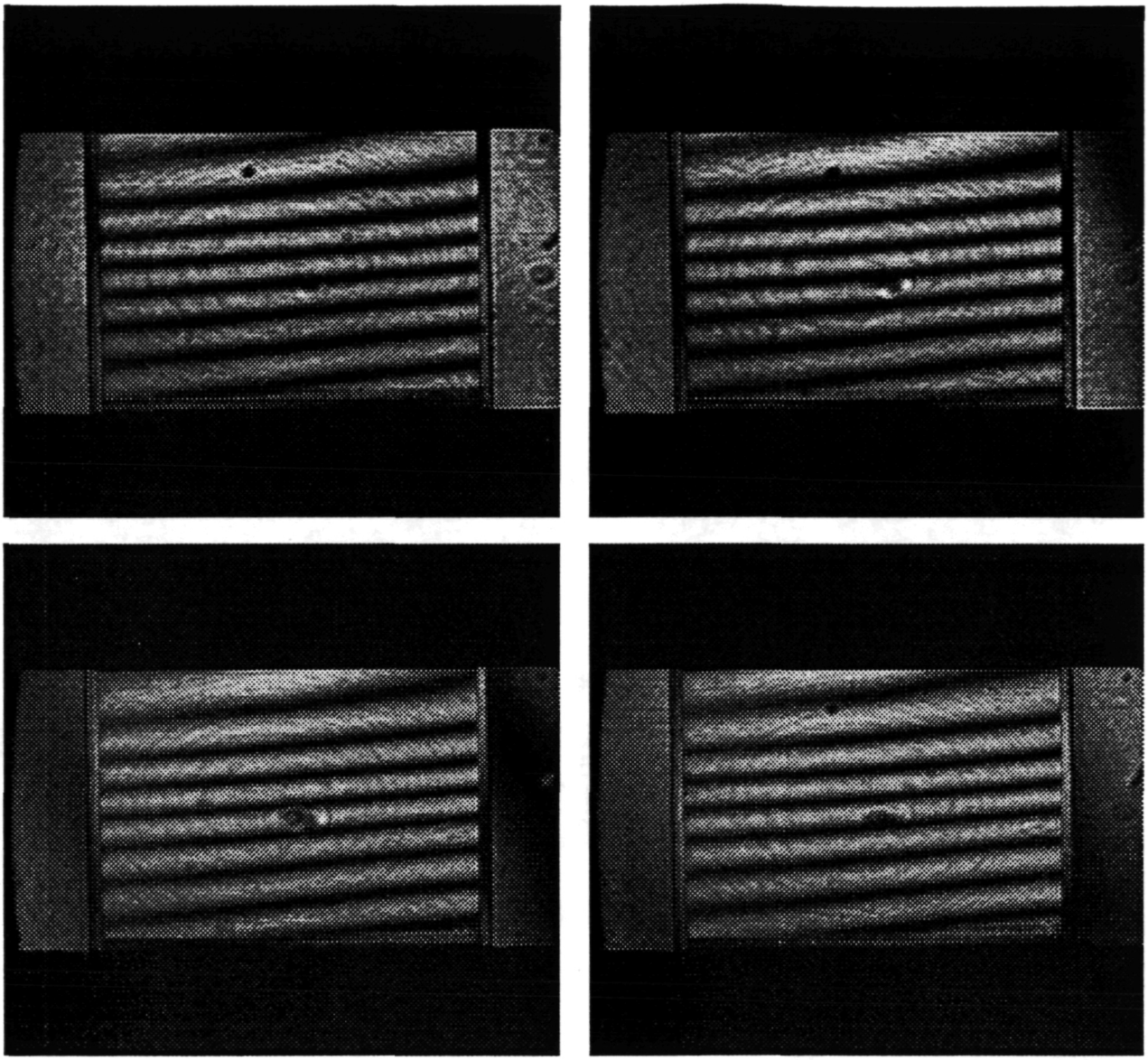

Figure 5.2. Four blue light interferogram (number BB1 from the seventh experimental series) in which the test cell contained both temperature and concentration gradients. Each interferogram is phase shifted 90° from the previous.

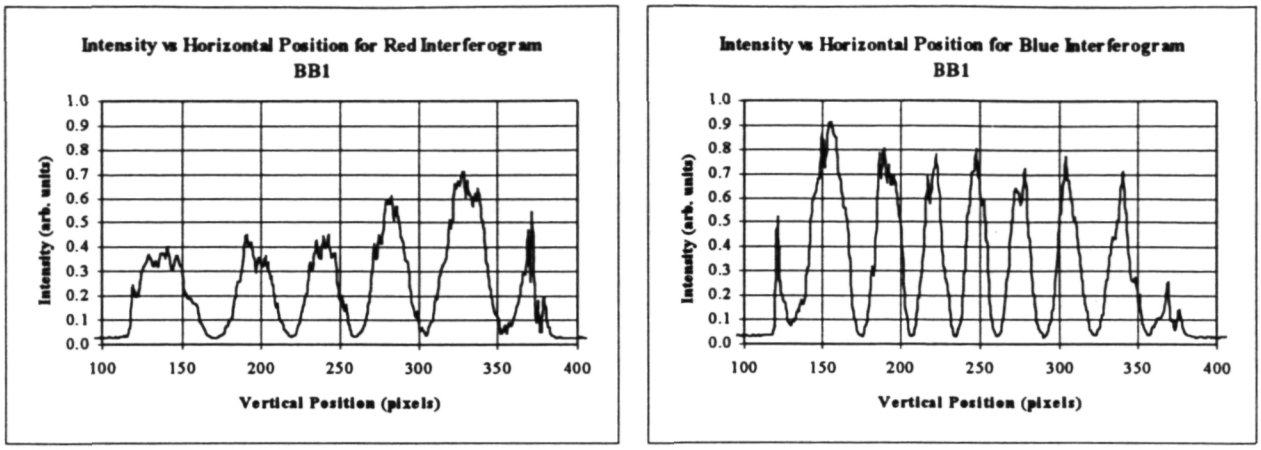

Figure 5.3. Intensity of light along a vertical line near the center of the interferograms shown in Figures 5.1 (right) and 5.2 (left).

5.2 Phase Maps

The interferograms shown in **Figures 5.1** and **5.2** were used to produce phase maps for each color laser using the phase shifting algorithm previously outlined. The phase maps produced from the above interferograms are shown in **Figures 5.4** and **5.5**. Each change in intensity from zero to maximum represents a crossover to the next fringe order. The red phase map indicates that the gradients in the test cell caused the optical path length to change by about five fringes, while the change for the blue light is a little over seven. The tilt of the holographic plate about the horizontal axis is much more evident now by the change in color in the vertical direction in the air gaps to either side of the cell. The ability to filter out intensity effects can be noted by comparing **Figures 5.1** and **5.3** or **5.2** and **5.4**. For example, a spot near the top center of the test cell, probably caused by a piece of dust on the test cell wall, can be readily noted in **Figure 5.1**, but is completely gone from **Figure 5.3**. This is because the blemish effects only the intensity of the light at the camera, not the phase of the light. This is one reason why phase shift interferometry is superior over simply using a single interferogram for determining phase.

Figure 5.6 shows how the phase shifts from top to bottom varies along the center of the cell for each color. Notice that the sinusoidal variation in **Figure 5.3** is replaced by a generally linear relation, with each cycle starting at zero and going to a maximum of 1. It can also be seen that the phase shifting algorithm has filtered out much of the noise seen in the previous interferograms (**Figure 5.3**).

Figures 5.7 and **5.8** show red and blue phase maps of the same test cell before the temperature gradient was added (concentration gradient only). Fewer fringes are seen here than in the phase maps of both temperature and concentration gradients, since each individual gradient is in the direction that caused solution density to increase from top to bottom (i.e., the bottom contained the coolest solution and the highest concentration). This was done to minimize convective currents that would have resulted if a higher density fluid element were above a lower density fluid element.

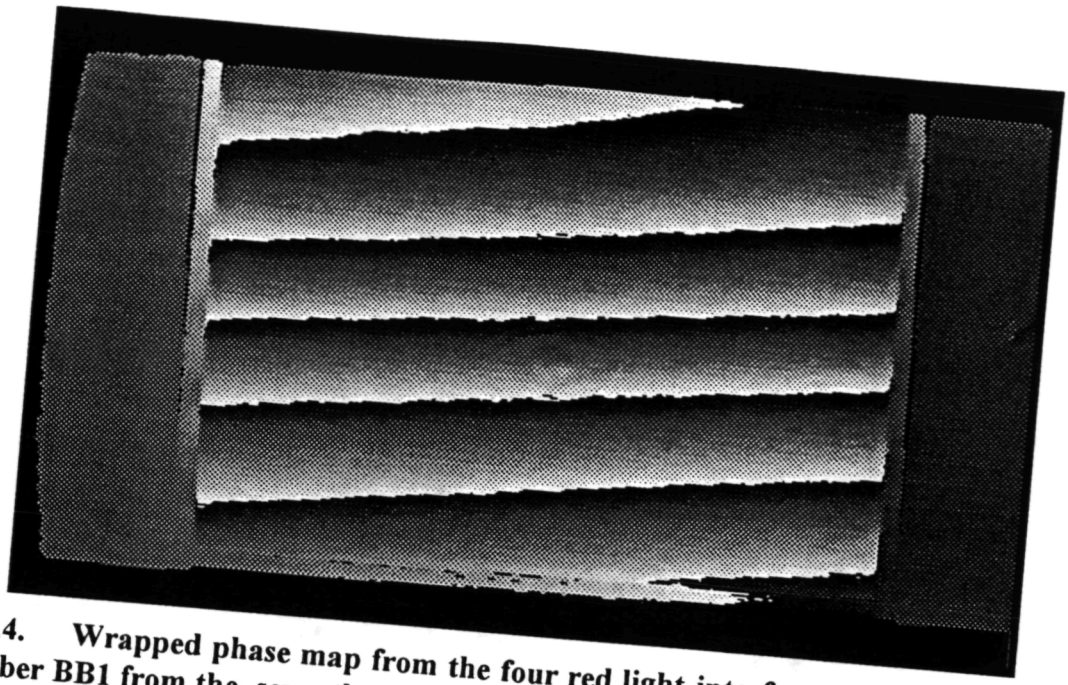

Figure 5.4. Wrapped phase map from the four red light interferograms shown in Figure 5.1 (number BB1 from the seventh experimental series).

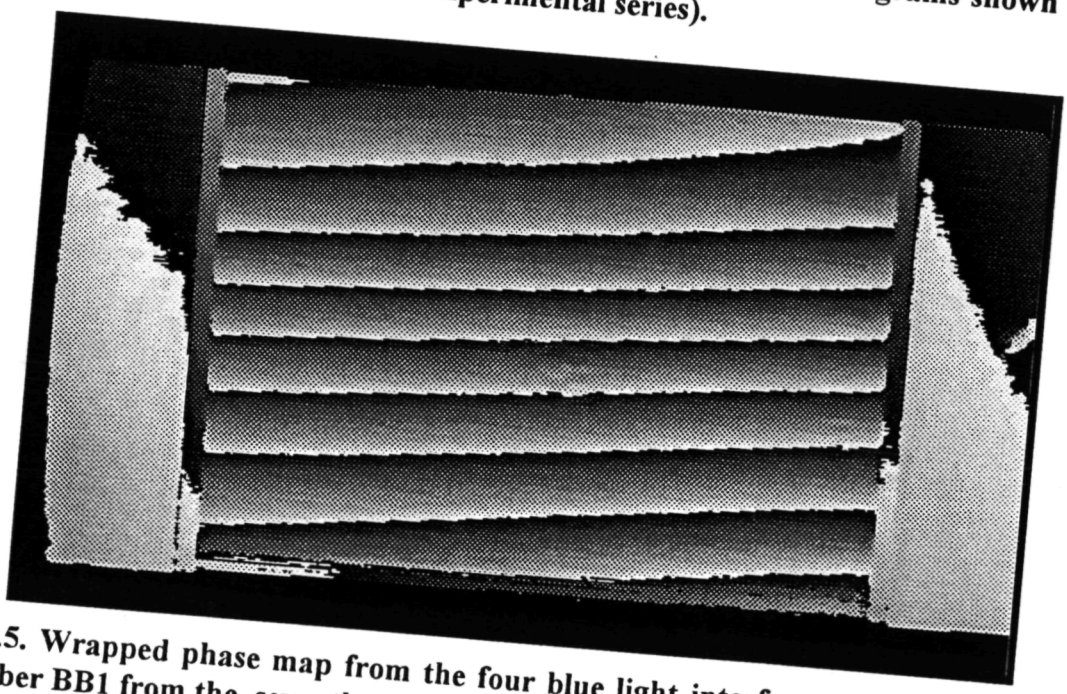

Figure 5.5. Wrapped phase map from the four blue light interferograms shown in Figure 5.2 (number BB1 from the seventh experimental series).

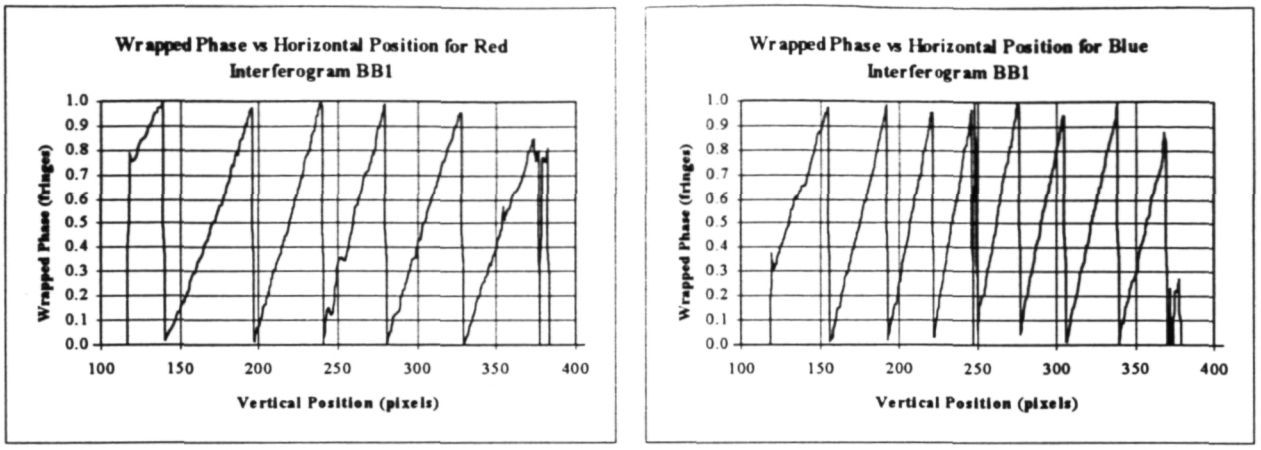

Figure 5.6. Phase along a vertical line near the center of the phase maps shown in Figures 5.4 (left) and 5.5 (right).

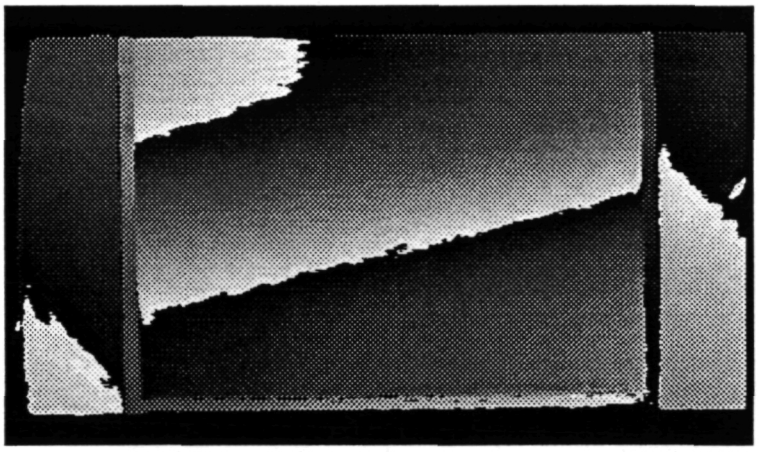

Figure 5.7. Wrapped phase map for red light of the test cell containing only a concentration gradient (number BC6 from the seventh experimental series).

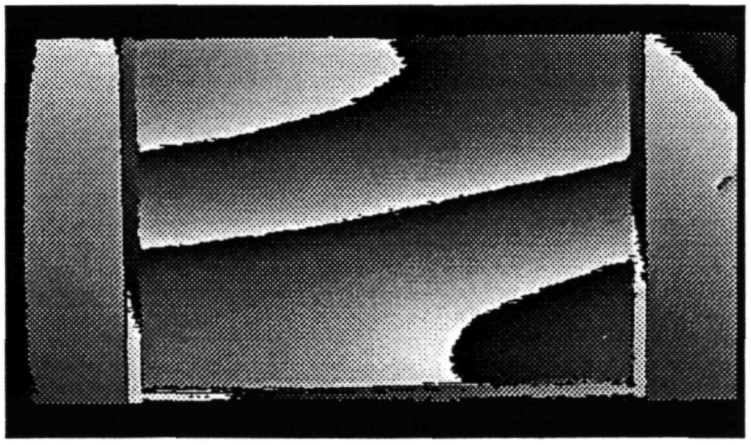

Figure 5.8. Wrapped phase map for blue light of the test cell containing only a concentration gradient (number BC6 from the seventh experimental series).

5.3 Determination of Δc and ΔT

To confirm the TCHI results, it was necessary to obtain estimates of the actual temperature and concentration differences of the two horizontal rows between which ΔT and Δc were to be measured interferometrically. The ΔT estimate was based on the fact that the temperature difference between the top and bottom of the cell was controlled to be 3 ± 0.05 °C and that the temperature profile was linear from top to bottom. The distance between the two horizontal rows in the test cell between which measurements were made was between 17.46 mm and 18.37 mm, depending on which of two methods was used to calibrate the vertical scale of the camera used to capture the interferograms. The distance between the inside bottom of the test cell and the copper heat sink in the top of the test cell was measured directly to be 39.79 mm. Based on this data, the expected ΔT between test points would be,

$$\Delta T = 3\ ^{\circ}C * (17.46\ mm \text{ to } 18.37\ mm) / 39.79\ mm = 1.32 \text{ to } 1.38\ ^{\circ}C.$$

The temperature difference between these two locations was, therefore, taken to be 1.35 ±0.05 °C when the temperature difference between the top and bottom of the cell was set at 3 °C. This temperature profile was found to remain very consistent over time, as is seen from **Figure 5.1** in the previous section. The ΔT estimate of about 1.35 °C should, therefore, be good for all experiments, since the top and bottom thermoelectrics were always set at room temperature +1.5 °C and -1.5 °C, respectively.

Determination of Δc was a little less direct, but should be good to within 10%. Two solutions were used for all salt water experiments (6th and 7th experimental series), a 0.03% and a 0.10% solution. The TCHI demonstration solution was prepared carefully so that, at least initially, the top contained only 0.03% solution and the bottom contained only 0.10% solution. Density measurements were made of these two solutions to confirm these concentrations. **Figure 5.9a** shows the concentration distribution (in terms of fringe order) in the vertical direction, shortly after the concentration gradient was put in place. The left side of the plot (from about pixels 120 to 180) is relatively flat, indicating that the concentration near the top of the test cell did not change with vertical position. The phase then begins to change with position due to the presence of the concentration gradient. Toward the right side of this plot (near the bottom of the test cell), the slope begins to decrease once again as the change in concentration becomes less. **Figure 5.9b** shows what happened to the gradient over time, with the interferogram being made after the TCHI demonstration had been run and the temperature gradient removed from the test cell. The decrease in the fringe order from top to bottom indicates that the solution has mixed over time and that the concentration gradient has diminished in this direction. Note that the left side of this plot is no longer flat, indicating that the top of the cell is no longer at the initial concentration of 0.03% as salt slowly migrated into the weaker solution. The slope at the bottom of the cell (right side of plot) has remained fairly constant, indicating that this area of higher concentration probably did not change much during five hours.

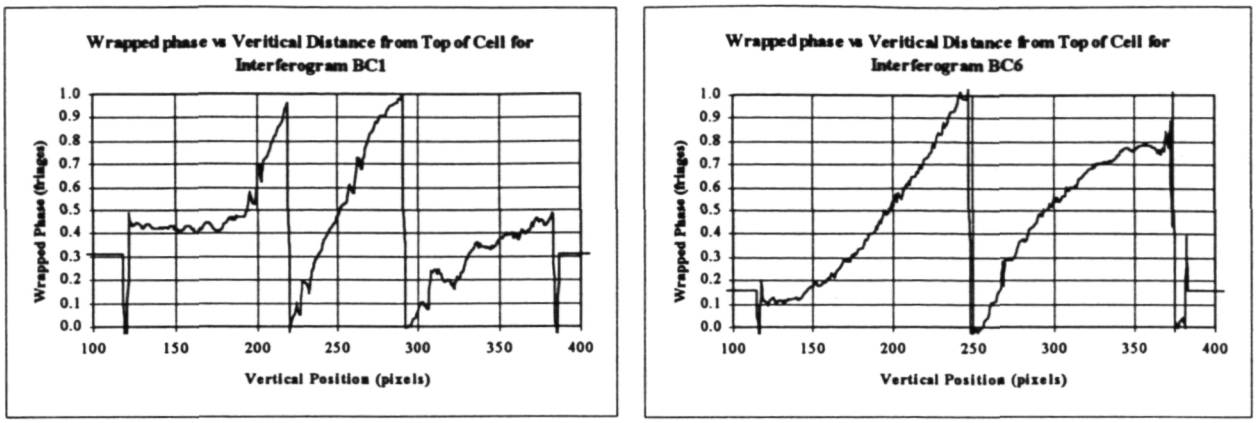

(a) (b)

Figure 5.9. Wrapped phase maps along a vertical axis the of test cell with a only concentration gradient. Interferograms made at 12:58 p.m. and 5:55 p.m., respectively (note: hologram tilt has been corrected for, so the decreased phase change in (b) is due to mixing of the solution over time).

Phase measurements from the interferograms were made at vertical positions of 140 and 340 pixels from the top of the cell. From **Figure 5.9a** it can be seen that the initial concentration of these vertical positions is very close to the extreme values of 0.03% and 0.10%. The initial value of Δc was, therefore, taken to be 0.07%. The value of Δc at any other time was deduced by comparing the phase change of the interferogram of interest with the phase change initially in the test cell. Δc and ΔN were assumed to be proportional, with the proportionality constant defined by the initial conditions shown in **Figure 5.9a**. The value of Δc during the TCHI demonstration, when both temperature and concentration gradients existed in the test cell, was determined by assuming that this value varied linearly with time between interferograms BC5 and BC6 (the interferograms made just before and just after the TCHI demonstration).

5.4 Calibration of dn/dT and dn/dc

Determination of dn/dc and dn/dT became necessary when it was discovered that the values obtained using the equations by Lu, which give refractive index of salt water as a function of temperature and concentration, were not as accurate as claimed by the author. The way this was discovered is outlined in Section 4.6.1.1.

Calibration was accomplished in the following manner. Values for dn/dT were calculated based on the Tilton paper, while values for dn/dc were based on Lu's equation. Even though the values for dn/dc were known to be off, they were the only data available and were, therefore, the best starting point. Next, the relation given in Equation 1.6 was used for the case of only a temperature gradient and for each color laser:

$$\Delta N_j = \left(\frac{\partial n}{\partial T}\right)_j \left(\frac{L\Delta T}{\lambda_j}\right), \tag{5.1}$$

$$\Delta N_k = \left(\frac{\partial n}{\partial T}\right)_k \left(\frac{L\Delta T}{\lambda_k}\right), \tag{5.2}$$

where j and k are the two colors (441.6 nm and 632.8 nm). The values of dn/dT were based on Tilton for pure water and the ΔNs and ΔTs were measured between the top and bottom of the test cell. These calculations were done at thirty different locations along two horizontal lines across the test cell (one near the top of the cell, the other near the bottom). The value of the dn/dT_k was optimized to make $\Delta N_j = \Delta N_k$, which makes Equation 5.2:

$$\Delta N_k = s_{dn/dT,k}\left(\frac{\partial n}{\partial T}\right)_k \left(\frac{L\Delta T}{\lambda_k}\right), \tag{5.3}$$

where $s_{dn/dT,k}$ is the multiplicative factor that produced agreement between Equations 5.1 and 5.3. In a similar manner, a test cell condition in which only a concentration gradient was present was used to find the value of a multiplicative factor, $s_{dn/dc,k}$, to correct for inaccuracies in the relative values of dn/dc at the two wavelength. The results of these corrections are shown in Figures 5.7 and 5.8. It can be seen in these plots that there was a slight variation in ΔT and Δc across the test cell. There variations were, however, too small to be detected in the TCHI results where errors due to phase sensitivity were larger than the small variations across the cell.

While the relative values of dn/dT and dn/dc at the red and blue wavelength were found to quite close, there was actually considerable errors in the absolute values of these parameters. These differences were attributed to the fact that the measurements being made in both Lu and Tilton was a refractive index, and not their derivatives with respect to temperature or concentration. Since the refractive index is essentially the same to the fifth decimal place in the refractive indices at similar conditions, very small errors in the refractive index measurement can result in very large errors when this data is used to calculate the local derivatives. Again referring to Equations 5.1 and 5.2, a **direct measurement of dn/dT and dn/dc** can be made using the TCHI laboratory breadboard even though the actual refractive index is totally unknown. Rewriting Equations 5.1 and 5.3 we have:

$$\Delta T = \left(\frac{\lambda_j \Delta N_j}{L}\right) \Bigg/ \left[s_{dn/dT}\left(\frac{\partial n}{\partial T}\right)_j \right], \tag{5.4}$$

$$\Delta T = \left(\frac{\lambda_k \Delta N_k}{L}\right) \Bigg/ \left[s_{dn/dT} s_{dn/dT,k}\left(\frac{\partial n}{\partial T}\right)_k \right], \tag{5.5}$$

where $s_{dn/dT}$ is the correction factor that, for the measured values of ΔN_j and ΔN_k, gives the value of ΔT given in the previous section (1.35 °C). Again, a similar approach was used to determine the correction factor for dn/dc at the two wavelengths, $s_{dn/dc}$. The values of these correction

factors based on the various corrections made to the interferograms themselves are given in Section 5.5.4.

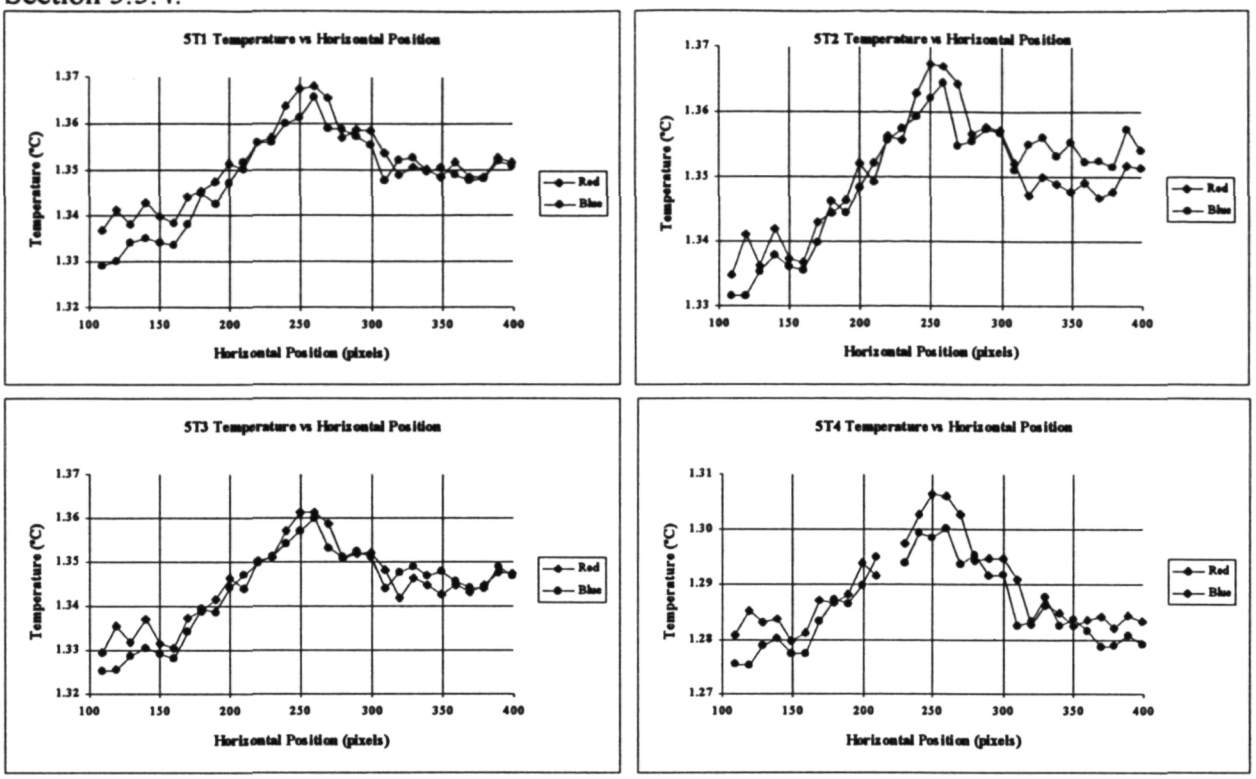

Figure 5.7. ΔT measurements from four different interferograms at various locations across the test cell based on corrected values of dn/dT_k. Interferograms were recorded at 7:05, 7:08, 8:15, and 9:05 p.m., respectively. Interferogram 5T4 was made after increasing the top and bottom control temperatures by 0.8 °C (ΔT was maintained at 3 °C).

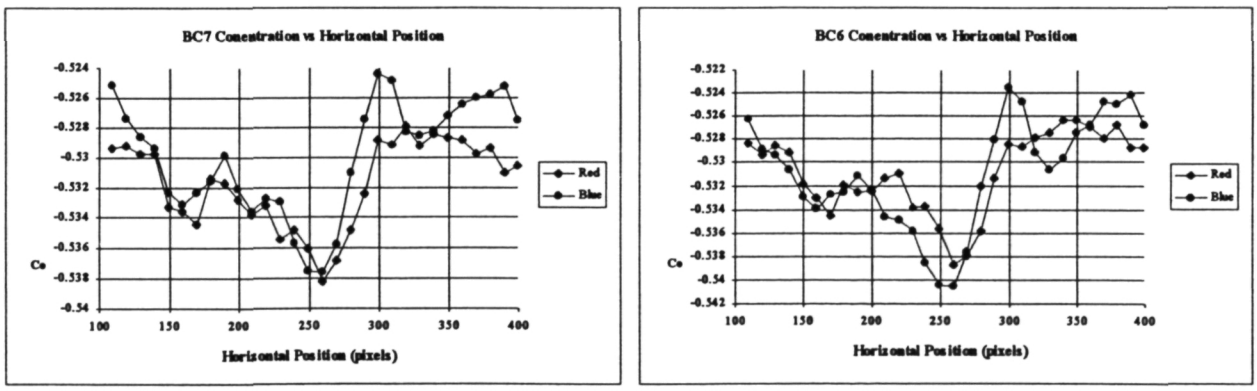

Figure 5.8. Δc measurements from two different interferograms at various locations across the test cell based on corrected values of dn/dc_k.

5.5 Data Interpretation

Several corrections had to be made to the raw phase maps before acceptable results were obtained in the calculation of ΔT and Δc. The effect of these corrections, along with the final results and a comparison of those results to expected inaccuracies based on the error analysis are given in this section.

5.5.1 Phase Error

In order to assess the quality of the data, error in the phase measurement used in the TCHI equations was determined. As outlined previously, each data point in the reduced phase maps was actually the averaged value of ten adjacent, horizontal pixels. Each phase map reduced in this manner contained 30 data points along two horizontal rows, one near the top of the test cell and one near the bottom. The standard deviation of the ten pixels making up each of these 60 data points was also calculated along with the average. This allowed an assessment of the accuracy of the fringe measurement. The fringe measurement error for the phase map was defined as the average standard deviation of the 60 data points used. The values for both red and blue interferograms is shown in **Table 5.1** for two of the holograms from the seventh experimental series (several interferograms were made from each hologram). **Table 5.2** shows the same data for four interferograms from the fifth experimental series. Improvements in the set up and use of frame averaging account for the decrease in error from around 0.03 fringes ($\lambda/33$) in the fifth series to generally better than 0.01 fringes ($<\lambda/100$) in the final series where TCHI was successfully demonstrated. Plots of the error of each data point for selected red/blue interferograms are shown in **Figures 5.10** and **5.11** for Holograms 5 and B from the seventh experimental series.

Table 5.1

Fringe error for various interferograms from the seventh experimental series.

	Average Error (fringes)	
Interf.	**Red**	**Blue**
5R3	0.006	0.004
5R4	0.007	0.005
5R5	0.006	0.005
5R6	0.006	0.006
5T1	0.009	0.010
5T2	0.009	0.011
5T3	0.008	0.010
5T4	0.008	0.010

	Average Error (fringes)	
Interf.	**Red**	**Blue**
BR1	0.008	0.009
BR2	0.008	0.009
BR3	0.009	0.011
BR4	0.010	0.013
BC6	0.010	0.013
BC7	0.010	0.013
BB1	0.012	0.015
BB2	0.012	0.015

Table 5.2.

Fringe error for various interferograms from the fifth experimental series

Interf.	Average Error (fringes)	
	Red	Blue
6C0	0.022	0.023
8R2	0.015	0.046
8R3	0.016	0.022
8R4	0.015	0.024
8C0	0.019	0.032
8C1	0.039	0.038
8T3	0.021	0.032
8T4	0.019	0.027
8B0	0.022	0.027
8B1	0.036	0.046
9R0	0.025	0.098
9B0	0.039	0.044
AC0	0.037	0.049

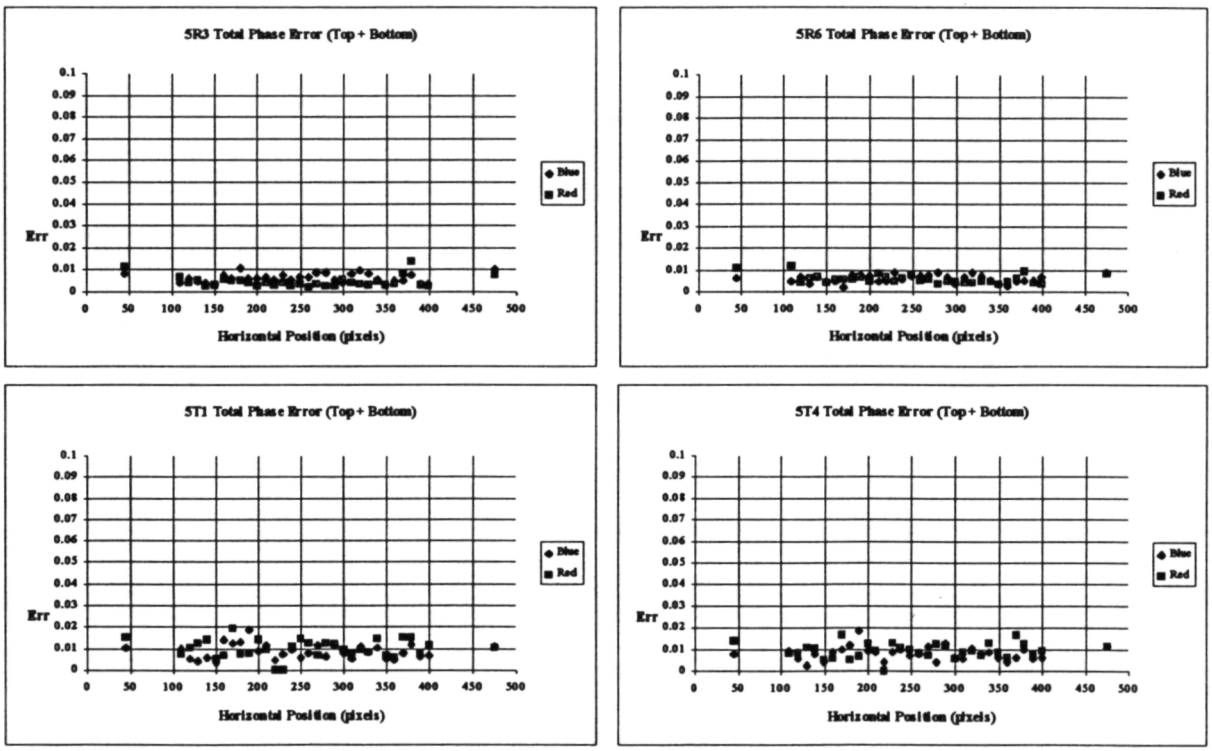

Figure 5.10. Phase error for selected interferograms from Hologram 5 (seventh experimental series).

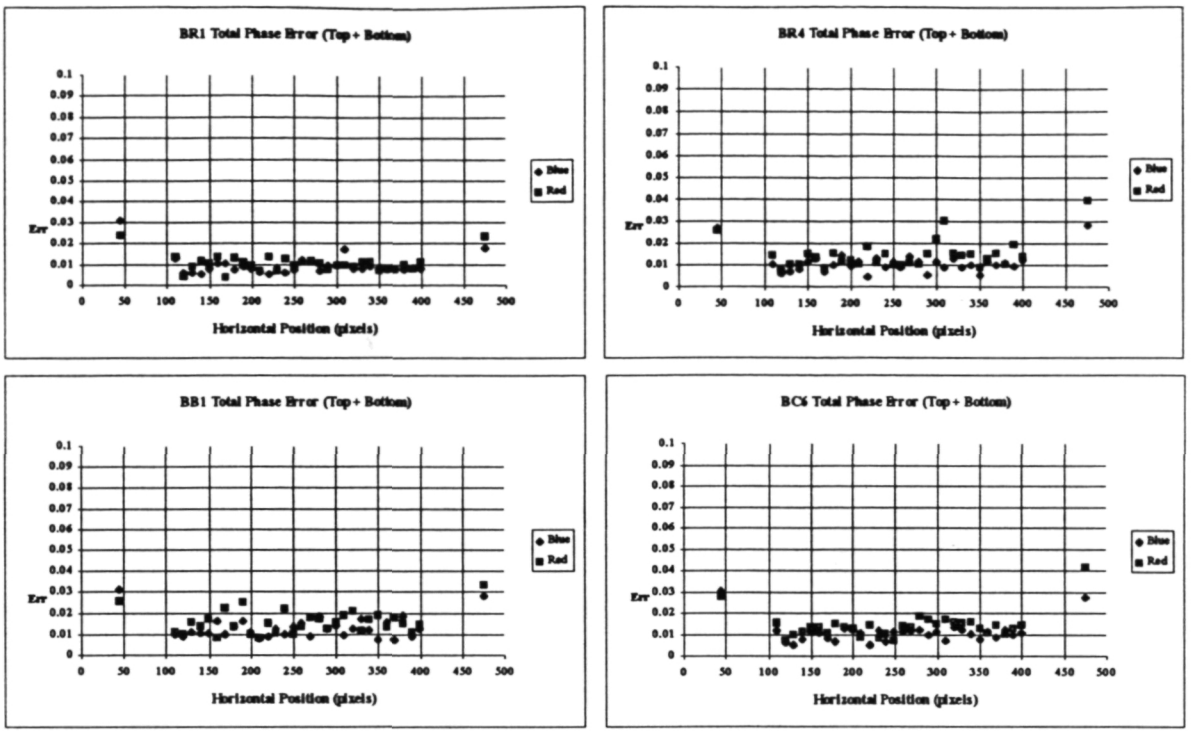

Figure 5.11. Phase error for selected interferograms from Hologram B (seventh experimental series).

Another way of determining fringe error is suggested by examining **Figures 5.7** and **5.8**. Here the value of dn/dT or dn/dc at the blue wavelength have been corrected such that the average value of the gradient is the same based on either the red or blue fringe measurement. Since the red and blue interferograms were taken within seconds of one another, the cell conditions must have been essentially identical in both cases. Therefore, any discrepancy in the relative phase between any to points in the cell for the red and blue measurements must be attributed to errors in those phase readings. In **Table 5.3**, the average discrepancy between the calculated values of temperature or concentration for the 30 sets of points in the test cell are given for Holograms 5 and B. The first column in each case is the actual error in either units of °C or g/liter, while the second column converts these values in terms of fringes based on using the average λ's and dn/dT's or dn/dc's for the red and blue wavelengths. This indicates the amount of fringe error that would account for the amount of observed discrepancy between the two measurements (red and blue fringe measurements). For these interferograms, fringe error measurement of a little better than 0.01 (λ/100) is observed, which agrees with the value calculated above. The exception is Interferogram BC5, which has an error of 0.043: four times higher than the other cases.

Table 5.3.

Fringe error based on difference in phase reading between red and blue laser light.

Interferogram	Red/Blue Discripency	
	(°C)	(fringes)
5T1	0.005	0.009
5T2	0.005	0.009
5T3	0.004	0.007
5T4	0.005	0.010

Interferogram	Red/Blue Discripency	
	(g/liter)	(fringes)
BC5	0.018	0.043
BC6	0.004	0.009
BC7	0.003	0.008

5.5.2 Reference Interferogram

During the seventh experimental series, a sequence of reference interferograms were made to determine the stability of system over time. **Figure 5.12** shows the phase maps of this set of interferograms for both wavelengths. The phase is actually the relative phase difference between the top and bottom of the cell. Ideally, this phase difference is exactly zero at any horizontal position. It can be seen, however, that the phase across the cell varied by approximately $\lambda/20$. The error bars show the $\lambda/100$ error in the phase measurement. It was found necessary to subtract this phase information from later interferograms containing concentration and/or temperature gradients in order to produce the best results.

As can been seen from the log for this experimental series, these interferograms were made over a period of almost nine hours. Over such a long period of time the structure of the relative phase from top to bottom is seen to gradually change, indicating that the cause of these small phase shifts is not static. In particular, the overall relative phase is seen to gradually increase over time to almost a full fringe for the blue hologram. This is probably due to relation of the plate holder and can be easily corrected for by using the reference air gaps to either side of the cell. This dramatic shift emphasizes the importance of having a reference area when applying the TCHI technique.

Figure 5.13 show similar reference interferograms for Hologram B of the seventh experimental series. The change is much smaller in this case since the elapsed time is only about half an hour. The details of the phase across the cell are seen to be more consistent between interferograms, indicating that it cannot be attributed to errors in the phase measurement itself. Again, even in this much shorter time frame, an overall increase in the relative phase shift can be seen to occur as time passes.

The gradual phase shift over time can be seen to be quite linear from **Figure 5.14** which shows the relative phase shift between the top and bottom of test chamber for Hologram 5 of the seventh experimental series. Phase shifts are shown for the air gaps to the left and right of the test cell as well as in the center of the test cell itself. Data is also shown for the phase shift in the air gaps for interferograms made when a temperature gradient was present in the test cell.

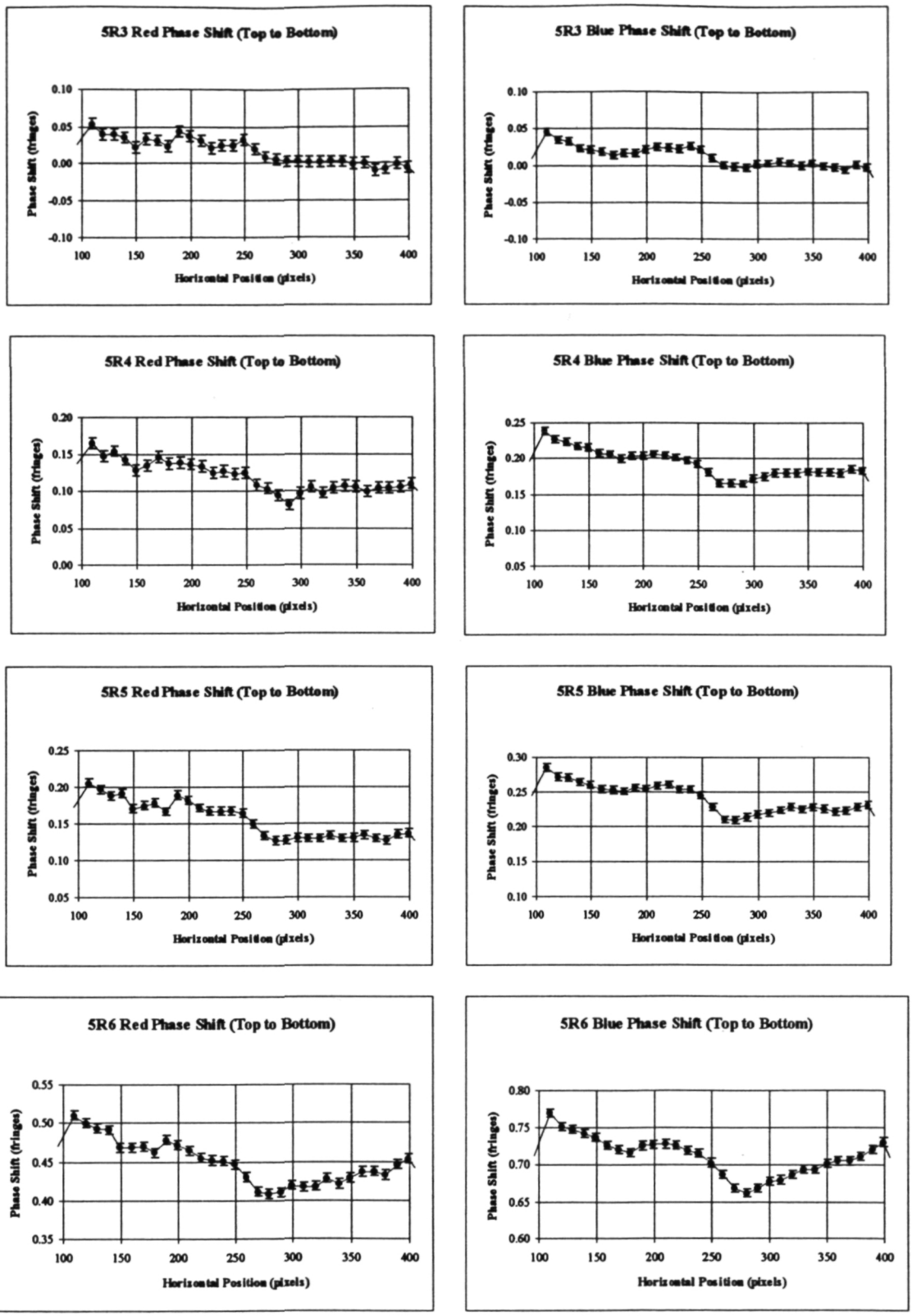

Figure 5.12. Reference interferograms from Hologram 5 of the seventh experimental series.

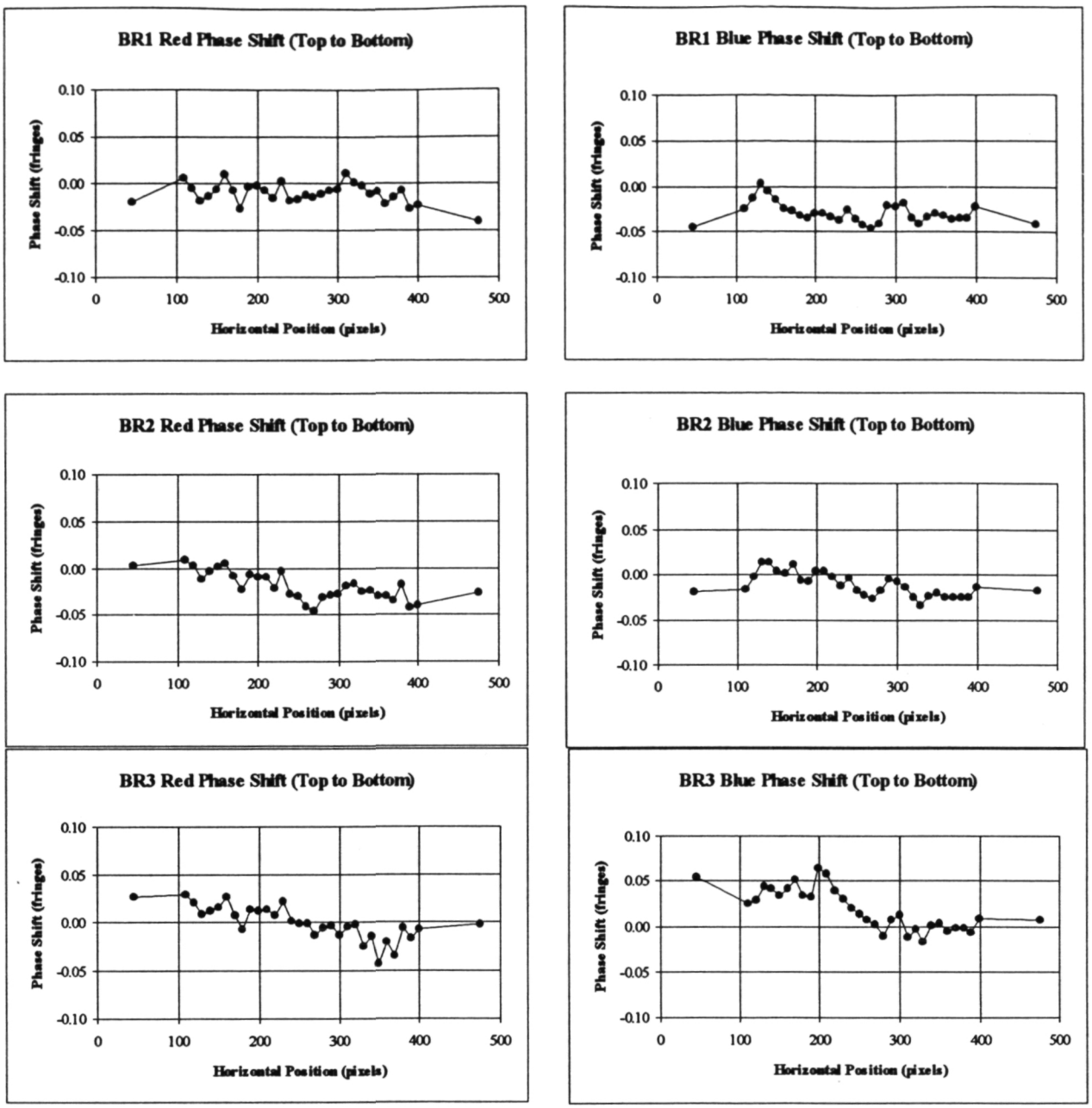

Figure 5.13. Reference interferograms from Hologram B of the seventh experimental series.

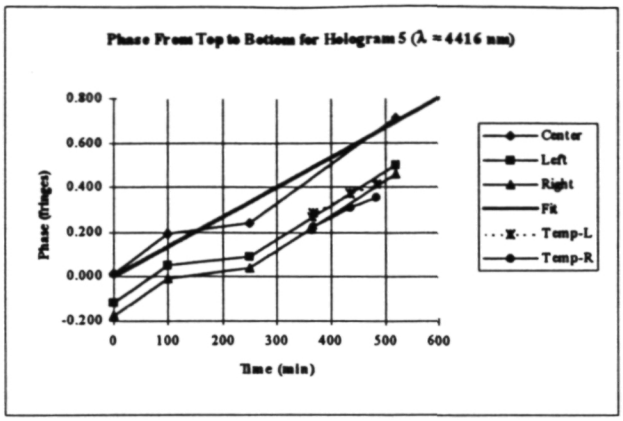

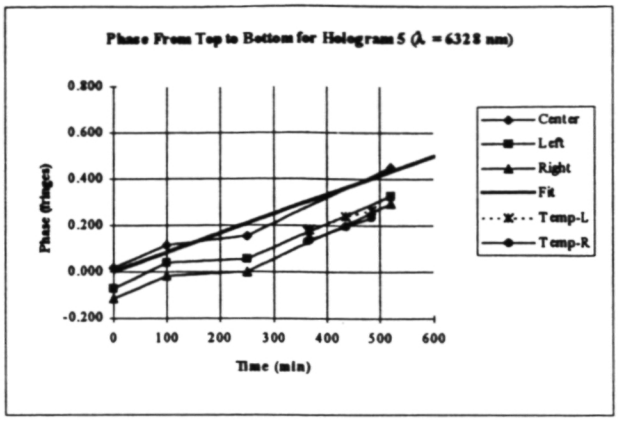

Figure 5.14. Relative phase shift between top and bottom of test chamber for Hologram 5 of the seventh experimental series as a function of time. Phase shifts are shown for the air gaps to the left and right of the test cell as well as in the center of the test cell itself.

5.5.3 Relative Phase Between Top and Bottom of Test Cell

The temperature and concentration measurements made using the TCHI technique are based on the relative difference between two points in the test cell (in this case, one near the top of the test cell and the other located directly below the first near the bottom). **Figures 5.15 - 5.18** show the relative phase measurements made for both the red (right) and blue (left) laser light. Each point along the x-axis represents a different horizontal location for the set of two points between which the phase measurement is made. The error bars are the average error for all data points for the particular phase map from which that graph is based. In each figure, the top set of graphs is of the raw phase data, while the bottom set has been corrected by the reference interferogram (an interferogram made from the hologram and the live test cell with no gradients). The bottom set generally shows obvious improvement from the top in the sense that the phase across the cell is closer to being flat. The improvement in other cases is more subtle and is really only appreciated when the temperature and concentration calculations are made based on the phase measurements. Relative changes in the red and blue measurement of a few hundredths of a fringe can result in dramatic differences in the calculated values of temperature and concentration based on the TCHI equations.

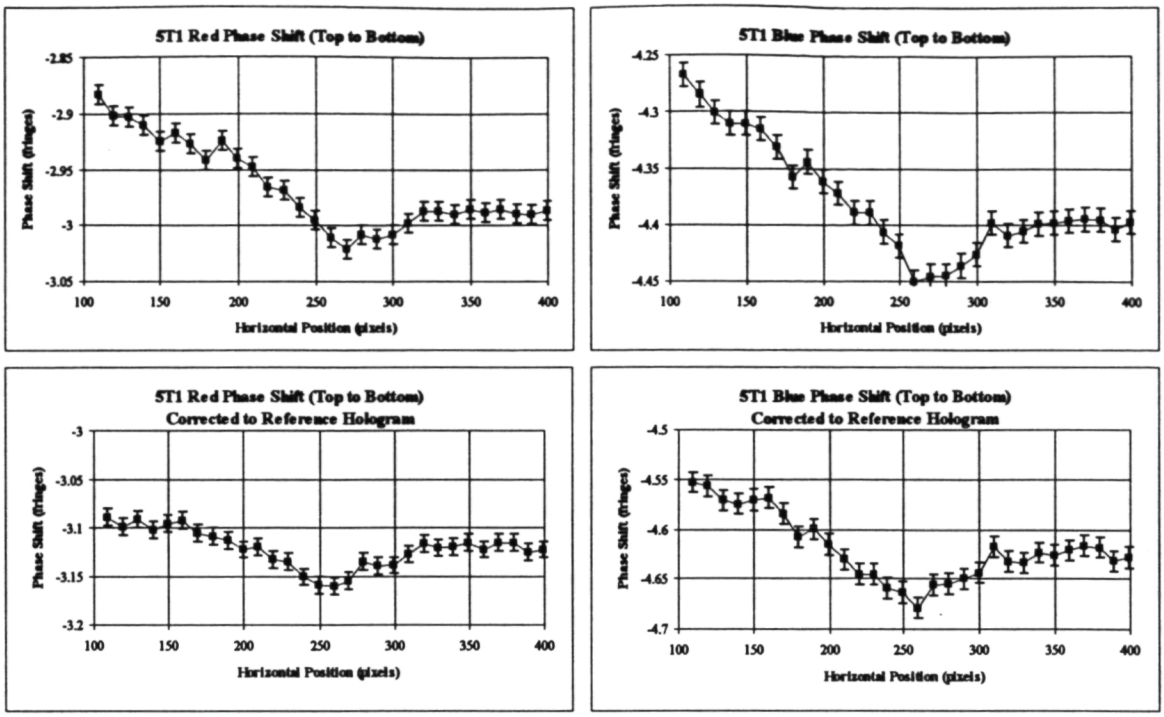

Figure 5.15. Relative phase measurement between points along a horizontal lines near the top and bottom of the test cell for Interferogram 5T1.

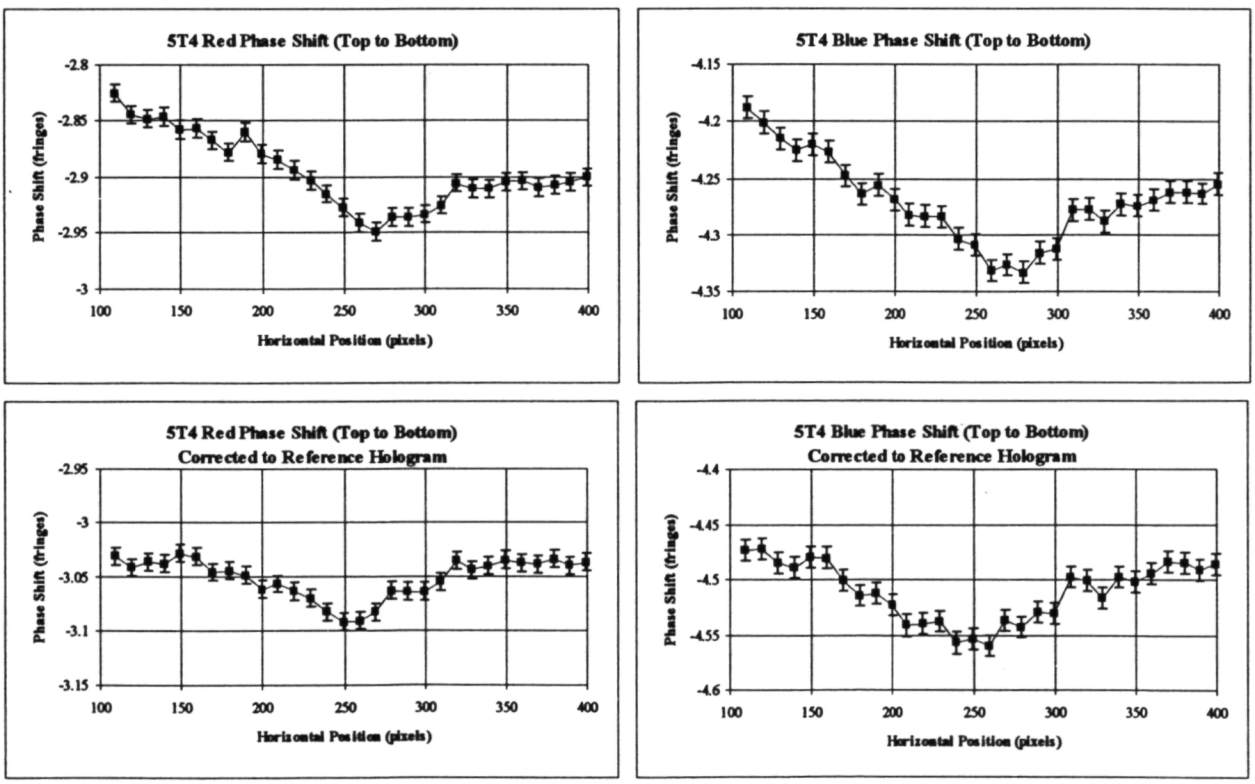

Figure 5.16. Relative phase measurement between points along a horizontal lines near the top and bottom of the test cell for Interferogram 5T4.

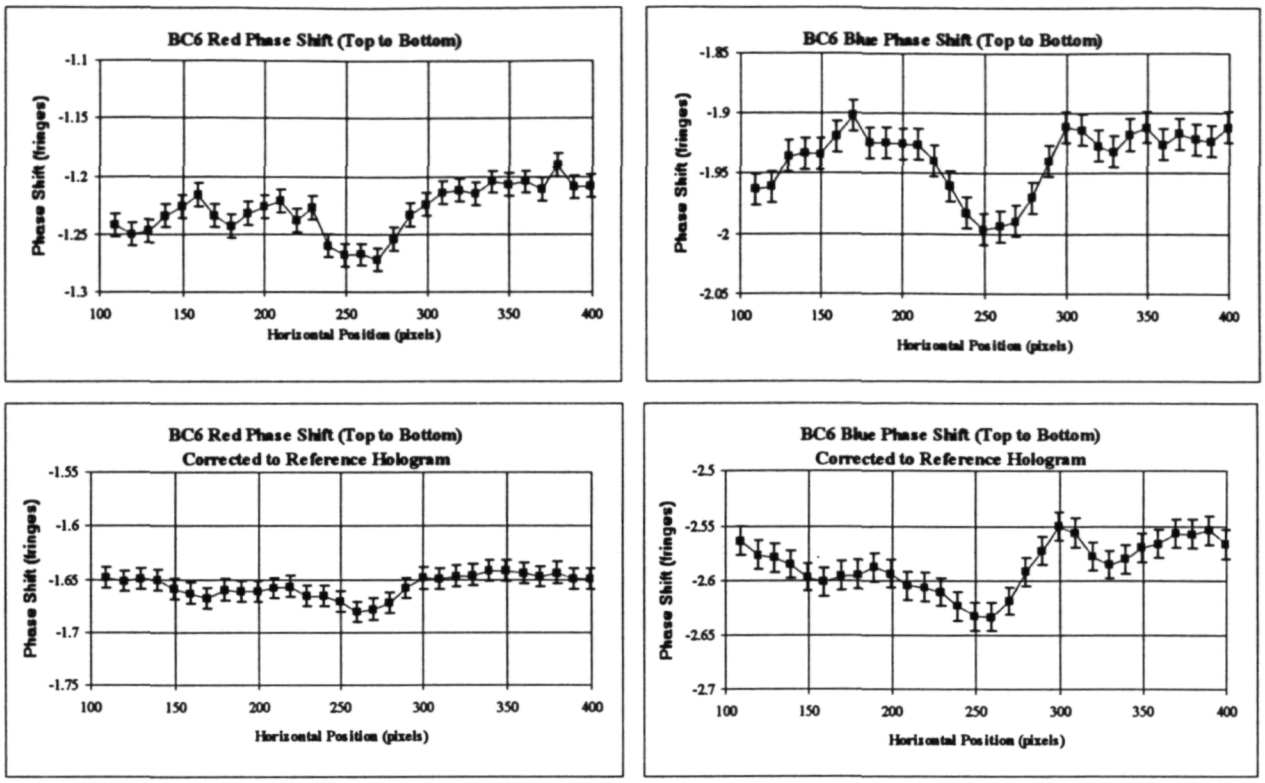

Figure 5.17. Relative phase measurement between points along a horizontal lines near the top and bottom of the test cell for Interferogram BC6.

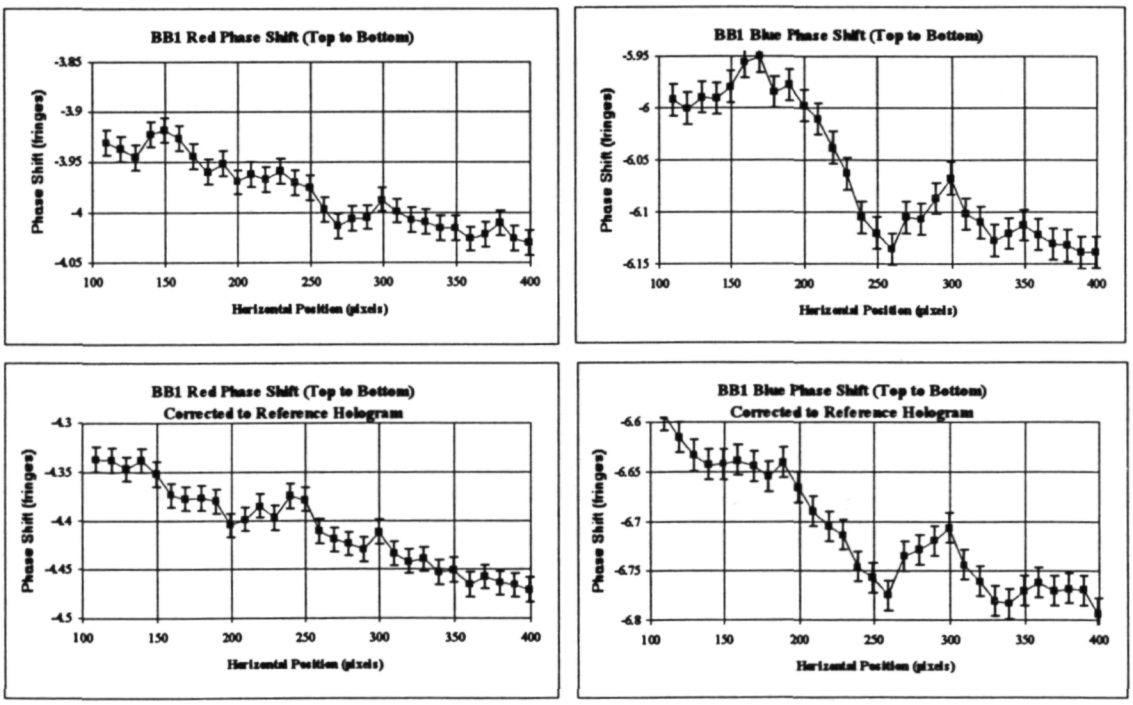

Figure 5.18. Relative phase measurement between points along a horizontal lines near the top and bottom of the test cell for Interferogram BB1.

5.5.4 TCHI Results

As outlined in Section 3.3, several corrections in the phase data were required before successful results could be obtained. For each correction in the phase data, new values of the scale factors in Section 5.4 for dn/dT and dn/dc based on published values had to be made ($s_{dn/dT}$, $s_{dn/dc}$, $s_{dn/dT,k}$, and $s_{dn/dc,k}$). This was necessary because the phase change from top to bottom was different when the phase map of the interferogram was altered by one of these corrections. A list of the three types of corrections evaluated, along with the corresponding scale factors for dn/dT and dn/dc, are given below in Table 5.4. These scale factors are multiplied by the value of $dn/dc_{441.6}$ based on Lu's equations and the value of $dn/dT_{441.6}$ based on the Tilton water data.

Table 5.4.
Correction factors for dn/dT and dn/dc at $\lambda = 441.6$ nm for the various types of corrections made to raw phase data.

	Correction Factors to dn/dT and dn/dc			
	Red Interferograms		Blue Relative to Red	
Type of correction	dn/dT	dn/dc	dn/dT	dn/dc
No Correction	1.2435	1.585	1.0201	0.9984
Plate tilt	1.374	1.585	1.0222	1.0021
Plate tilt & subtract ref. hologram	1.445	1.605	1.0156	1.0241
Plate tilt, ref. hologram, chromatic aberation	1.446	1.605	0.9981	1.0233

Figure 5.19 shows the results of applying the TCHI equations to the raw phase data. The four plots show temperature and concentration difference between points near the top and bottom of the test cell at various locations across the cell. One interferogram from each of the four possible gradient conditions possible is shown. Those conditions are:

1. No gradient (reference interferograms). $\Delta T = 0$ °C, $\Delta c = 0$ g/liter.
2. Temperature gradient only (used also to calibrate $dn/dT_{441.6}$). $\Delta T = 1.35$ °C, $\Delta c = 0$ g/liter.
3. Concentration gradient only (used also to calibrate $dn/dc_{441.6}$). $\Delta T = 0$ °C, $\Delta c \approx -0.55$ g/liter.
4. Both temperature and concentration gradients. $\Delta T = 1.35$ °C, $\Delta c \approx -0.55$ g/liter.

The broad variations, especially evident in the plots for interferograms BC7 and BB2, are a result of the values of dn/dT and dn/dc producing a very small denominator term, $(\partial n/\partial c)_j(\partial n\partial T)_k-(\partial n/\partial c)_k(\partial n/\partial T)_j$, which makes the equations extremely sensitive to the slightest phase variations. It is interesting to note that even in these cases, the correct value of Δc is calculated at data points where the correct value of ΔT resulted from the phase measurement. It is this fact that gave us confidence that the correct answer really was contained in the phase data, even though the initial results looked so chaotic.

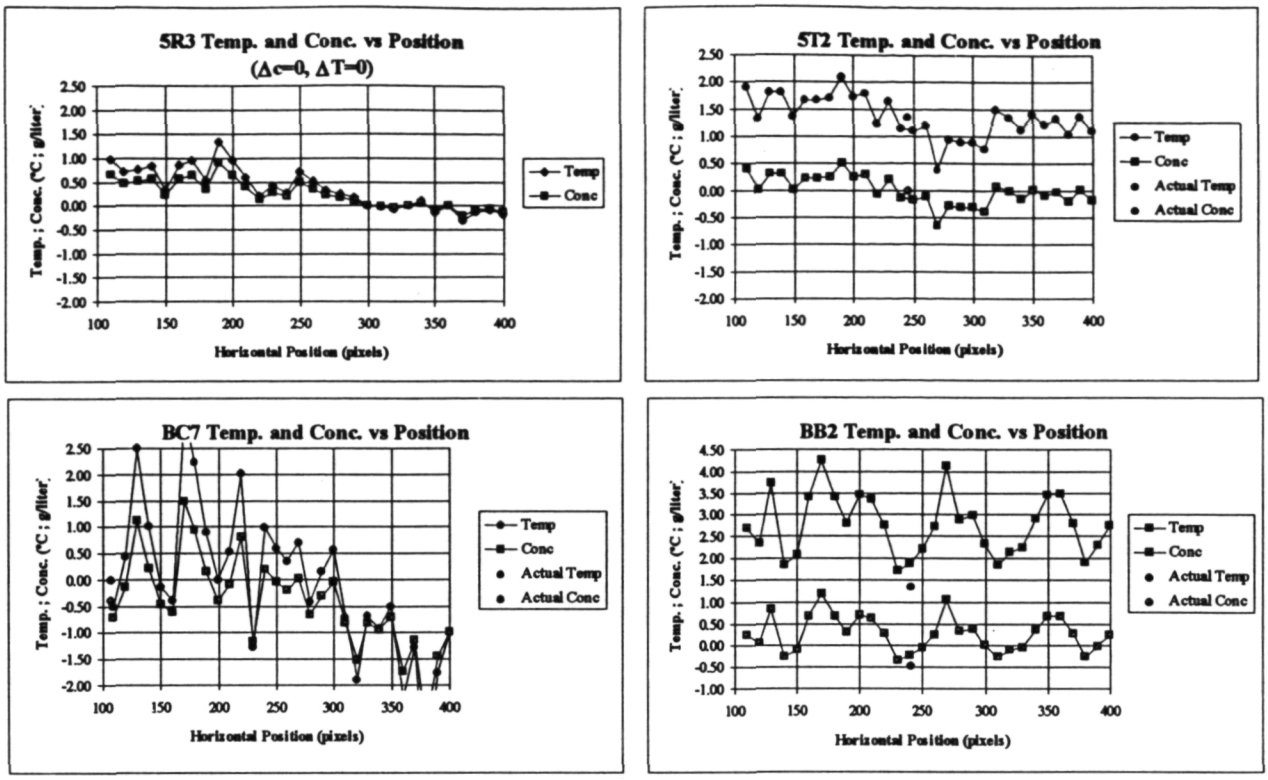

Figure 5.19. TCHI results using raw phase data.

The most obvious correction to make in the phase data was to correct for tilt in the hologram. The method for doing this has been given in Section 3.3, and the results of correcting the phase measurements in this manner are given in **Figure 5.20**. While fluctuations are still broad in many cases, the average values for the 30 different locations across the cell are seen to be approaching the correct values for ΔT and Δc.

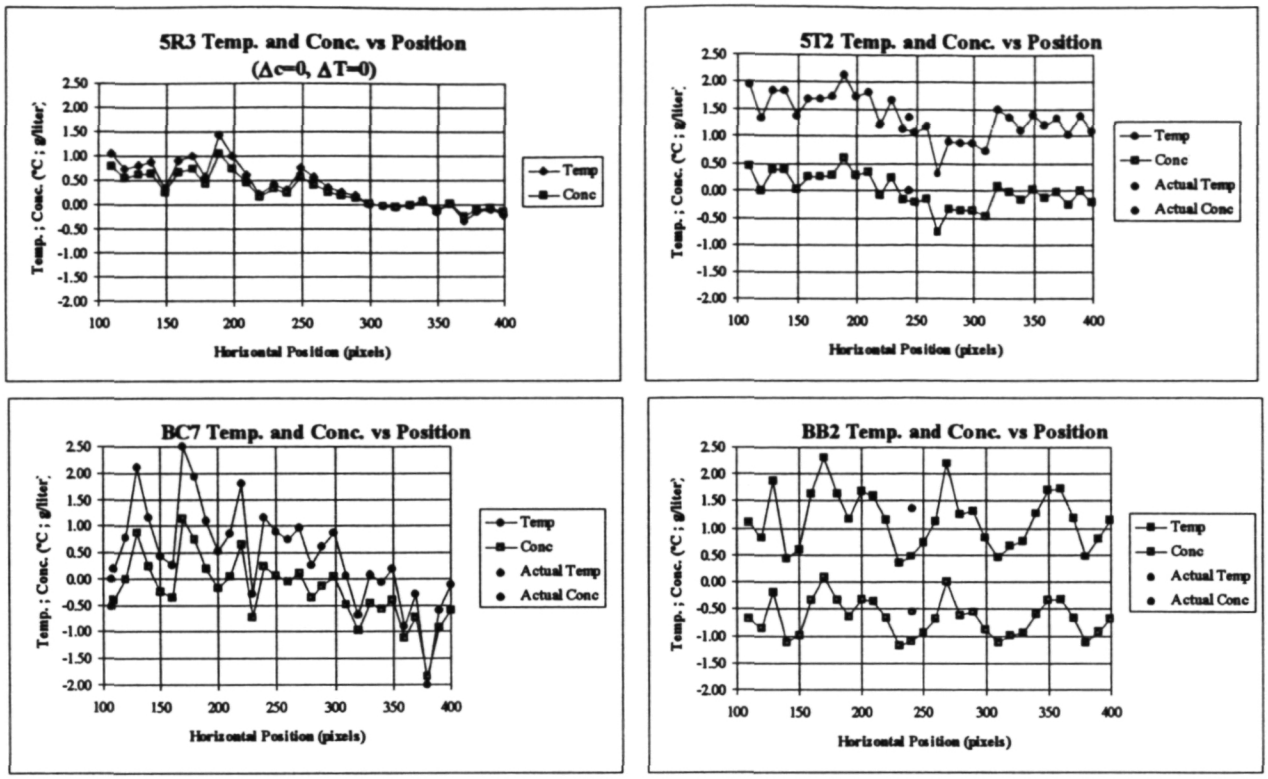

Figure 5.20. TCHI results when hologram tilt corrections are incorporated into the phase measurement data.

The next correction made to the phase data was to subtract off the reference interferogram from all subsequent interferograms containing temperature and/or concentration gradients. The wild fluctuations in ΔT and Δc are now seen to dampen considerably. Of special interest is the dramatic change in the reference hologram, 5R3. The average values of ΔT and Δc in this case is significantly closer to zero, which is the expected value if not gradients are present in the test cell. The interesting aspect of this is that 5R3 is not directly effected by the subtraction of the reference interferogram, since it is the reference interferogram (if 5R3 were subtracted from itself, then the red/blue phase measurements would be exactly zero at all locations, and the plot of ΔT and Δc would simply be a straight line at $\Delta T = \Delta c = 0$). The superior results in this particular case stem from the fact that the derived value of $dn/dT_{441.6}$ and $dn/dc_{441.6}$ are such that the denominator of the TCHI equations is now larger and small phase errors are therefore less critical.

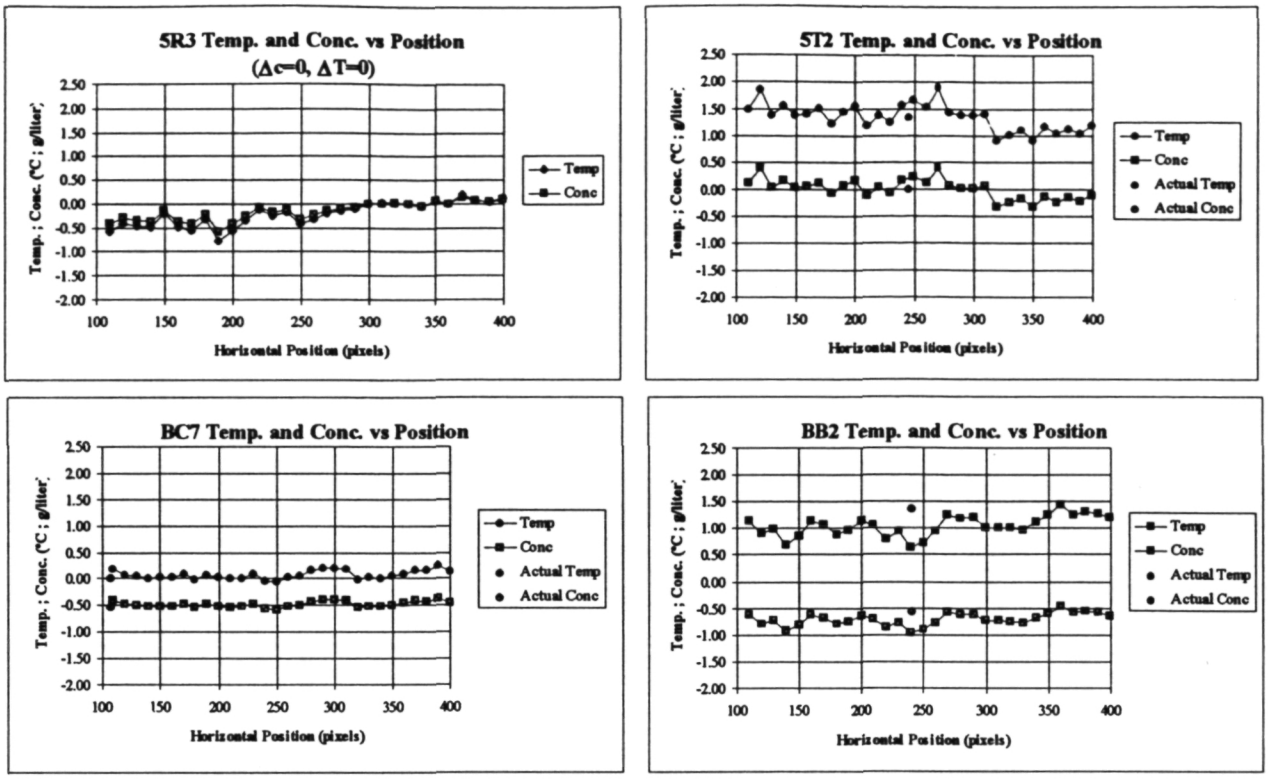

Figure 5.21. TCHI results when phase data is corrected for hologram tilt and the reference interferogram is subtracted off all subsequent interferograms.

The last correction to be applied to the phase data was to adjust for the change in magnification between the red and blue interferograms. The resulting plots are shown for a large number of cases in **Figures 5.22** and **5.23**. Variations in the calculated values of ΔT and Δc across the cell are even smaller now, with the average value being very close to that measured by independent means. A summary of the results for each case is shown in tabular form in Table 5.4. The last two columns show the amount of phase shift in the red and blue phase data resulting from the tilt and magnification corrections. The table shows that the variation of the calculated values of ΔT was $\pm$ 0.14 °C to $\pm$ 0.27 °C, while Dc variations were between $\pm$ 0.06 g/l to $\pm$ 0.19 g/l, while the average values were within 0.2 °C and 0.15 g/l of the values determined using other means for ΔT and Δc, respectively.

Table 5.5 summarizes the cell conditions for each interferogram analyzed and **Table 5.6** shows the values of dn/dT and dn/dc calculated based on the conditions in **Table 5.5**. The last two columns of **Table 5.6** show the corrected values of dn/dT and dn/dc for the blue light after all corrections were made in the phase data.

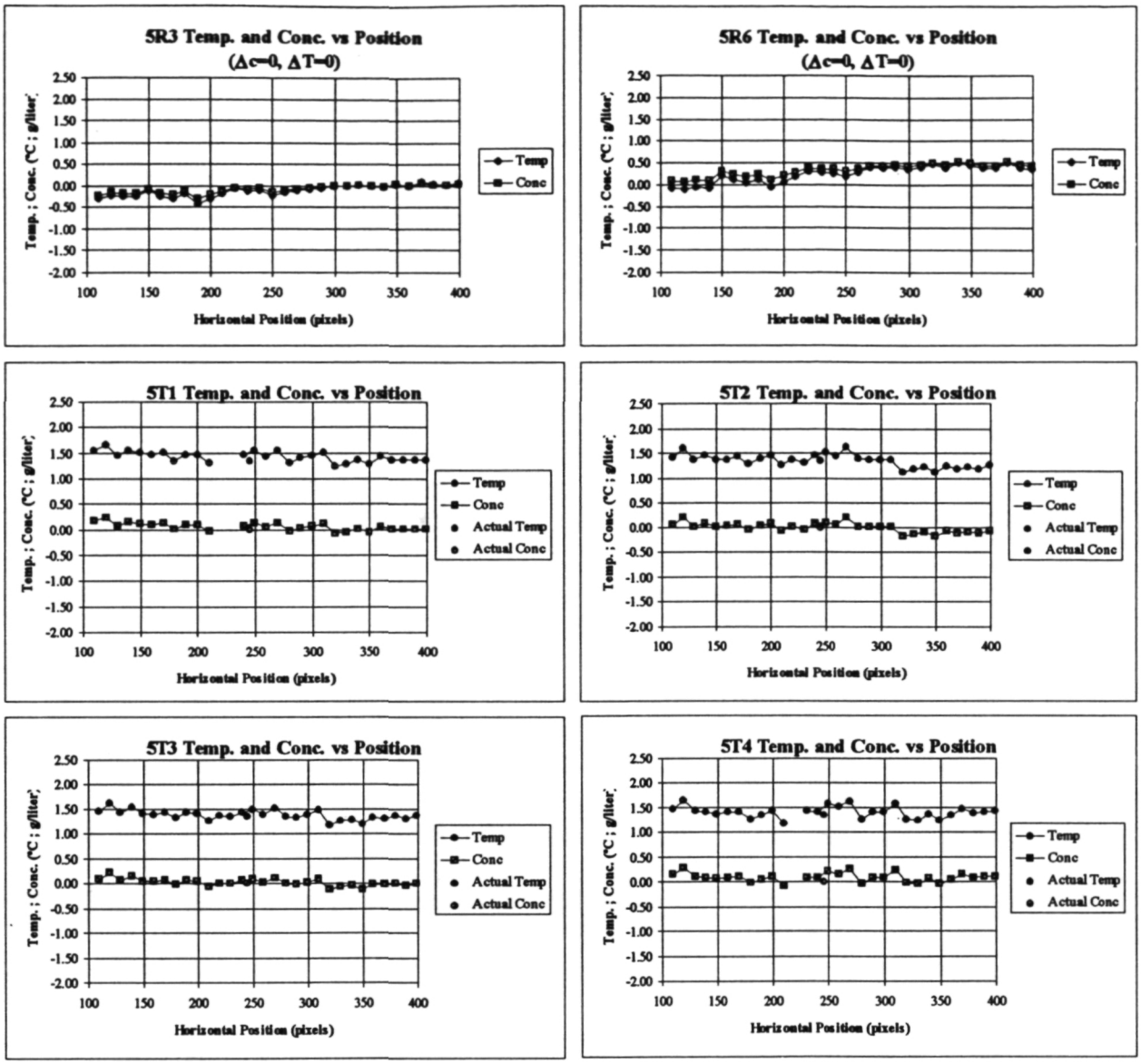

Figure 5.22. TCHI results using Hologram 5 of the seventh experimental series when all phase corrections are made to interferograms.

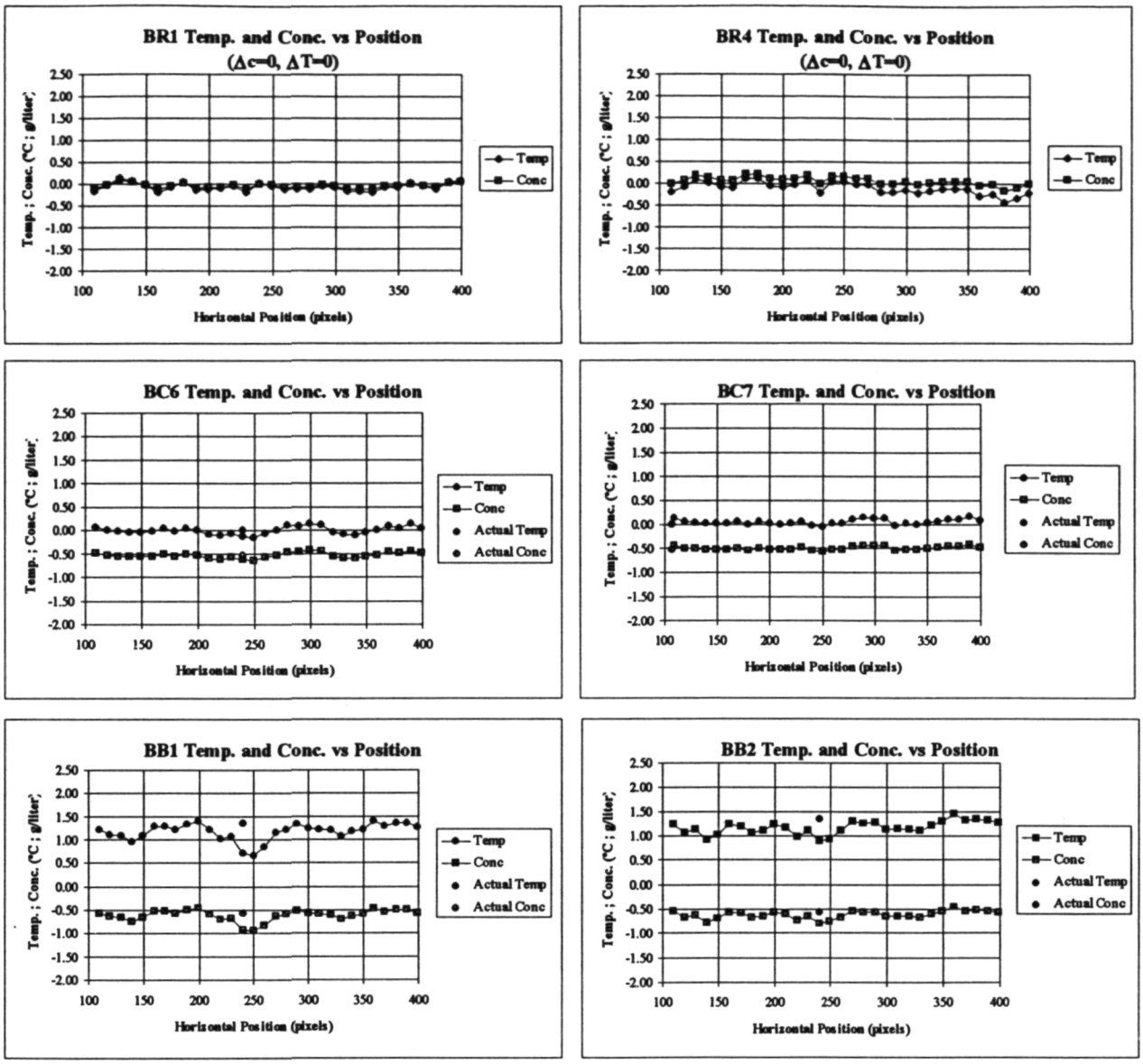

Figure 5.23. TCHI results using Hologram B of the seventh experimental series when all phase corrections are made to interferograms.

Table 5.4.
Summary of final results from TCHI demonstration.

	Actual Values		Two Color Values		Two Color Std. Dev.		Phase correction	
	Temp	Conc	Temp	Conc	Temp	Conc	Red	Blue
Interferogram	(°C)	(g/liter)	(°C)	(g/liter)	(°C)	(g/liter)	(fringes)	(fringes)
5T1	1.35	0.00	1.43	0.06	0.10	0.08	0.279	0.306
5T2	Áš¢x¢õxõ	0.00	1.35	0.00	0.13	0.10	0.282	0.319
5T3	1.35	0.00	1.38	0.03	0.10	0.07	0.340	0.406
5T4	1.35	0.00	1.41	0.09	0.12	0.09	0.374	0.456
BC6	0.00	-0.50	0.00	-0.53	0.08	0.06	-0.002	0.061
BC7	0.00	-0.50	0.05	-0.50	0.05	0.04	0.016	0.079
BB1	1.35	-0.53	1.17	-0.62	0.18	0.12	-0.217	-0.293
BB2	1.35	-0.53	1.16	-0.62	0.14	0.08	-0.174	-0.229

Table 5.5.
Temperature and concentration conditions for the various interferograms made using Holograms 5 and B.

Interf. Name	Temperature (°C)				Conc.	Δ^T	Δ^c
	Top	Bottom	Average	Block	g/liter	°C	g/liter
5R1	---	---	22.60	22.60	0.000	0.00	0.000
5R2	---	---	22.60	22.60	0.000	0.00	0.000
5R3	22.60	22.60	22.60	22.60	0.000	0.00	0.000
5R4	23.96	23.96	23.96	23.96	0.000	0.00	0.000
5R5	23.95	23.95	23.95	23.95	0.000	0.00	0.000
5R6	24.66	24.66	24.66	24.66	0.000	0.00	0.000
5R7	24.66	24.66	24.66	24.66	0.000	0.00	0.000
5T1	25.47	22.54	24.01	24.50	0.000	1.35	0.000
5T2	25.48	22.54	24.01	24.50	0.000	1.35	0.000
5T3	25.48	22.57	24.03	24.67	0.000	1.35	0.000
5T4	26.26	23.33	24.80	24.70	0.000	1.35	0.000

Interf. Name	Temperature (°C)				Conc.	Δ^T	Δ^c
	Top	Bottom	Average	Block	g/liter	°C	g/liter
BR1	20.00	20.20	20.10	20.13	0.000	0.00	0.000
BR2	20.10	20.30	20.20	20.27	0.000	0.00	0.000
BR3	20.20	20.30	20.25	20.30	0.000	0.00	0.000
BR4	21.95	22.00	21.98	22.07	0.000	0.00	0.000
BC1			20.25		0.649		-0.700
BC4	20.90	21.10	21.00	21.00	0.649	0.00	-0.586
BC5	21.00	21.00	21.00	21.07	0.649	0.00	-0.569
BC6	21.90	22.00	21.95	21.95	0.649	0.00	-0.531
BC7	21.90	22.00	21.95	21.97	0.649	0.00	-0.531
BB1	22.67	19.73	21.20	21.27	0.649	1.35	-0.562
BB2	22.67	19.73	21.20	21.53	0.649	1.35	-0.554

Table 5.6.

Refractive index information for the various interferograms made using Holograms 5 and B.

	Red (λ=632.8 nm)			Blue (λ=441.6 nm)		
Interf. Name	n	dn/dc	dn/dT	n	dn/dc	dn/dT
	—	liter/g	1/°C	—	liter/g	1/°C
5R1	1.331507	1.962E-04	-1.398E-04	1.33903024	2.126E-04	-1.447E-04
5R2	1.331507	1.962E-04	-1.398E-04	1.33903024	2.126E-04	-1.447E-04
5R3	1.331507	1.962E-04	-1.398E-04	1.33903024	2.126E-04	-1.447E-04
5R4	1.331376	1.937E-04	-1.460E-04	1.33889825	2.075E-04	-1.511E-04
5R5	1.331377	1.937E-04	-1.460E-04	1.33889924	2.076E-04	-1.510E-04
5R6	1.331306	1.924E-04	-1.491E-04	1.33882788	2.049E-04	-1.543E-04
5R7	1.331306	1.924E-04	-1.491E-04	1.33882788	2.049E-04	-1.543E-04
5T1	1.331371	1.936E-04	-1.462E-04	1.33889377	2.073E-04	-1.513E-04
5T2	1.331371	1.936E-04	-1.462E-04	1.33889328	2.073E-04	-1.513E-04
5T3	1.331369	1.936E-04	-1.463E-04	1.33889178	2.073E-04	-1.514E-04
5T4	1.331292	1.922E-04	-1.497E-04	1.33881411	2.044E-04	-1.549E-04

	Red (λ=632.8 nm)			Blue (λ=441.6 nm)		
Interf. Name	n	dn/dc	dn/dT	n	dn/dc	dn/dT
	—	liter/g	1/°C	—	liter/g	1/°C
BR1	1.331735	2.008E-04	-9.158E-05	1.33925658	2.221E-04	-9.498E-05
BR2	1.331726	2.006E-04	-9.194E-05	1.33924793	2.217E-04	-9.534E-05
BR3	1.331722	2.005E-04	-9.211E-05	1.33924359	2.215E-04	-9.552E-05
BR4	1.331566	1.973E-04	-9.808E-05	1.33908881	2.150E-04	-1.016E-04
BC1	1.331723	2.005E-04	-9.211E-05	1.33924458	2.216E-04	-9.552E-05
BC4	1.331656	1.992E-04	-9.473E-05	1.33917851	2.187E-04	-9.819E-05
BC5	1.331656	1.992E-04	-9.473E-05	1.33917851	2.187E-04	-9.819E-05
BC6	1.331569	1.974E-04	-9.799E-05	1.33909208	2.151E-04	-1.015E-04
BC7	1.331569	1.974E-04	-9.799E-05	1.33909208	2.151E-04	-1.015E-04
BB1	1.331638	1.988E-04	-9.542E-05	1.33916057	2.180E-04	-9.890E-05
BB2	1.331638	1.988E-04	-9.542E-05	1.33916057	2.180E-04	-9.890E-05

5.5.5 Comparison to Expected Results Based on Error Analysis

The expected error of the measurements of ΔT and Δc using the TCHI technique, based on uncertainties in the ΔN measurement and on the temperate and concentration conditions of the solution, can be seen in Table 3.1 to be around 0.11 °C and 0.08 g/l, respectively. These numbers represent the average error expected in calculated values of ΔT and Δc based on the given measurements error in ΔN. Inspection of Table 5.4 shows that the actual variation in the data was between 0.05 and 0.18 °C for ΔT and between 0.04 and 0.12 g/l for Δc, depending on the interferogram. This shows a remarkable correlation to the predicted results and demonstrates the capability of the analytical error analysis to predict how well the TCHI method will work in a particular set of circumstances. The average error in the ΔT and Δc readings from the "actual" values was about 0.07 °C and -0.05 g/l (or 5.4 % and -9.8%), based on the data in Table 5.4.

Statistically, for a sampling of 30 data points (the case for these interferograms), the average error might be expected to be smaller. This discrepancy can be attributed to inaccuracies in the independent measurements of ΔT and Δc and in some systematic, unaccounted-for error in the phase measurements. Overall, the results seem extremely good, given the many corrections that had to be implemented into the raw data.

5.5.6 Comparison of 4 and 5 bucket Algorithms

The phase shift interferometry algorithm used by MetroLaser was utilized for what is known as a four bucket algorithm to calculate phase (i.e., four interferograms were used to produce a phase map). An algorithm using 5 interferograms has also been written, and was utilized by Bill Witherow at MSFC in producing phase maps from interferogram data. A comparison was done on some of the earlier data obtained using sucrose (experimental series 5) to see if any improvement was gained using the 5 bucket algorithm. The results of the comparison are shown in Tables 5.7 and 5.8 below. In each table, the minimum, maximum, and average fringe error is reported after eliminating points that had extremely high errors were eliminated (the number eliminated in each case is seen in the last column). As can be seen by comparing the two tables, the average error was usually better for the five bucket algorithm, though only by a slight amount. The maximum error for each data set showed even less difference between the two algorithms. The difference between the two approaches was slight enough that the four bucket algorithm, which had been used initially, continued to be used in later data. Though never tested, it is thought that the difference in the two approaches would be even less in data from the seventh experimental series, where frame averaging and improvements in the breadboard resulted in a noise improvement by more than a factor of 2.

Table 5.7.

Maximum, minimum, and average error for selected interferograms from the fifth experimental series using the four bucket algorithm.

Four Frame Phase Map Error

Interferogram		Error (fringes) Min	Max	Ave	# of Pts. Eliminated
6C0	Red	0.006	0.191	0.021	1
	Blue	0.004	0.089	0.023	18
8B0	Red	0.004	0.048	0.021	1
	Blue	0.004	0.088	0.027	0
8R3	Red	0.004	0.044	0.016	0
	Blue	0.004	0.088	0.023	0

Table 5.8.

Maximum, minimum, and average error for selected interferograms from the fifth experimental series using the five bucket algorithm.

Five Frame Phase Map Error

Interferogram		Error (fringes) Min	Max	Ave	# of Pts. Eliminated
6C0	Red	0.004	0.238	0.018	2
	Blue	0.003	0.057	0.021	3
8B0	Red	0.004	0.038	0.018	0
	Blue	0.007	0.093	0.025	0
8R3	Red	0.004	0.040	0.014	0
	Blue	0.004	0.091	0.021	0

6. FLIGHT BREADBOARD PROGRAM

6.1 Breadboard Description

A schematic of the flight breadboard is shown in **Figure 6.1** along with a photograph of the system before the optical isolator (described later) was added. The breadboard was developed and evaluated at MetroLaser for its suitability to function as a flight system to be used in TCHI. A variety of designs were considered in the production of the breadboard. The philosophy taken was that we should not duplicate the excellent TCHI breadboard already in operation at MSFC employing conventional optics, large lasers, and standard optical components. Instead, we opted for the design of a system that could be used to develop the advanced optical concepts that ultimately would be employed in a spaceflight system, such as fiber optics, diode lasers, and holographic optical elements.

The system consisted of two lasers with couplers to launch their output into a fiber optic system. The fiber optic system contained two inputs from each laser along with hardware to split each input into two outputs and to control or shift the phase of each input. Only one input was used for each laser, with the remaining input incorporated for use in the potential implementation of a feedback controller. The four output fibers (two for each laser) were paired together with one output from each laser constituting a set that was mounted in a special holder that allowed the fiber centers to be placed within approximately 200 um of one another. One output set was used as a reference/reconstruction beam, while the other was used as the object/live beam. The special fiber holders were placed in tilt stages for directing the output toward the only conventional optics in the system: two four inch collimating lenses.

An in-house test cell, originally constructed for another program, was used as the subject of holograms and interferograms produced during evaluation of the breadboard as a TCHI system. The cell consisted of a Plexiglas container and a thermoelectrically controlled crystal growth sting of the variety used in the IML-1 Spaceflight. A temperature gradient could be produced in the test solution by controlling current through a thermoelectric inside the sting. Since the cell and sting were not configured with a temperature controller, no quantitative measurements were

available in the initial tests performed at MetroLaser. To set up a temperature gradient, a current of approximately 200 mA was run through the thermoelectric, resulting in a steady-state condition around the sting.

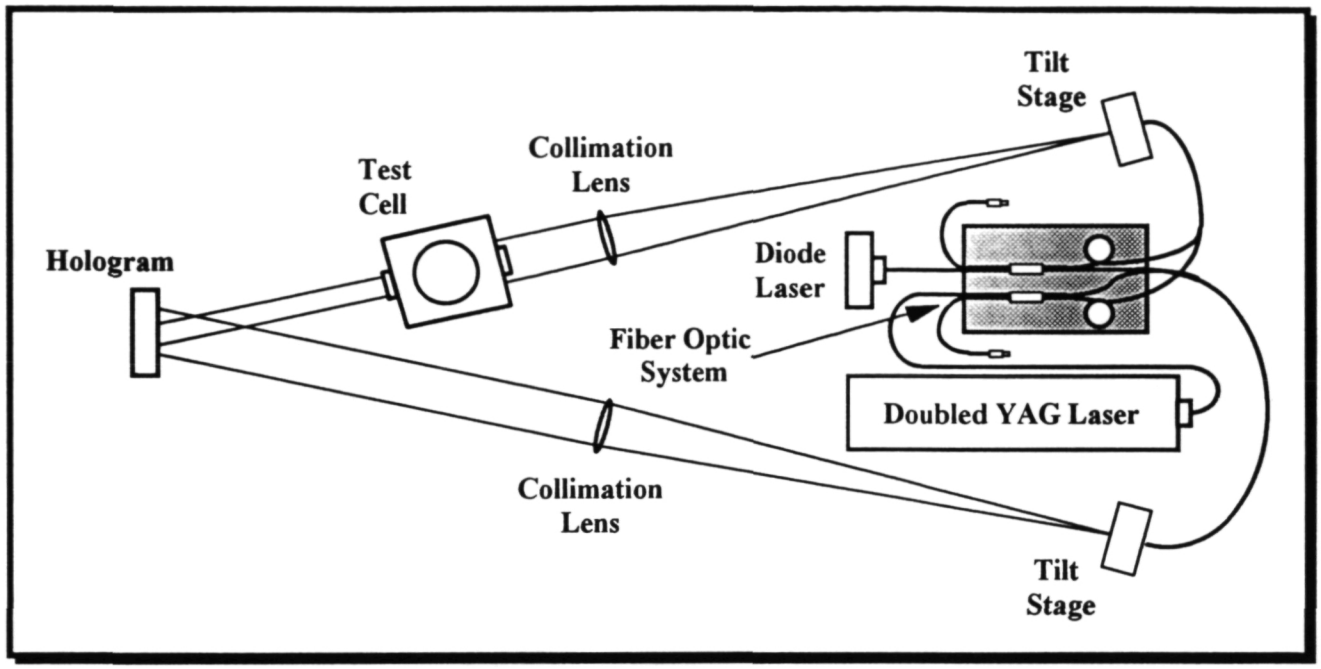

Figure 6.1. Schematic of the advanced fiber optic flight breadboard tested at MetroLaser.

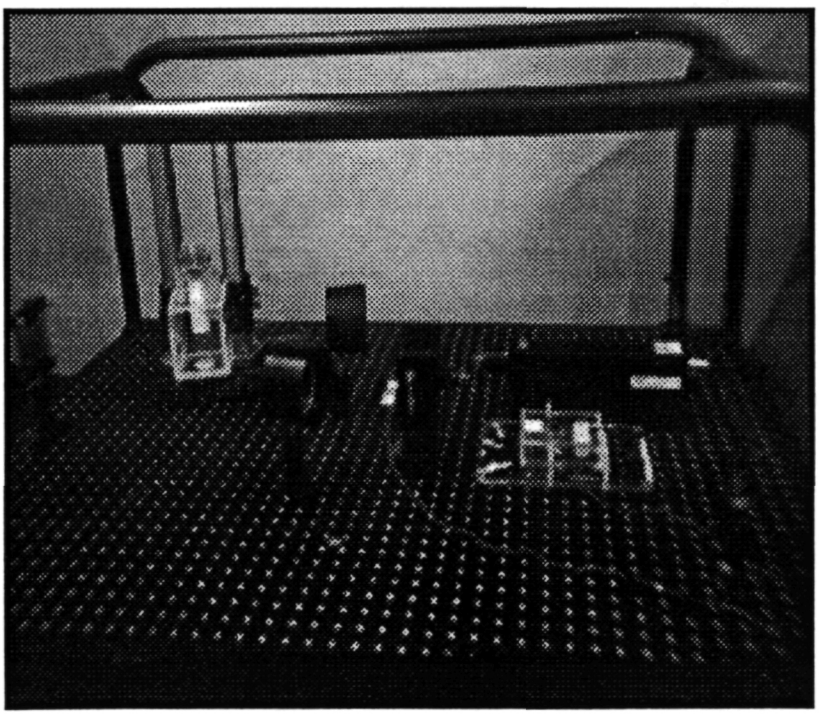

Figure 6.2. Photograph of the fiber optic flight breadboard tested at MetroLaser.

The fiber optic based design has several advantages. Most importantly, it completely eliminates the need for mirrors that require careful alignment, are very sensitive to vibration, and consume a great deal of physical space. The fiber system also allows phase modulation to be introduced directly onto the fiber by using a piezo-electric element to stretch the fiber. This phase modulation scheme can be used both in the reconstruction process and as an active fringe stabilization mechanism during recording. Because the fibers are of such a small diameter (typically 100-200 μm), it is possible to place them close together and use the same collimating optics, reducing the complexity of the optical layout and alignment requirements. **Figure 6.3** illustrates the errors introduced from using a single achromatic collimating lens for both colors.

The two offsets introduced from using the same lens for both colors are 1) a linear displacement d, and 2) an angular deviation θ. The linear displacement is equal to the fiber core separation distance. Because the fiber diameters are so small, the cores can be placed very close together by simply gluing the two fibers together. This results in a linear displacement of less than 400 μm. The angular deviation is a simple ratio of the core separation to the focal length (for small angles). Expanding the output of the fiber for a 2 inch collimated beam requires a 30 cm focal length lens (light exits the fiber at approximately 10 degrees) which results in an angular displacement of 0.06 degrees. This small misalignment would have a negligible effect.

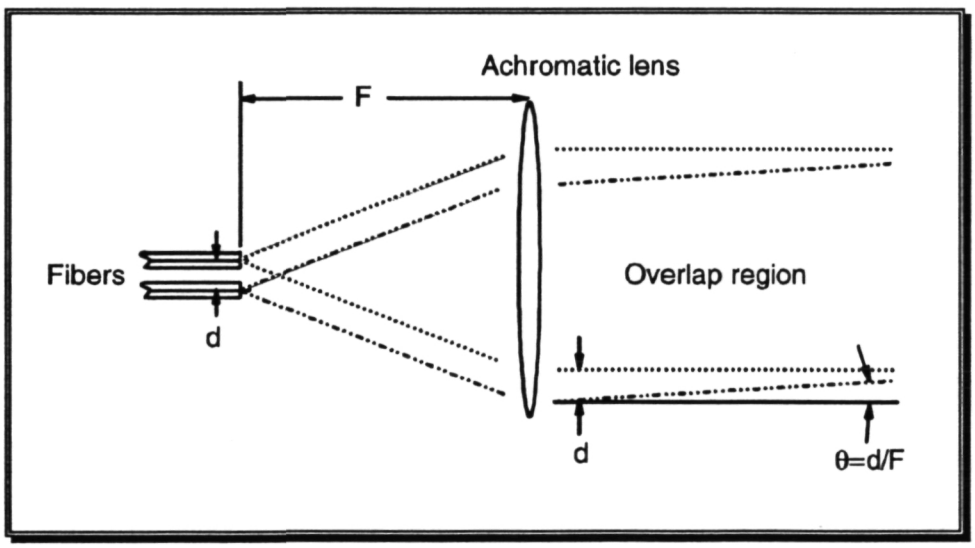

Figure 6.3. Recombination of the Two Colors from a single lens.

6.1.1 Lasers and Associated Hardware

Two laser were used in the TCHI flight breadboard. A frequency doubled YAG made by ADLAS was used to produce a 50 mW beam with a wavelength of 532 nm, while a diode laser from Laser Max was used to produce a 20 mW beam at 680 nm. The two were chosen in an effort to provide the greatest difference in wavelength in units that were extremely small and light, and therefore suited for space flight experimentation. Each laser was couple to the fiber optic system using a compact, rugged fiber launcher suitable for flight systems and manufactured by OZ Optics, Ltd. in Canada.

The YAG laser was especially well suited for the holographic application since it had a rated coherence length of 25 meters. The unit was cooled with a fan that could be removed in the final system so long as good thermal contact is provided with a suitable heat sink. This laser was used in the system almost immediately to produce phase shifted interferograms of a temperature gradient around a crystal growth sting. The YAG laser produced holograms with a diffraction efficiency of approximately 8%.

In order to be suitable for holography, the diode laser required a temperature controller that would maintain a constant temperature to within 0.1 °C. Unlike the YAG laser, initial use of the diode laser produced very poor quality holograms with a diffraction efficiency of much less than 1%. A series of repeatable vertical lines appeared on the holograms that seemed to have at least two different spatial periods. We postulated that these lines were caused by the interference of two or more modes from the laser interfering with one another at the hologram plane. The origin of the multiple wavelengths was believed to be the result of mode hopping in the laser cavities due to reflections from the fiber tips back into the laser. To test this hypothesis we performed a variety of experiments. A holography system was assembled using conventional optics in place of the fiber system. With no temperature control of the diode, a hologram with the same set of vertical lines resulted. However, when the temperature controller was used with the diode laser, the mode lines disappeared and a hologram with a diffraction efficiency of approximately 5% resulted. Similar behavior of a diode laser had been observed in experiments by Bill Witherow at MSFC. This seemed to confirm that the problem was due to multiple modes set up by fiber reflections.

Since the input ends of the fibers had been cut with a 7° angle, the feedback problem appeared to be from the output end of the fiber. The feedback problem had been previously observed in the YAG laser in terms of power fluctuations, especially during warm up. In the case of the YAG laser, the doubling crystal appeared to offer sufficient isolation from the laser cavity to prevent any modal problems. Putting a cut on the output end of the fiber was considered as a solution to the diode laser feedback problem. This should have worked if the cut angle were greater than the acceptance angle of the single mode fiber (approximately 6°). The major drawback to this solution, if it did indeed work, was that the feedback from the output face could no longer be used to control and step the phase of the holograms as has been previously proposed.

An alternative solution that, in the end, was actually implemented was an optical isolator between the diode laser and the fiber coupler that incorporated a Faraday rotator. The Faraday rotator is used to rotate the polarization of the laser output by 45 degrees. Any retroreflected light passes back through the Faraday rotator a second time and is rotated an additional 45 degrees. A polarizer between the laser and the Faraday rotator is then used to attenuate the light 30 to 40 dB before entering the laser cavity. Suitable units of this type were found at a cost of $2,400 to $4,800 depending on the vendor and particular configuration chosen. The unit selected was bought from OZ Optics, Ltd., the same company that manufactured the fiber launcher. The impact to the program was a slightly larger unit (approximately 1" x 1" x 4") and an increase in material cost.

Holograms were successfully made using the fiber optic system once the optical isolator was incorporated.

6.1.2 Fiber Optic Assembly

The fiber optic system constituted the heart of the flight breadboard design and is represented schematically in **Figure 6.4**. The system consisted of four FCPC connectors, two fiber optic couplers and a special output coupler. One of the two FCPC connectors going into each of the couplers was connected to each of the two lasers. The fibers into and out of each coupler were single mode fibers that were optimized, along with the coupler itself, for the wavelength of the laser to be used (λ=532 and 680 nm). Each coupler was designed to produce a 50/50 output into the two fibers on the output side of the coupler for the design wavelength. The other input into the coupler was incorporated for potential use as a feedback for either stabilizing or controlling the phase of the output from the fiber. One fiber from each of the couplers was cemented together in the special output coupler. This special arrangement allowed the core of each of the two fibers to be located within approximately 200 μm of one another, thereby virtually eliminating the alignment errors between the two colors in each output leg.

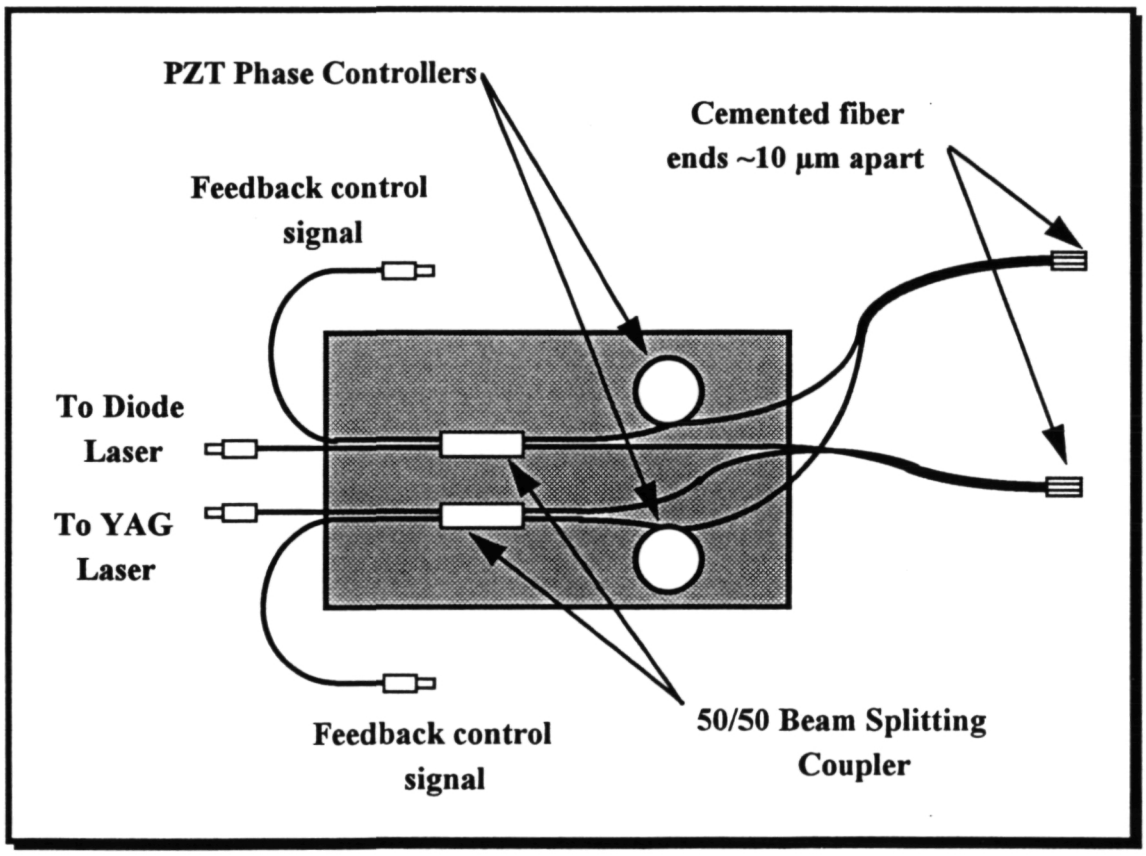

Figure 6.4. Schematic of the fiber optic system manufactured by Canadian Instruments.

Once aligned, the output characteristics from each laser were determined. The results of this testing are shown in **Table 6.1**. The uneven split of the power out of the diode laser between the

output legs shown in this table appears to be a result of improper design by the vendor of the coupler to produce a 50/50 split. The vendor did not actually have a laser with the 680 nm wavelength of the diode laser to be used in the system, but presumed he could extrapolate the performance at 680 nm based on the HeNe laser (λ=633 nm) he had in-house. It appears his extrapolation was either invalid or improperly calculated. Due to the long lead time involved in fabrication and subsequent modification of this system, it was decided to live with the current system which seemed to otherwise perform acceptably. The 3-to-1 split in the power can even be beneficial for holography, where a stronger reference beam can actually improve some aspects of the hologram.

Table 6.1.

Experimentally measured performance of the fiber optic breadboard.

				Power Efficiency at Fiber Output		
Laser	Rated Output	Measured Output	Extinction Ratio	Leg 1	Leg 2	Total
	(mW)	(mW)		(%)	(%)	(%)
Diode	20	18	90	10.5	37	47.5
YAG	50	55	30	25.5	22	47.5

The output from each leg for both lasers was set up as a Michelson interferometer to test the coherence of the output. The beams from each leg were approximately collimated and their interference resulted in a fringe pattern consisting of a set of concentric rings. The location of the one leg was changed to determine the coherence length of each laser. The diode laser was found in this manner to have a coherence length of approximately 5 cm, which slightly exceeded the manufacturer's specification, (assuming temperature could be controlled to within a 0.1 °C). This was enough to make holograms, although careful attention had to be made in matching path lengths of the object and reference waves. The YAG laser has a rated coherence length of greater than 25 m, which could obviously not be confirmed with the simple setup used here. A path length difference of approximately one-half meter was, however, tested and the fringes were still quite visible, as would be expected.

6.2 Experiment Description

Several experiments were performed to test both the individual components and the system as a whole. Component testing was described primarily in Section 6.1. Experiments to evaluate the system's suitability as a flight system for producing TCHI data is described in the this section.

6.2.1 Phase Shift Interferometry

The first experimentation done on the integrated system was to evaluate its ability to incorporate phase shift interferometry. The objective was to produce a usable hologram in two colors of a phase object and produce a phase map of this object using phase shift interferometry. The phase shifted interferograms were produced using a control circuit that drove the piezo-electric phase controllers. The circuit provided not only high voltage control to the piezo-electric driver, but also had a built-in ramp generator whose characteristics could be set using two pots.

Interferograms were captured of the hot and cold sting holograms interfered with the live test cell (sting off) using a Cohu CCD camera and a frame grabber manufactured by Imagination, Corp. The piezo-electric driver, which is part of the fiber optic assembly, was used to produce the phase shifted data. A ramp generator, which is included on the piezo-electric driver card, was utilized to produce a linear change in the phase with time. The ramp cycle was adjusted to approximately 5 seconds, over which time the voltage to the piezo-electric driver varied from -10 to +180 volts. With the fiber wrapped twice around the piezo-electric driver, this corresponded to a phase shift of about 3π. A program was written to grab four frames of data while the phase was being ramped with an equal time between frames of about 0.6 ±0.008 seconds; in which it stored the data to hard disk; and reformated the files with the correct header for the fringe analysis software. This resulted in four frames of data with equal phase shifts of close to 90°.

This capability of the breadboard may or may not ultimately be used in the actual flight system, since this system's primary purpose is to produce the holograms for TCHI interrogation. Reconstruction of the images in the holograms and production of phase shifted interferograms could use the same system, but might just as likely use a dedicated, ground based system using conventional optics such as the one currently set up at MSFC to actually prove the TCHI technique. The phase control capabilities may prove invaluable, however, if real time holographic interferometry were needed during the flight itself.

This experimentation, done early in the program, was carried out only with the double YAG laser portion of the system since, at the time, the diode laser could not be used to produce holograms in the fiber optic configuration due to the mode hopping problem discussed earlier. Successful results with the double YAG were sufficient, however, to prove this capability of the system in this regard and can easily be extrapolated to the diode laser leg now that it can also successfully produce usable holograms.

After checking out the system, holograms were then made with the YAG using the configuration shown in **Figure 6.1**. Holograms were made both with a steady temperature in the cell and with a temperature gradient created by running a constant current through the sting thermoelectric. These holograms were reconstructed and combined with the "live" image, and the results were digitized using a Cohu CCD camera. The gradient could be clearly seen in either hologram when the cell condition (either constant or gradient) was reversed during reconstruction. By varying the intensity of the live image, a very high fringe contrast was observed.

6.2.2. Demonstration of TCHI

Once the optical isolator was installed into the system, holograms could be successfully produced with both lasers. Two color holograms were then made using two collimated beams (**Figure 6.1** without the test cell). This demonstrated the capability of the fiber optic based system to produce holograms containing phase data that could later be used in a TCHI analysis.

6.2.3. Simulation of Microgravity

The optical components used to achieve miniaturization can be tested in terms of their ability to produce high quality TCHI data comparable to that produced in the laboratory breadboard and all appear to be excellent candidates for spaceflight. However, the question remains as to the unknowns that will be added by microgravity. The flight breadboard was designed and constructed so that it could be a candidate for testing in KC135 tests if these were deemed important. The factors that are obvious include the changes in stress placed on all components when gravity is removed. Secondly, the removal of convection as a cooling agent on the electronics and lasers becomes a signficant factor. These could be tested in KC135 flights. The expense of such flights are an incentive to searching for alternatives. The effects of removing gravity can be simulated by changing the orientation of the breadboard with respect to gravity. A worst case scenario would be to turn the breadboard upside down. In lieu of expensive KC135 tests, we elected to use these low cost simulations of gravity that would also give us the convenience of working in the laboratory environment where effects could be studied more carefully (and possibly be remedied).

7. EXPERIMENTAL RESULTS FROM FLIGHT BREADBOARD

Holograms have been made using the test cell for both hot and cold stings as well as with the sting off. The hot and cold sting holograms were interfered with the live test cell without any temperature or concentration gradients. This simulated the type of situation that would typically occur in actual space flight data in which the hologram contains the optical conditions of the cell during crystal growth and is interfered with a "neutral" cell (no temperature or concentration gradients) once it is on the ground.

A typical phase map produced from four phase-shifted interferograms from the fiber optic flight breadboard are shown in **Figure 7.1** for light from the YAG laser. The fringe analysis software was applied to these images to produce this phase map of a hot sting interfered with the neutral live test cell. **Figure 7.2** shows data from a vertical scan across this phase map.

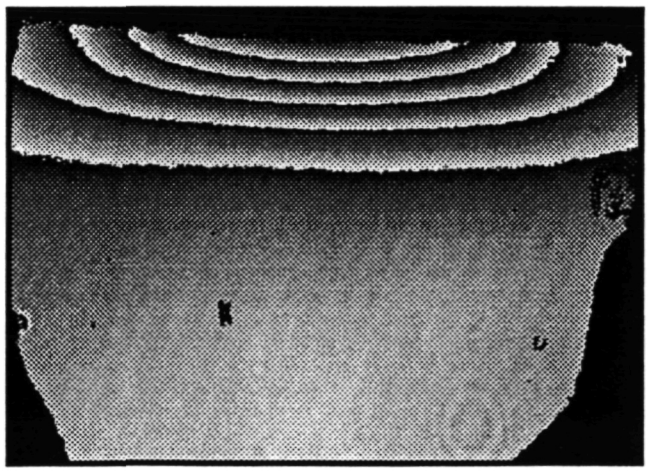

Figure 7.1. Phase map of a hot sting interfered with a live test cell (sting off) using directly digitized frames and the fiber optic breadboard.

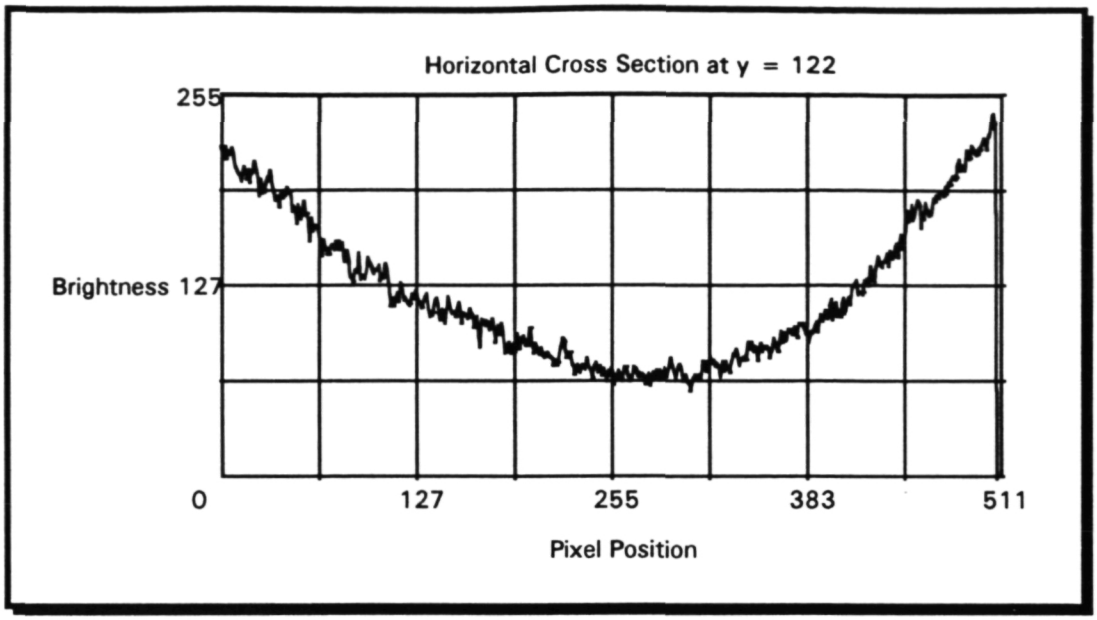

Figure 7.2. Phase data from fiber optic breadboard using the image directly from the frame grabber.

The frame grabber used at MetroLaser would only hold one frame of data, making it necessary to store each frame onto disk before the next frame was digitized. This slowed the rate at which the four frames of data could be taken. Files were written to a ram disk to speed this process, but the images could still not be stored faster than approximately 600 msec. The frame grabber used at MSFC allowed multiple frames to be grabbed at each phase and at rates of approximately 30 Hz. This permited the digitized data to be gathered more quickly, thus lowering the noise due to air currents and acoustics between frames. This type of system could also be incorporated into the fiber optic system.

As stated previously, the fiber optic system was used to produce two color holograms of a collimated beam. A photograph of the TCHI interferogram using the diode laser is shown in **Figure 7.3**. The lightest area in the right portion of the circle is undiffracted light that passed through a 2" aperture in front of the holographic plate used during recording and reconstruction. The darker area in the circle is the intersection of the diffracted and undiffracted light passing through the aperture (i.e., the hologram). The interferogram is essentially an infinite fringe, as would be expected from the interference of the two collimated beams.

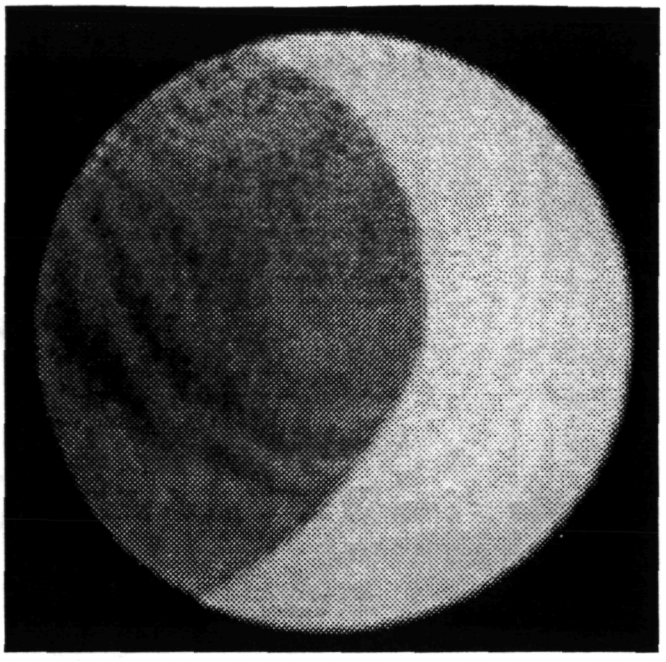

Figure 7.3. Diode laser (λ = 680 nm) reconstruction of an interferogram made from a TCHI hologram.

To simulate microgravity, the breadboard was tilted at an angle of approximately 20°, as shown in **Figure 7.4**. The result of this change in orientation is shown in **Figure 7.5**, where the horizontal fringes in the combination of the live beam and the hologram of the same beam are attributed to bowing in the 2" thick breadboard. The fringes could be removed by slight adjustments in the tilt of the fiber output, thus returning to an infinite fringe condition as in **Figure 7.3**. This demonstrated that holograms made in an environment producing different stresses on the flight breadboard (such as in microgravity), could be corrected through simple procedures.

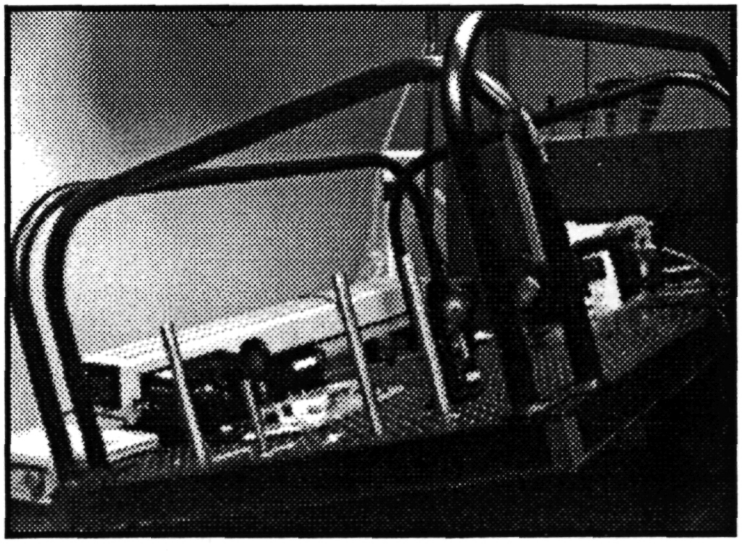

Figure 7.4. Photograph of breadboard tilted to simulate the effects of a microgravity environment on the system.

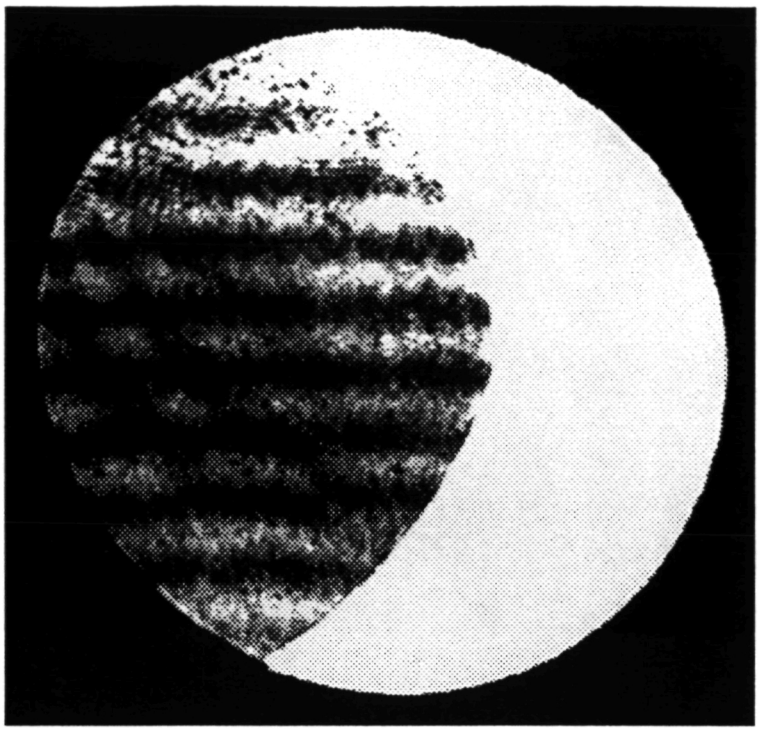

Figure 7.5. Diode laser (λ = 680 nm) reconstruction of an interferogram made from a TCHI hologram after breadboard was tilted.

8. CONCLUSIONS

In the foregoing study, the theory of two color holographic interferometry has been tested experimentally over a large range of interest for materials processing in space where measurements of temperature and concentration in a solution are required. In the course of the work, new techniques were developed and applied to stretch some of the limits beyond what could be done with existing procedures. The study resulted in the production of one of the most advanced, enhanced sensitivity, holographic interferometers in existence. The interferometric measurements made at MSFC represent what is believed to be the most accurate holographic interferometric measurements made in a fluid to date. The tests have provided an understanding of the limitations of the technique in practical use.

The feasibility of the TCHI technique itself was demonstrated using the laboratory breadboard located at MSFC. The importance of precise values of the partial derivatives of refractive index with respect to temperature and concentration in determining the sensitivity of the TCHI method became apparent during experimentation with the system. The scarcity of this information also became evident and obtaining it was perhaps the major difficulty in successfully demonstrating the feasibility of the method. While very accurate data is available on refractive index for a variety of solutions over temperature and concentration (especially at the Sodium line wavelength), this data is generally not adequate for determining dn/dT and dn/dc to better than within several percent points, since the variation of refractive index with these parameters is usually in the fifth or sixth decimal point. We found, however, that the same breadboard used to demonstrate the TCHI technique could also be used to obtain sufficiently precise values of these derivatives, apart from

knowing the exact value of the refractive index itself. This was a major discovery because it meant that since the same setup can be used to, in essence, "calibrate" the system, the technique can be used for any crystal growth solution of interest, independent of published information about these material properties. The subtlety of this is that knowledge of the refractive index of the material is not actually required for the technique to work; only the derivatives with respect to temperature and concentration are needed.

The value of having a reference area for normalizing holograms to the live view was also demonstrated during the experimental program. Corrections made for hologram tilt proved to be vital in order to obtain correct results; corrections that could not have been made if air gaps to either side of the test cell had not been provided as a reference area. The use of a "reference hologram" was also found to be important for producing highly corrected interferogram data. This reference interferogram was formed by interfering the stored wavefront of the test cell with that from the live test cell under the exact same conditions.

An analysis of the sensitivity of the TCHI equations to errors in the various parameters revealed that the most critical determinate in evaluating the sensitivity of the method for a particular set of conditions was the denominator term $(\partial n/\partial c)_j(\partial n\partial T)_k-(\partial n/\partial c)_k(\partial n/\partial T)_j$ found in Equations 1.9 and 1.10 (referred to in this report as the parameter, d). The reason for this is that not only are the derivatives almost equal at each wavelength, but each product is made up of a partial at each wavelength. If, for example, the variation in $(\partial n/\partial c)$ with wavelength exactly matched the variation in $(\partial n/\partial T)$, then d would be exactly zero and the method would not work since the TCHI equations would be infinitely sensitive to <u>any</u> error in <u>any</u> of the parameters (c.f. Equations 2.2 - 2.11 for $d = 0$). We have proposed that d is a useful descriptor of a material under study whose value can vary with temperature and concentration. Determining d for a particular material at a particular nominal state will go a long way in establishing what phase error, for instance, can be tolerated in order to obtain a given accuracy in the temperature and concentration measurements.

The experimental results using the laboratory breadboard confirmed the accuracy of the analytical error analysis and established the value of these equations in determining the sensitivity of the method to uncertainties in the values of the parameters found in the two TCHI equations. It is important to realize that the sensitivity of the TCHI equations to errors in its parameters actually establishes the sensitivity of the method itself. This is true since variations in the actual temperature or concentration below the values obtained in the error equations (Equations 2.13 - 2.22) would not be detectable, since that change would not be distinguishable from uncertainties in the phase measurement.

The phase error for the laboratory breadboard used in the TCHI demonstration was found to be $\lambda/100$ on average. The error was evaluated two different ways with essentially the same result. Camera intensity resolution (at best 1 part in 255) was probably the limiting factor. Based on the error analysis equations, this would lead to a sensitivity in the TCHI technique of ±0.08 g/l and ±0.12 °C. These results matched with the experimentally observed variations in temperature and concentration readings (see columns 6 and 7 in **Table 5.4**). Phase variations across the cell with no (known) gradients were observed to be anywhere from $\lambda/100$ to $\lambda/33$, depending on the

hologram and time. These variations cannot be attributed to temperature or concentration variations, since no gradients existed in the cell. Where variations were $\lambda/100$, the problem could be either electronic noise or optical (phase) noise, since this was also determined to be the noise level of the phase readings themselves. We concluded that the noise was optical for those cases where the variation across the cell was larger. This suggests that a limit may have been reached for the holographic method using silver halide glass plates where it is hypothesized that factors such as emulsion shrinkage due to processing may have accounted for the observed variations. Use of a liquid gate could have mitigated this effect to some extent.

Based on these experiments we have concluded that TCHI can provide useful measurements in the materials processing in NASA space programs.

In a second part of the program, techniques for miniaturizing the system and its associated hardware, so that the method could be implemented in space, were tested. Procedures were identified and tested that would allow the TCHI system to be constructed in a small, lightweight, compact, low power requirement package that could be implemented on a crystal growth cell. The use of fiber optics and solid state lasers provide a key to such implementation. By way of comparison, the two color holocamera unit we built on a flight breadboard is smaller in weight and volume by over an order of magnitude than the holocamera used in the FES for Spacelab 3 and IML-1 spaceflights and yet it is considerably more powerful. A simple simulation of the change in stresses on the system due to the microgravity environment was performed. We concluded that the resulting changes in the interferogram formed using a hologram made in a different stress environment could be easily corrected by simple tilt adjustments in the horizontal and vertical axes.

The information resulting from this project is extremely critical for the design and construction of a practical, spaceflight TCHI system that could be extremely useful to NASA's materials processing in space programs.

REFERENCES

[1] Creath Katherine, "Phase-measurement Techniques for Nondestructive testing" in Hologram Interferometry and Speckle Metrology, the Proceedings of The Society for Experimental Mechanics Baltimore, November 5-8, 1990. pp. 473-479. Note: the latter proceedings has a large collections of papers dealing with automated data reduction using the various techniques discussed in this report.

[2] Brophy, C.P., "Effects of Intensity Error Correlation on The Computed Phase of Phase Shift Interferometry," J. of The Optical Society of America, Vol. 7, No.4, April 1990. pp. 537-541.

[3] Trolinger, J., Craig, J. and Dean, P., "Advanced Holographic Diagnostic Method For 3D Hypersonic Flow Fields," AIAA Paper 88-4653-CP, AIAA/NASA/AFWAL Sensors & Measurement Techniques For Aeronautical Applications Conference, Atlanta, GA., September 1988.

[4] Yanta, W.J., Spring, W.C., Gross, D.U. and McArthur, J.C., "Phase Measuring Laser Holographic Interferometer For Use In High Speed Flows," ICIASF 13TH Congress on Instrumentation In Aerospace Simulation Facilities, September 1989.

[5] W. Lu and W.M. Worek "Two-wavelength interferometric technique for measuring the refractive index of salt-water solutions." Applied Optics, Vol. 32, No. 21 p. 3992, 20 July 1993.

[6] L.W. Tilton and J.K. Taylor, "Refractive index and dispersion of distilled water for visible radiation at temperatures 0 to 60°C", Journal of Research of the National Bureau of Standards, Vol. 20, April 1938.

APPENDIX A

INSTALLATION INSTRUCTIONS FOR TEST CELL CHAMBER

The hardware is comprised of four major components:

1. Computer Card
2. Interface Box
3. Thermo Couples
4. Test Cell

Test Chamber & Cell

To install the test chamber and test cell, follow the nine simple steps listed below:

1. Set test chamber in desired location with the side mount power connect in a position of easy access.

2. Connect the six pin connector from the interface box into its mating connector on the test chamber.

3. Check that the copper chamber body is seated and centered in the polypropylene chamber body.

4. Remove the copper chamber body cap.

5. Place one drop of mineral oil on the bottom of the cooler plate.

6. Place the quartz test cell on the bottom cooler plate. Be sure that the mineral oil spreads out under the bottom of the test cell to ensure good thermal contact. Use care not to get mineral oil on the optical surfaces because these are very difficult to clean.

7. Carefully place the copper chamber cap back in place. NOTE: The upper cooler plate protrudes into the test cell so *use care!* Pressure on the test cell ***will*** damage it!

8. Insert the polypropylene chamber cap into place.

9. Attach the front plate to the front of the test chamber and the back plate to the back of the test chamber.

The test chamber and cell are now installed.

To install the computer card, power down the computer and remove the cover. Find an open card slot, remove the screw holding the cover in place and insert the comp card. Secure the card in place by replacing the screw you just removed. The computer card is now in place.

Place the interface box next to the computer and remove the top. On one end you will find a ribbon cable and on the other end there is a strain relief clamp for the input and output wires. There will already be one wire placed in the strain relief.

At this point you will need to connect the ribbon cable to the computer card. The ribbon connector is notched so that the connector can only be installed in one position. Next, the thermocouples (TC) will need to be connected. To connect the thermocouples, first note that the TC's are in three parts. Two single TC's and one group of four. The two single TC's can be identified by the cables 1 and 6 on the blue connectors. Due to poor labeling, the connectors have two ID marks. The first is the numbers and second is a set of dots. TC #1 has one dot, TC #2 has two dots, and so on. The dots are on the top side of the connectors. On the interface box, there are two sections; digital I/O and analog output.

The digital I/O has already been wired and should not need to be adjusted. The analog output is where the TC's are to be connected. The analog outputs have eight channels. Label 1-8 from the bottom left, clockwise. They consist of three poles (+, -, common). There is a 10K resistor between the negative and the com pole of the first six channels. When connecting the TC's , the copper prong on the TC is connected to the positive; while the silver prong is connected to the negative. Remember that the resistor needs to stay connected between the negative and com. Once these connections are made, the TC's are ready for reading.

Software Installation

1. Place the supplied floppy disk into the "A" drive.

2. First create the directory to which the software will be installed.

3. At the C:> prompt, type: **MD METRO**

   You have now created a directory called "Metro". Now copy the contents of "A" drive to the METRO directory by doing the following:

4. From the C:> prompt, type **\METRO**. From the C:\METRO> prompt, type: **COPY A:*.***.

To add the rotational stage software:

1. Create a subdirectory in METRO by typing **MD MOVER** at the C:\METRO> prompt.

   You now have a subdirectory in METRO called MOVER. Change to this directory at the C:\METRO> prompt by typing **CD\MOVER**. You should now be in C:\METRO\MOVER> directory.

2. Insert the MOVER disk into the "A" drive and type: **COPY A:*.***.

3. Now type **CD..** until you are at the C:\METRO> prompt and type **TEMP1.** You are now in the "Temperature Monitor and Control Program". When the program starts up, a title screen appears. Press any key to continue. The next screen will display inputs and outputs. The screen should read:

8 - Analog inputs installed.
12 - Digital outputs installed
8 - Channels with valid calibration

If your screen does not display these numbers, check to make sure that all your connections are solid. If your screen displays the correct numbers, then press any key to continue. You are now in the Temperature Monitoring screen. A brief description of the display screen is as follows:

On the left hand side is a graphic displaying the test cell and the locations of the thermocouples. These are lines leading from the thermocouples to the corresponding temperature readings. The temperature readout displays current temperature, minimum temperature of current run and maximum temperature of current run.

At the bottom of the temperature readout display, between ΔT TC 2 and 5 MIN & MAX, at the bottom of the screen are five function operations.

Starting from the left operation, type P-(PRINT DATA). These will print the temp readout to the printer on LPT1.

R - (RESET STATISTICS) will reset MIN and MAX temperature readout.
S - (SETUP) will call up the Set-Up Menu. The Set-up Menu will be discussed later.
D - (DATAFILE) calls up the DATAFILE Menu. (To be discussed later).
T - (TOGGLE) toggles the phase shift software.
X - (EXIT) To exit the program.

S - SETUP

The Set-Up menu consists of four functions:

1. The first: the number of average samples: 10. This is the number of samples taken for each reading displayed.

2. The second: Heater control is: enabled/disabled. This function turns the temperature control on or off.

3. The third: Control Mode: Dual heater, ABSOLUTE T (Top) = :21 T (Bottom) = 21

   Dual heat is an obsolete function. ABSOLUTE gives the adjustment of setting a temp. for the top plate and for the bottom plate. (Example: if you wanted to maintain a temp. of 21°C in the cell, you would set T (Top) at 21 and T (Bottom) at 21. If you wanted to put a 1°C gradient across the cell, you should lower T (Top) .5°C and raise T (Bottom) .5°C. This will give you a full ° of gradient.

4. The fourth is the calibration setting. This should not require adjusting. To exit the Set-up screen, type X then enter (or carriage return).

DATAFILE FUNCTION

1. Current storage delay (seconds): 10. The time between DATA collection.

2. Current save file name: Run 1. This is your spec. file name and path. The user must specify the name for each data collection.

3. Save to disk: DISABLED/ENABLED. Once this function is switched to ENABLED, the program will start saving data.

4. Type X to exit.

Report Documentation Page

Form Approved
OMB No. 0704-0188

Public reporting burden for this collection of information is estimated to average 1 hour per response, including the time for reviewing instructions, searching existing data sources, gathering and maintaining the data needed, and completing and reviewing the collection of information. Send comments regarding this burden estimate or any other aspect of this collection of information, including suggestions for reducing this burden, to Washington Headquarters Services, Directorate for Information Operations and Reports, 1215 Jefferson Davis Highway, Suite 1204, Arlington, VA 22202-4302, and to the Office of Management and Budget. Paperwork Reduction Project (0704-0188), Washington DC 20503.

1. AGENCY USE ONLY *(Leave blank)*	2. REPORT DATE	3. REPORT TYPE AND DATES COVERED
	23 February 1995	Final Report: POP: 07/21/92 - 02/21/95

4. TITLE AND SUBTITLE

Two Color Holographic Interferometry for Microgravity Application

5. FUNDING NUMBERS

DCN 1-2-ES-44818

6. AUTHOR(S)

James D. Trolinger, Ph.D. and David C. Weber

7. PERFORMING ORGANIZATION NAME(S) AND ADDRESS(ES)

MetroLaser
18006 Skypark Circle #108
Irvine, CA 92714-6428

8. PERFORMING ORGANIZATION REPORT NO.

TNM4DWF

9. SPONSORING/MONITORING AGENCY NAME(S) AND ADDRESS(ES)

Chief, Technology Utilization Office, AT01
NASA Marshall SFC
Attn: COTR William Witherow/ES74
Marshall SFC, AL 35812

10. SPONSORING/MONITORING AGENCY REPORT NUMBER

11. SUPPLEMENTARY NOTES

12a. DISTRIBUTION/AVAILABILITY STATEMENT

12b. DISTRIBUTION CODE

16. Abstract

Holographic interferometry is a primary candidate for determining temperature and concentration in crystal growth experiments destined for space. The method measures refractive index changes within the fluid of an experimental test cell resulting from temperature and/or concentration changes. When the refractive index changes are caused by simultaneous temperature and concentration changes, the contributions of the two effects cannot be separated by single wavelength interferometry. By using two wavelengths, however, two independent interferograms can provide the additional independent equation required to determine the two unknowns. There is no other technique available that provides this type of information.

The primary objectives of this effort were to experimentally verify the mathematical theory of two color holographic interferometry (TCHI) and to determine the practical value of this technique for space application.

In the foregoing study, the theory of TCHI has been tested experimentally over a range of interest for materials processing in space where measurements of temperature and concentration in a solution are required. New techniques were developed and applied to stretch the limits beyond what could be done with existing procedures. The study resulted in the production of one of the most advanced, enhanced sensitivity holographic interferometers in existence. The interferometric measurements made at MSFC represent what is believed to be the most accurate holographic interferometric measurements made in a fluid to date. The tests have provided an understanding of the limitations of the technique in practical use.

14. SUBJECT TERMS	15. NUMBER OF PAGES
Holographic Interferometry, crystal growth	77
	16. PRICE CODE

17. SECURITY CLASSIFICATION OF REPORT	18. SECURITY CLASSIFICATION OF THIS PAGE	19. SECURITY CLASSIFICATION OF ABSTRACT	20. LIMITATION OF ABSTRACT
Unclassified	Unclassified	Unclassified	Unlimited